Coventry University

Coventry University

DOCTOR OF PHILOSOPHY

Numerical analyses of proton electrolyte membrane fuel cell's performance having a perforated type gas flow distributor

Virk, Muhammad Shakeel

Award date:
2009

Awarding institution:
Coventry University

Link to publication

Numerical Analyses of a Proton Electrolyte Membrane Fuel Cell's Performance having a Perforated Type Gas Flow Distributor

Muhammad Shakeel Virk

A Thesis Submitted in Partial Fulfilment of the Requirements of the Coventry University for the Degree of Doctor of Philosophy

The Programme of research was carried out at the Energy & Environmental Technology Applied Research Group, Faculty of Engineering and Computing, Coventry University, UK

August 2009

Dedicated To

Dada Abu and Dadi Amaa

Acknowledgements

I would like to take this opportunity to thank a number of people for their assistance and guidance throughout this research. Special thanks must go to my supervisor Professor Arne Erik Holdø who has always been an example of relentless and energetic researcher for his patience and guidance. It has been really a nice learning experience to work under his kind guidance. Our in-depth discussions and his enthusiasm allowed me to see the light on several occasions during times of frustration and despair. I also want to say thanks to Dr William Hall and all my fellow researchers at the *' Energy and Environmental Technology Applied Research Group'* of Coventry University for their friendship and the pleasant working environment.

Special thanks to my small, but larger than life family: my father, mother, wife, brother, sisters and cute son (Ismael) for their social and moral support. All your help and guidance has been invaluable, because without you I could never have followed this path.

Muhammad Shakeel Virk
Coventry, 2009

Table of Contents

List of Figures

viii

ix

List of Tables

Nomenclature

u, v, w	Velocity Components in x, y and z direction (m/sec)
P	Pressure (Pa)
M	Molecular weight of reactant species
t	Time (sec)
R	Universal gas constant, 8.314 (J/mol .K)
T	Temperature (K)
D	Diffusion coefficient (m^2/sec)
h	Enthalpy
E	Energy (Joule)
V	Atomic diffusion volume of reactant species
S	Source term
D_f	Diffusion flux of reactant species
K_p	Permeability (m^2)
K_s	Thermal conductivity of solid (W/m.K)
K_f	Thermal conductivity of fluid (W/m.K)
W	Mass fraction of reactant species
E	Activation Energy (KJ/Mol)
$C_{o2,ref}$	Local oxygen concentration (mol/m^3)
$C_{H2,ref}$	Local hydrogen concentration (mol/m^3)
i_0	Reference exchange current density
i	Current density (A/cm^2)
F	Faraday constant, 96747 (C/mol)
n_e	Number of electron transfer

q^0	Heat generated (W/m^2)
a	Membrane water activity
$A_{1,2,3}, B_{1,2,3}$	Constants
n_d	Electro-osmotic drag coefficient
F	Pulsating frequency
A	Pulsating amplitude

Subscripts

i	Oxygen and Hydrogen species
j	Water species
c	Cathode
a	Anode
g	Gas phase
l	Liquid phase
H_2	Hydrogen
O_2	Oxygen
H_2O	Water
act	Activation
oc	Open circuit
s	Electrode
m	Membrane
eff	Effective
rev	Reversible

Greek Symbols

ρ	Fluid density (kg/m^3)
μ	Fluid dynamic viscosity (kg/m-sec)
ε	Porosity
λ	Membrane water content
α	Symmetry parameter
φ	Cell potential (Volts)
σ	Ionic conductivity (S/m)
β	Heat transfer coefficient (W/m^3)
η	Cell over-potential (Volts)
τ	Stress tensor

Abbreviations:

PEM	Proton electrolyte membrane (or) Proton exchange membrane
MEA	Membrane electrode assembly
GDL	Gas diffusion layer
CL	Catalyst layer
FC	Fuel cell
SS	Stainless Steel
PTFE	Polytetafluor-ethylene

ABSTRACT

This thesis presents a compendium of work related to performance analyses of a proton electrolyte membrane (PEM) fuel cell with two novel design configurations. The finite element based numerical analysis has been carried out to solve the numerical transport models involved in a PEM fuel cell coupled with the flow in a porous medium, charge balance, electrochemical kinetics and membrane water content. The scope of this research work focuses on improving the performance of the PEM fuel cell by optimizing the thermo-fluid properties of the reactant species instead of analysing the complex electro-chemical interactions. Two new design configurations have been numerically analyzed; in the first design approach, a perforated-type gas flow distributor is used instead of a conventional gas flow distributor such as a serpentine, straight or spiral shape; the second design approach examines the effect of reactant flow pulsation on the PEM fuel cell performance. Results obtained from the numerical analyses were also compared with the experimental data and a good agreement was found.

Performance of the PEM fuel cell with a perforated-type gas distributor was analyzed at different operating and geometric conditions to explore the merits of this new design configuration. Two-dimensional numerical analyses were carried out to analyze the effect of varying the different operating parameters; three-dimensional numerical analyses were carried out to study the variation of different geometric parameters on overall performance of the new design configuration of the PEM fuel cell.

The effects of the reactant flow pulsation on the performance of PEM fuel cell were analyzed using a two-dimensional numerical approach where both active and passive design configurations were numerically simulated to generate the pulsations in the reactant flow. The results showed a considerable increase in overall performance of the PEM fuel cell by introducing pulsations in the flow.

CHAPTER 1

1   Introduction

1.1   Background

Increasing levels of pollution and possible anthropogenic global warming resulting from the combustion of fossil fuels have urged scientists to consider alternative energy conversion and power generation systems that could satisfy the global energy demands in more environmental-friendly ways. Wind, tidal, solar and hydrogen based renewable energy systems are some of the potential areas in this regard [1, 2]. Hydrogen-based renewable energy systems such as fuel cells offer a promising pathway with the prospect of low- to zero-emissions during power generation for sub-watt to megawatt applications in transportation, manufacturing and communications [3-5]. The combination of high efficiency, environmental benefits and versatility make fuel cells a suitable power generation device for both terrestrial and space applications. Despite these potential benefits, the commercial deployment of fuel cells faces many challenges such as; high operating cost and a lack of existing hydrogen infrastructure [6, 7].

The fuel cell was first demonstrated by Lawyer-cum-inventor William Grove in 1839, but no further significant research was carried out in this field until the late 1940s [8]. The first commercial application of a fuel cell was in space and military systems [9]. Among the different types of fuel cells, the polymer electrolyte membrane (PEM) fuel cell is considered a promising approach due to its low operating temperature and simple design configuration [10, 11].

The basic operating principle of a fuel cell is simple, but involves the coupling of complex transport phenomena such as species transport by convection and diffusion, heat transfer, charge balance and electrochemical kinetics. These

transport phenomena lead to certain efficiency losses in the fuel cell that affect its overall performance. The performance of a fuel cell can be investigated in two ways; either by experimental techniques or by numerical simulations. Experimental methods have limitations when investigating the complex interaction of transport phenomena taking place inside the fuel cell, whereas numerical modelling provides a better insight into the problem [12, 13]. Furthermore, it is not possible to perform detailed in-situ measurements of a fuel cell during its operation because of its reactive environment [14, 15]. The complex experimental setup of the fuel cell system has stimulated efforts to develop sophisticated numerical models of the fuel cell that can simulate and predict the coupled transport of reactant and product species, heat transfer and charge balance along the fuel cell domain.

The performance of a PEM fuel cell can be improved by improving the reaction rate and the species distribution along its domain [3]. The reaction rate is a function of the electro-chemical properties of the catalyst layer and distribution of the reactant species. The electro-chemical properties of the catalyst layer depend upon the material and chemical composition, whereas the distribution of the reactant species can be improved by certain changes in the PEM fuel cell design. Therefore, innovative fuel cell designs are required to improve the distribution of reactant species along the fuel cell domain and particularly along the catalyst layer [16]. Numerical modelling can provide detailed information into the effects of design changes on the overall distribution of the reactant species and can contribute to significantly shortening the design and optimization cycle.

The present research was carried out at the *'Energy and Environmental Technology Applied Research Group, Faculty of Engineering and Computing, Coventry University, UK'*. It primarily focuses on computational fluid dynamics (CFD) based multi-physics numerical modelling of the coupled transport phenomena that occur in two novel design configurations of the PEM fuel cell. In the first design approach, a perforated-type gas flow distributor is examined instead of a conventional type of gas flow distributor (such as serpentine, spiral or parallel flow channels). The second design approach studies the effects of reactant flow pulsation on the distribution of the reactant and product species along the PEM fuel cell domain. These numerical analyses have been carried out using both two- and

three-dimensional numerical modelling techniques, and the results obtained from the numerical analyses have been compared with experimental data to validate the method, numerical model and the design concept.

1.2 Aim and Objectives

This research work primarily aims to enhance the performance of a PEM fuel cell by improving the distribution of reactant/product species along its domain by simplifying the design configuration and by optimizing the behaviour of the thermo-fluidic parameters along its domain [17]. To date, most research and development activities examining PEM fuel cells have focused on the electro-chemistry, and in particular on the membrane electrolytes. However no major research activity has been carried out to study the thermo-fluidic properties of the PEM fuel cell [18].

This research work also aims to reduce the manufacturing efforts and cost of the PEM fuel cell by simplifying its design configuration through optimizing the design of the gas flow channels and the use of less exotic materials. The electrode plates, usually termed as bipolar/end plates in fuel cell literature, are very important components of the PEM fuel cell which significantly contribute towards its total weight and cost. As such, attention has been paid in this research work to select the optimum materials for these electrode plates as well as simplifying their design specifications.

The main objectives of this research can be described as follows:

1) To understand and numerically model the coupling of complex transport phenomena taking place inside the PEM fuel cells.

2) To reduce the manufacturing cost of the PEM fuel cells by selecting optimal materials for the electrode plates and simplifying their gas flow channel design configuration.

3) To improve the performance of PEM fuel cells by enhancing the distribution of reactant species along their domain instead of dealing with the complex electro-chemical properties of the membrane electrode assembly. For this purpose, two new design configurations of the PEM fuel cell are analyzed and discussed in this research work:

a) In the first design approach, a perforated stainless steel gas distributor is used instead of the conventional serpentine or parallel shaped gas flow distributor based on graphite. The perforated-type gas distributors significantly reduce the manufacturing effort and cost as they are readily available on the market and can be readily customized without any extra machining cost.

b) In the second design approach; the concept of cathode flow pulsations is introduced to improve the diffusive properties and overall distribution of reactant and product species inside the PEM fuel cell domain.

1.3 Outline

This thesis consists of seven chapters in addition to the introduction in chapter 1. Chapter 2 is a review of the recent published literature on this field of the fuel cell science, where the current state of knowledge and existing literature concerning PEM fuel cells are examined; this includes the basics of typical PEM fuel cell design and fuel cell numerical models used by different researchers. The numerical methodology and governing transport equations used for the numerical simulation are presented in Chapter 3 while a case study used for the validation of the numerical model in comparison to experimental data is discussed in Chapter 4. Chapter 5 introduces a parametric study of the effects of different operating conditions and geometric parameters on the performance of a perforated-type PEM fuel cell. Chapter 6 describes the transient numerical analyses involving the effect of cathode flow pulsations on the performance of PEM fuel cells having a straight-type gas flow channel. In Chapter 7 the important findings of this study are

4

discussed, and finally the conclusions and recommendations for future work are presented in Chapter 8.

1.4 Summary

The performance of a fuel cell can be analysed using both numerical and experimental techniques. In this work numerical techniques were used to conduct the performance analyses of a PEM fuel cell and experimental data were used to validate the numerical model. The primary focus of this research work is to improve the performance of PEM fuel cells by improving the distribution of reactant species instead of enhancing the complex electro-chemical properties of the membrane electrode assembly. Further aims and objectives of this research work have been described earlier to clearly define the basis and direction of this research.

CHAPTER 2

2 Literature Review

2.1 Introduction

A fuel cell is an electro-chemical conversion device that directly converts the chemical energy of reactants into electricity without combustion [8]. In spite of the complexities involved in the manufacturing of a fuel cell system, the basic operating principle of a fuel cell is relatively simple. A typical fuel cell consists of two electrodes (anode and cathode) separated by a conducting ionised electrolyte. At the anode side, the incoming hydrogen gas atoms are oxidised into positively charged protons and negatively charged electrons. The positively charged protons travel through the electrolyte membrane while the negatively charged electrons travel through an external circuit to the cathode side, where they chemically react with reduced oxygen atoms, forming heat and water as a by-product [19].

A fuel cell is different from a battery as it is only an energy *conversion* device, whereas a battery is an energy *storage* device. The electrode of a battery is consumed during the reaction that eventually stops the delivery of power from the battery. However, in a fuel cell the energy conversion and storage functions are separated from each other, such that the fuel cell can operate as long as reactants are supplied. The overall composition of a fuel cell itself remains unchanged during the whole electro-chemical process [9].

The fuel cell systems are superior to existing conventional power generation systems in many regards; for example:

i. Fuel cells operate in an environmental friendly manner as they do not produce any harmful by-products like most conventional power generation

6

systems. Conventional power generation systems use different types of fuels such as coal, petrol and diesel that result in the emission of harmful by-product gases that pollute the atmosphere.

ii.   In comparison to other conventional power generation systems, fuel cell systems produce far less noise during their operation. The noise level at 30 meters from a fuel cell power plant has been measured at only about 55 db [20].

iii.   Fuel cells do not cause any significant thermal pollution as only a very small amount of heat is produced in the electro-chemical reaction. The low amount of heat generated by a fuel cell means that the heat can be exhausted directly into the air rather than into a specialised heat sink, such as water.

iv.   Fuel cell systems do not have a striking visual impact, as no smokestacks or cooling towers are required. It is possible to enclose a fuel cell system inside a small building without the extensive special arrangements required by conventional energy generation methods [19].

v.   Fuel cells are safer and more reliable when compared to other conventional power generation systems. The US aerospace programme has proven the reliability of fuel cells for steady, uninterrupted power generation, as not a single failure of a fuel cell system has occurred in NASA programmes [19].

vi.   Maintenance of a fuel cell system is simple because a fuel cell is mechanically static, and as such there are no moving parts. Due to this, the maintenance of the fuel cell system is required only at infrequent intervals. Moreover, fuel cells can be used for unmanned operations with automatic or remote dispatch of generated electricity [19].

As well as the above mentioned benefits of a fuel cell system, there are some fundamental drawbacks such as:

i. The slow reaction rate leads to low current outputs and power densities. This problem can be dealt with by the selection of proper material composition for the membrane electrode assembly and catalyst layer and optimizing the design of the fuel cell gas flow channels

ii. Hydrogen fuel is not readily available and a completely new infrastructure is required for the hydrogen distribution.

iii. Like other emerging power generation systems, fuel cells are limited by current materials technology, but this problem is much less critical than those associated with magneto-thermodynamics and nuclear fusion [19].
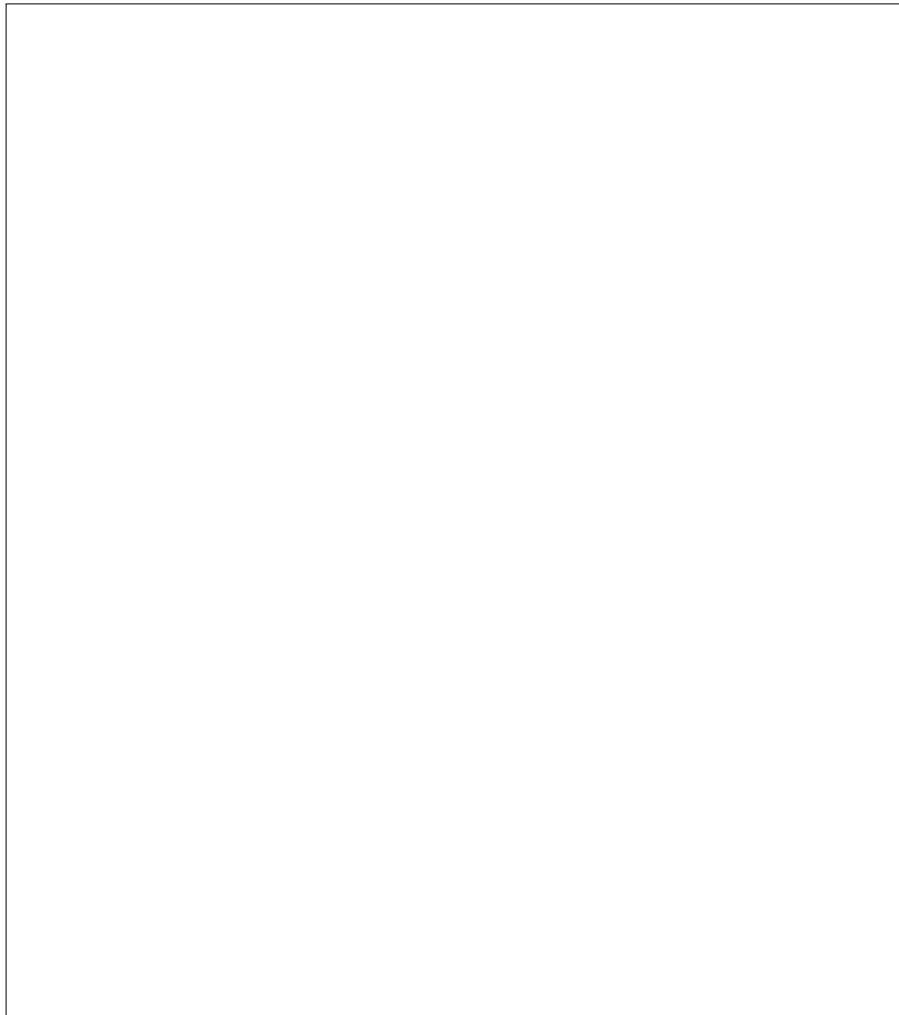
Figure 2-1: Basic operating principle of a fuel cell [21]

2.2 Types of Fuel Cell

Different types of the fuel cell systems have been investigated by researchers to improve their performance and promote their commercialisation. Currently, five classes of fuel cells have emerged as viable power systems for the present and near-future applications. Each type of fuel cell has some merits and drawbacks. A brief description of the major types of fuel cells is presented in the following sections.

2.2.1 Polymer Electrolyte Membrane (PEM) Fuel Cell

The polymer electrolyte membrane (PEM) fuel cell is regarded as one of the most promising types of fuel cells due to its simplicity and low operating temperature. This type of fuel cells generally operate between 50 to 100 ^{o}C, which makes them suitable for automotive and mobile applications [8]. In this type of fuel cells, the electrolyte is a solid polymer which contains mobile protons. The major drawback of the low operating temperature of PEM fuel cells is the low electro-chemical reaction rate, which can be addressed using sophisticated catalysts and electrodes.

2.2.2 Alkaline Fuel Cell

The alkaline fuel cell is one of the most developed types of fuel cells which was used by NASA moon missions in the late 1960s [8] . This type of fuel cells produces power through a 'redox' reaction between hydrogen and oxygen. The anode and cathode are separated by a porous matrix saturated with an aqueous alkaline solution of potassium hydroxide (KOH). Pure oxygen reacts with the potassium hydroxide to make potassium carbonate as a by-product. This potassium carbonate causes a blockage of pores that slowly reduces the performance of this type of fuel cells.

Alkaline type fuel cells operate at fairly high temperatures ranging between 50 to 200 ^{o}C and they have higher efficiency when compared to the PEM fuel cells. Alkaline fuel cells also have an edge over PEM fuel cells due to their low activation

overpotential at the cathode, but conversely they need pure hydrogen and oxygen to achieve optimum performance which makes their operation costly [8, 22].
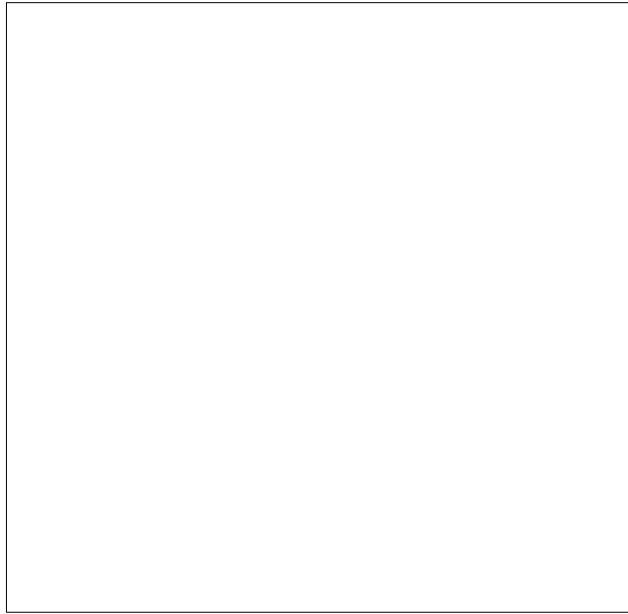
Figure 2-2: Operating principle of alkaline type fuel cells [8]

2.2.3 Phosphoric Acid Fuel Cell

This type of fuel cells uses liquid phosphoric acid as an electrolyte. Hydrogen is introduced at the anode side and is oxidised to produce positively charged protons and negatively charged electrons. The ionic conductivity of the phosphoric acid is low at low temperatures. Furthermore, it solidifies at temperatures below 40 ^{o}C, which makes the initial start-up difficult and restricts the continuous operation of this type of fuel cells [23].

Phosphoric acid fuel cells operate at a temperature of around 220 ^{o}C and can tolerate carbon monoxide, which is not acceptable for many other types of fuel cells. Moreover, In this type of fuel cells, the hydrogen fuel problem can be solved by reforming natural gas (CH_4, methane) to hydrogen and carbon dioxide, but the equipment required for this adds considerable cost, complexity and size to the fuel cell system [22].

2.2.4 Solid Oxide Fuel Cell

Solid oxide fuel cells are made up of four layers, three of which are ceramic. Ceramics do not become ionically active until they reach at very high temperature and therefore the solid oxide fuel cell is only operational in the region of 800 – 1200ºC. Oxygen gas enters at the cathode side while fuel enters at the anode side. Light hydrocarbon fuels such as methane, propane and butane are mostly used as fuels in this type of fuel cell. Oxygen is reduced into oxygen ions at the cathode side. These oxygen ions then diffuse through the solid oxide electrolyte to the anode where they electro-chemically oxidize the fuel.

This type of fuel cell is generally suitable for large industrial applications because of its high operating temperature range. Due to such high temperatures, a fast reaction rate can be achieved without using any expensive catalysts.
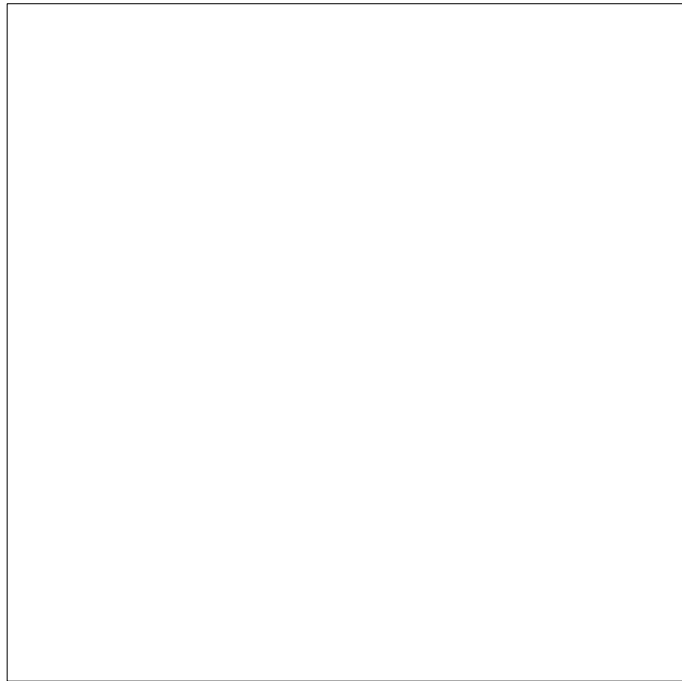
Figure 2-3: Operating principle of solid oxide fuel cells [8]

2.2.5 Molten Carbonate Fuel Cell

The electrolyte of a molten carbonate fuel cell is a mixture of molten alkali metal carbonates; usually a binary mixture of lithium and potassium, or lithium and sodium carbonates. To melt the carbonate salts and achieve high ion mobility through the electrolyte, this type of fuel cell operates at around 650 ^{o}C [24]. Due to the high temperatures, the alkali carbonates form a highly conductive molten salt with the carbonate (CO_3^{-2})ions, providing ionic conduction [8]. Unlike other types of fuel cells, molten carbonate fuel cells do not require any external reformer to extract hydrogen from energy-dense fuels. Due to the high operating temperature, the fuels are converted into hydrogen within the fuel cell itself by internal reforming.
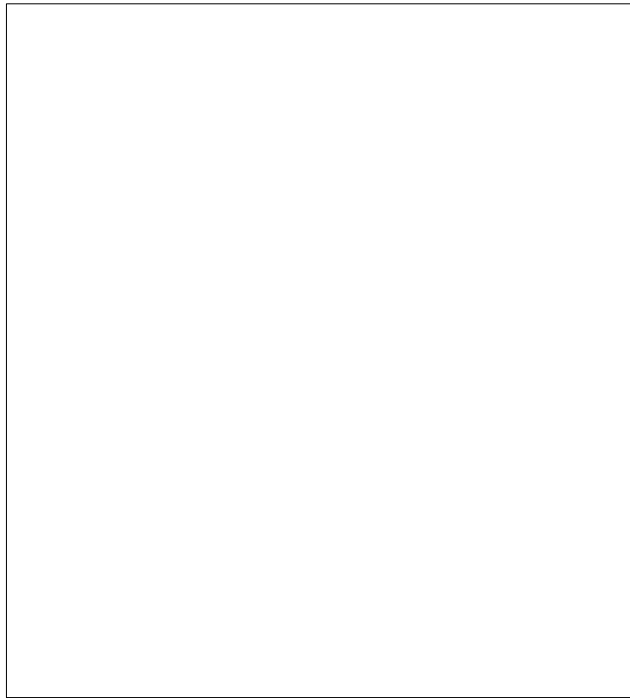
Figure 2-4: Operating principle of molten carbonate fuel cells [25]

2.3 PEM Fuel Cell: Description

Polymer electrolyte membrane (PEM) fuel cells are a relatively new technology within the fuel cell community. This type of fuel cell was first developed by *General Electric* in the USA in the 1960s for use by NASA on its manned space vehicles [26]. The development of PEM fuel stagnated in the 1970s and early 1980s. However, in the second half of the 1980s there has been a renaissance of interest in this type of fuel cell. Rapid development during the past decade has now brought the PEM fuel cell significantly closer to commercial reality.

PEM fuel cells consist of three major components: a negatively charged electrode (cathode), a positively charged electrode (anode) and a membrane electrode assembly. The membrane electrode assembly consists of a current collector, a porous gas diffusion layer, a catalyst layer and an electrolyte membrane. The operating principle of a PEM fuel cell is simple and can be considered to be the opposite of electrolysis. In electrolysis, an electric current is passed through water to produce hydrogen and oxygen, whereas in a PEM fuel cell, hydrogen and oxygen gases are passed at either side of the polymer electrolyte membrane where hydrogen is split into its elementary constituents - the positively charged proton ions and the negatively charged electrons.

The potential difference between anode and cathode attracts the protons from anode to cathode causing them to travel through the electrolyte membrane, whereas the electrons travel first through an external circuit and then to the membrane catalyst layer interface at the cathode side where they react with the reduced oxygen atoms, following this, the reduced oxygen atoms react with the protons diffusing through the membrane to produce heat and water as by-products [27]. The electro-chemical reactions for the PEM fuel cell can be stated as follows:

Anode Reaction:	$2H_2 \rightarrow 4H^+ + 4e^-$	(a)
Cathode Reaction:	$O_2 + 4H^+ + 4e^- \rightarrow 2H_2O$	(b)
Overall Reaction:	$O_2 + 2H_2 \rightarrow 2H_2O$	(c)
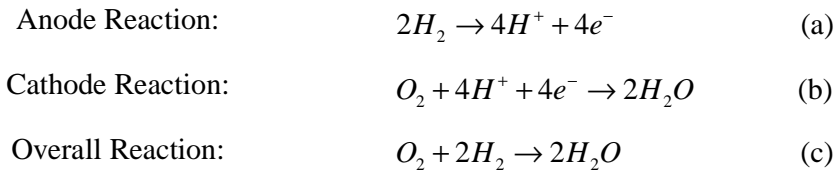
The following figure explains the basic operating principles of the PEM fuel cell and highlights its important components.

Figure 2-5: Schematic view of a PEM fuel cell and its operating principles [3]

2.4 PEM Fuel Cell Components

A PEM fuel cell consists of four major components. The following sections briefly describe these components and their role in the operation of the fuel cell.

2.4.1 Polymer Electrolyte Membrane

The polymer electrolyte membrane is the heart of a PEM fuel cell. It has two main functions; firstly, it works as a gas separator, preventing the reactant gases from directly reacting with each other; secondly, it acts as the proton conductor. Typically, the electrolyte membrane consists of a Perfluroinated polymer backbone with Sulphonic acid side chains [28]. *Nafion*® membranes by *Du-Pont* are typically used as the de-facto standard for most of the polymer electrolyte fuel cells. However, there are also other variants of electrolyte membranes, such as *Flemion*® and *Aciplex*® membranes, which are well known in the fuel cell industry [27, 29, 30].

Membranes have to be hydrated so as to sustain their protonic conductivity. It is therefore necessary for the membrane to retain a certain amount of water content so as to maintain its ability to transfer protons. This depends on two phenomena; firstly, that of the chemical affinity for water in hydrophobic regions of the membrane, which enables the membrane to absorb and retain water; secondly, that of the electro-osmotic drag phenomena, whereby each hydrogen ion is accompanied by one or two molecules of water [30, 31]. The requirement to keep the membrane hydrated restricts PEM fuel cell operation at higher temperatures. In general, to achieve high efficiency, the membrane must possesses the following properties [32, 33]:

a) High proton conductivity to support high currents with minimum resistive losses and zero electronic conductivity.
b) Adequate mechanical strength and durability.
c) Chemical stability under operating conditions.
d) Extremely low fuel or oxygen by-pass to minimise crossover current.
e) Reasonable production cost which is compatible with intended application.

2.4.2 Gas Diffusion Layer (GDL)

The gas diffusion layer enables efficient distribution of the reactant and product species along the fuel cell domain. The gas diffusion layer is made up of a sufficiently porous and electrically conductive material. Materials of a typical gas diffusion layer include carbon paper or carbon cloth with typical thicknesses of 100-300 μm [34]. The GDL is intentionally porous to increase the wetted surface area by hundreds and even thousands times the geometric surface area [26, 27].

The gas diffusion layer is characterized by its thickness, hydrophobic nature and dry resistance to flow and electric properties [35]. Performance of the PEM fuel cell is immensely influenced by the reactant/product species distribution along the gas diffusion layer since it can lead to issues such as water flooding and poor concentration distribution. To facilitate excess water removal from the fuel cell and minimize water flooding, the hydrophobicity of the GDL is increased by impregnating it with a hydrophobic material. The amount of hydrophobic agent used is a sensitive parameter as excess impregnation can result in the blockage of surface pores and thus a reduction of the GDL porosity [36].

Figure 2-6: Microscopic image depicting the random fibre structure of a GDL, formed of Toray carbon paper [3]

2.4.3 Catalyst Layer

A fine layer of catalyst, usually the noble metal platinum (Pt), is applied to both faces of the electrolyte membrane. A catalyst loading of 0.1-0.3 mg/cm^2 per membrane catalyst layer is typically used. The thickness of the catalyst layer is usually in the range 5-15 μm [37]. Due to the high cost of platinum, it must be used sparingly in order to reduce the overall cost of the PEM fuel cell [38]. The catalyst layer breaks the bonds between the atoms of the reactant species and promotes higher reaction rates. At the anode side, the hydrogen molecules are absorbed onto the surface of the catalyst and the bonds between the hydrogen atoms are stretched and weakened so that they eventually break. A similar mechanism occurs on the cathode side where the reduction of oxygen is promoted by the action of the catalyst [30].
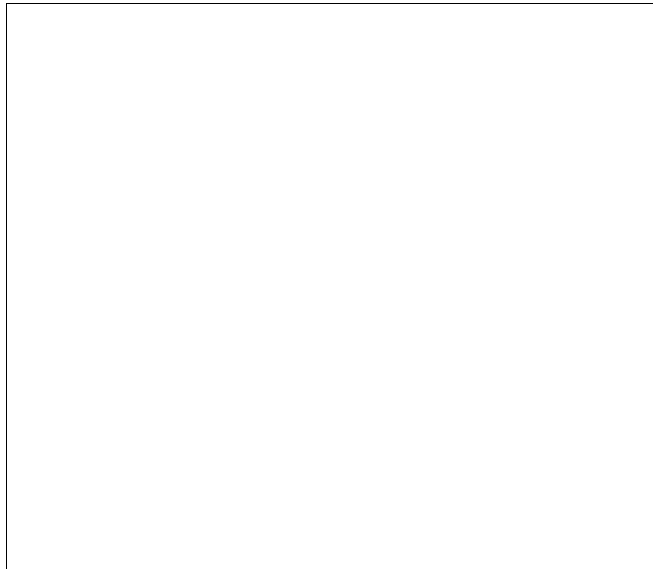
Figure 2-7: TEM Image of fuel cell catalyst (black specks show the platinum catalyst particles finely divided over the carbon paper) [8].

2.4.4 Bipolar / End Plates

The interconnection between the fuel cells in a stack is achieved using conductive plates. When machined on both sides, they are normally called *bipolar* plates. Plates which are fitted at the edges of the fuel cell stack and are machined on one side only are termed *end* plates. The term electrode plates will be used here to

refer to the bipolar and end plates. [30]. These plates are an important component of any fuel cell system because they assist the supply of fuel and oxidant to the reactive sites, remove reaction products, collect produced current and provide structural support [39]. Conventionally, when the electrode plates are made of graphite; they constitute around 60 % of the total weight, 30% of total cost and 80% of the total volume of a fuel cell; the weight and cost of a fuel cell can be reduced significantly by improving the design of these plates. The essential requirements for the electrode plates are [34]:

- High values of electronic and thermal conductivity;
- High mechanical strength;
- Impermeability to reactant gases;
- Resistance to corrosion;
- Low cost of production.

Bipolar plates are usually constructed from graphite. However, graphite is porous, fragile, and needs to be thick for the required strength, leading to an increase in weight, size and cost. As such, alternative materials have been under intense study by various researchers [40-43]. Different design topologies, i.e. straight, serpentine or spiral shapes have been used by the researchers to achieve the aforementioned functions efficiently with the aim of obtaining high performance and economic advantages. Around a 50% increase in fuel cell performance has been reported just by improving the distribution of the gas flow fields [44].

Bipolar/end plates typically have fluid flow channels stamped on their surfaces. Flow channel geometry at both the anode and cathode sides can be different from each other depending on their design requirements. The essential requirements for the bipolar plates with respect to physio-chemical characteristics are the uniform distribution of the reactant species over the active surface of the electrode to minimize the concentration overpotential. The choice of flow field configuration strongly affects the performance of a PEM fuel cell, especially in terms of water management and distribution of reactant species. Due to this, the effective design and optimization of the gas flow fields and the bipolar plates

remains a very important issue for cost reduction and performance improvement of the PEM fuel cell. The different types of flow field configurations that have been used by researchers are discussed in the following sections.

2.4.4.1   Serpentine Shaped Gas Flow Channel

The serpentine shaped gas flow channel configuration is a common option for many fuel cell designers. In this design configuration, only one flow path exists for the reactant gases across the flow field plate and any liquid water accumulating in the channel is quickly pushed out of the cell. Watkins *et al.* [45] studied the optimization of serpentine shaped flow channels. This type of flow field configuration results in high pressure losses and therefore needs a high pressure flow.
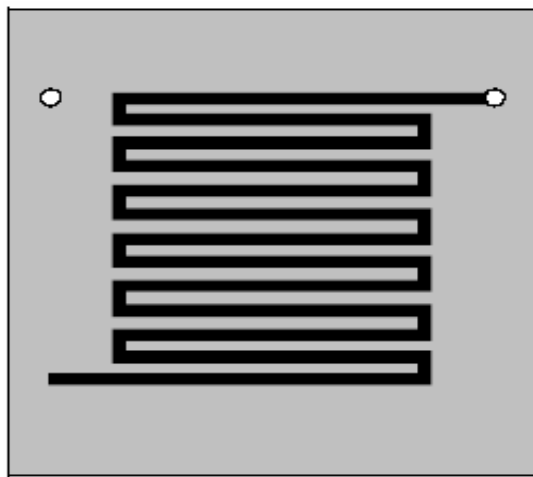
Figure 2-8: Serpentine shaped gas flow channel configuration

2.4.4.2   Parallel/Straight Shaped Gas Flow Channel

Pollegri *et al.* [46] introduced the concept of a parallel/straight type gas flow channel configuration. This type of flow field has an advantage over the serpentine shaped channels due to the lower pressure losses; on the other hand, a major drawback is that different paths exist across the bipolar plate for the reactant gases, potentially causing ineffective water removal because of the uneven flow distribution of the reactant flow through the fuel cell domain.
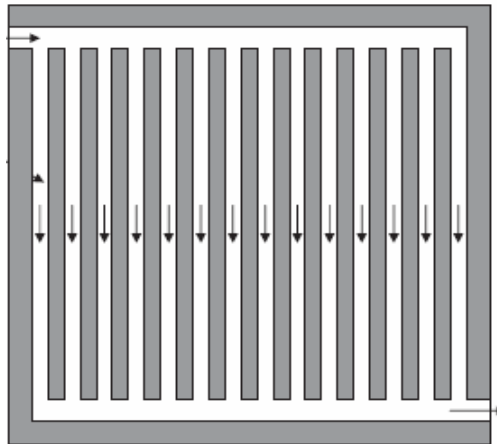
Figure 2-9: Parallel gas flow channel configuration

2.4.4.3 Discontinuous Type Gas Flow Channel

The discontinuous type gas flow channel configuration has been proposed as a solution to the problem of low diffusion rates along the gas diffusion layer in a fuel cell. Discontinuity of the gas channel passively forces the reactant species to diffuse along the gas diffusion layer and facilitates the removal of water. In this type of flow channel configuration, the transport of the reactant species in the gas diffusion layer is forced instead of relying on free convection [47].
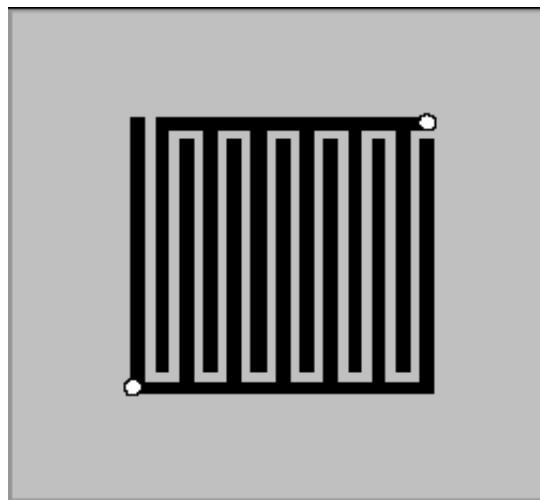
Figure 2-10: Discontinues flow field configuration

2.4.4.4 Spiral Shaped Gas Flow Channel

Kaskimies *et al.* [44] proposed a spiral shaped gas flow field configuration. This configuration combines the effective water removal of the single channel geometry with the advantage of having channels containing fresh and depleted cathode gas side by side, leading to better distributions of oxygen and water. However, the manufacturing cost of this type of flow field configuration is significantly higher.
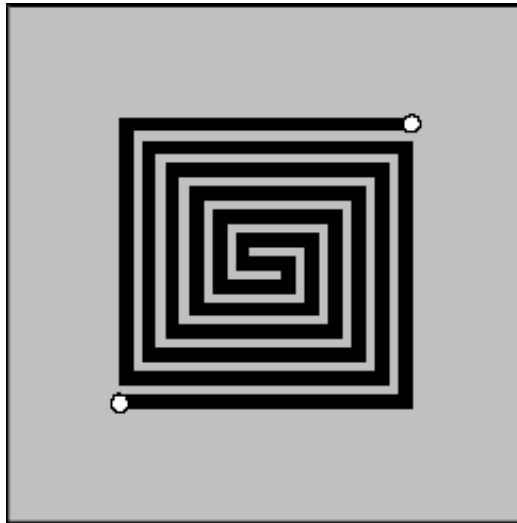
Figure 2-11: Spiral flow field configuration

2.5 Review of Numerical Modelling of PEM Fuel Cell Transport Phenomena

Fuel cells are increasingly viewed as a future power source. Researchers are actively enhancing PEM fuel cell numerical models to improve the understanding of the complex transport phenomena involved, and to use these numerical models to optimize fuel cell performance. The fundamental numerical model of a PEM fuel cell consists of governing equations for mass, momentum and energy conservation and the charge balance in order to model the flow in porous media and the electro-chemical kinetic reactions. The transport phenomena of PEM fuel cells are coupled to solve the multi-species transport model and have a significant effect on issues

related to the fuel cell performance, such as thermal and water management, and mass transport limitations [48, 49].

Numerical modelling of PEM fuel cell transport phenomena is not straight forward because of the diversity and complexity of the electrochemical processes involved. In spite of significant numerical and model developments, the underlying physics of the PEM fuel cell transport process is not fully understood [50]. Common issues with most numerical models of the PEM fuel cells involve the uncertainties associated with the specifications of boundary parameters that affect these transport processes.

Rational models based on the fundamental chemical processes and calibrated with experimental observations are commonly used as essential tools to gain an understanding of PEM fuel cell operation. Initial efforts towards the development of a numerical model for PEM fuel cells were focused on single phase, one dimensional (1D) numerical models. However, recent developments in computational technology have made it possible to simulate more accurate two phase and three dimensional computational models that account for fluid, thermal and electrical transport phenomena.

Initial numerical models of PEM fuel cells were developed in early 1990s by Springer *et al.* [51] and Bernardi *et al.* [52]. These were one dimensional, isothermal, single phase numerical models that considered only the mass, continuity and electro-chemical kinetics. These models provided a fundamental framework on which more advanced multi-dimensional numerical models of PEM fuel cells were built. As an extension of their previous work, Bernardi [6, 52] published another numerical model of a PEM fuel cell where he also focused on the calculation of activation overpotential, membrane resistance loss and Ohmic losses in the gas diffusion layer. Initial models by Springer *et al.* [52] used empirical relations for calculating the membrane conductivity based on water content in the membrane. Bernardi and Vebrunge implemented the Butler-Volmer equation to model the electro-chemistry and Schlogl's equation for the membrane transport behaviour. Broka and Ekdunge [53] made efforts to develop one dimensional agglomerated models for the catalyst layer of the PEM fuel cell.

In 1993 Nguyen *et al.* [6, 54] presented a two dimensional steady state numerical model of a PEM fuel cell that accounted for the mass transport of water across the membrane by electro-osmosis and diffusion. This model also accounted for the varying activation overpotential as a function of the local current density and oxygen partial pressure along the longitudinal channel by integrating the solution at different points along the fuel cell domain. The electro-osmotic drag coefficient of water across the membrane in this model was calculated based on empirical relations of water vapour pressure activities given by Springer *et al.* [51]. Lampimen and Fomino [55] introduced entropy changes in their two dimensional numerical model to calculate the heat transfer in a PEM fuel cell.

Newman and Fuller developed 2D numerical models of PEM fuel cells to study water effects and issues related to the thermal management. They used a concentrated solution theory for transport in the membrane [56]. Nguyen and White investigated and demonstrated the importance of water and heat management in order to maintain high performance of PEM fuel cells [57]. In 1998, Gurau *et al.* [58, 59] developed a two dimensional numerical model of a PEM fuel cell with different flow channel configurations and membrane types. This model fully accounted for the mass transport of reactant species that had been simplified in earlier models. Later, Yi and Nguyen formulated a two dimensional model of a PEM fuel cell to explore the hydrodynamics and multi-component transport on the cathode side with an inter-digitised flow field configuration [60].

Dutta *et al.* [61] described a three dimensional numerical model of a PEM fuel cell that included solutions of the governing equations of fluid flow (the Navier Stokes equations) for straight flow channels and discussed how the mass consumed in the electro-chemical reactions affected the momentum transport equation. Later, Baghdadi *et al.* [62, 63] presented a 3D numerical model for a PEM fuel cell in which they quantified the effects of operating, design and material parameters on fuel cell performance. Later Braden *et al.* [64] employed a novel method to reduce the computational effort required to simulate a pseudo three dimensional solution by implementing a hybrid numerical model. In this model, the membrane and anode were not considered, and the catalyst layer was modelled as a boundary condition

with the flux determined from a first order reaction expression. Um and Wang extended this work and studied the effect of varying flow channel geometries and overall layouts [65-67].

Earlier numerical models of PEM fuel cells by different researchers did not include descriptions of the two phase flow that actually takes place in the PEM fuel cell domain. In two phase models, the liquid and gas phases travel at different velocities, at the same time, the interfacial tension effects and GDL wetting abilities can be modelled, the later phenomena are essential to the operation of a PEM fuel cell. Advances in the numerical modelling of PEM fuel cells have spurred significant progress in two phase modelling of transport phenomena. Yu and Liu [68] and Natarajan and Ngyuen [69] presented two phase models of the PEM fuel cell in which they neglected the anode side of the PEM fuel cell and analysed the performance by modelling the cathode side only. Later, Djillali *et al.* [70] and Hu *et al.* [71, 72] developed full scale, three dimensional models of PEM fuel cells, taking into account two phase flow effects.

The internal temperature distribution has a significant effect on the amount of water that undergoes phase change and consequently on the overall performance of the PEM fuel cell. For this reason, the assumption of isothermal conditions can lead to results that are not physically representative when phase changes are accounted for. In PEM fuel cells, heat is generated by the entropic heat of reaction, the irreversibility of the electro-chemical reaction and the Ohmic resistances. The irreversible reaction, entropic and joule heating account for approximately 55%, 35% and 10% of the total heat released respectively [49]. Membrane hydration is also strongly effected by the temperature distribution along the fuel cell domain. Initial efforts to numerically model this heat transfer phenomena in PEM fuel cells was carried out by Nguyen *et al.* [73] and Newman *et al.* [74]. Nguyen developed a two dimensional model of the PEM fuel cell with heat transfer in the flow direction, while Newman developed pseudo-two dimensional models with heat transfer effects. These initial models did not include temperature variations in the membrane. Djilali and Lu [75] developed a three dimensional model of the PEM fuel cell including heat transfer. Later, Berning *et al.* [48] presented a three

dimensional model of a PEM fuel cell which included the irreversible and entropic heat source terms in the catalyst layer and joule heating in the membrane.

Three primary processes (electrochemical double-layer discharging, gas transport through the channel and hydration of the GDL and membrane) govern the time response of a PEM fuel cell. The time dependant constant for the double-layer discharging is fairly small (in the range of milliseconds) and thus can be ignored. The time dependant constant for the gas transport through the channel and hydration of the GDL ranges from 0.1 to 1s [49]. Finally, membrane hydration is the slowest process in PEM fuel cell operation and its time constant is around 25 seconds. Um *et al.* [67] was the first researcher to study the transient behaviour of PEM fuel cells and developed a 2D transient model to study the transport phenomena in the fuel cell domain at different time intervals; however, they did not include the membrane hydration process in their model. Their work was extended by Wang *et al.* [49] to include the effects of transient membrane hydration processes.

Despite of the extensive work done by different researchers, the numerical modelling of PEM fuel cells is still under intense development. Different computational tools are used for this purpose that allow systematic simulation and design optimization of fuel cell systems, and facilitate the integration of advances which can reduce the reliance on hardware prototyping, hence, reducing the development cycle time [3]. These '*computational fuel cell engineering tools*' (CFCE) require the robust integration of numerical models that represent a variety of complex multi-physics transport processes such as fluidic, ionic, electronic and thermal transport in concert with the electro-chemical reactions. Coupling of such models with modern CFD and multi-disciplinary optimization methods allows the creation of powerful CFCE tools.

The following sub-sections provide a comprehensive overview of the numerical models developed by different researchers for the analysis of coupled transport phenomena in each section of the polymer electrolyte membrane (PEM) fuel cell.

2.5.1 Gas Flow Channel

Flow characteristics in the PEM fuel cell gas flow channels are strongly influenced by the geometric configuration. Different gas flow channel design configurations, such as straight, parallel, U shaped, spiral and serpentine shaped have been studied by the researchers to explore their effects on the distribution of reactant/product species and the overall performance of the PEM fuel cells. Ming [76] investigated the effect of different flow channel design configurations on the performance of a PEM fuel cell. Hadi *et al.* [77] studied the effect of varying gas flow channel dimensions (channel width and shoulder size) on the performance of the PEM fuel cell finding that increasing the gas channel width improves the limiting current density. Li and Sabir extensively reviewed different configurations of PEM fuel cell gas channels and their effects on fuel cell performance [39].

Due to the small amounts of reactant gases entering the fuel cell, the velocity of flow is fairly low, hence laminar flow is assumed for the numerical modelling of the reactant fluids in PEM fuel cell gas flow channels. Different types of transport phenomena take place in the PEM fuel cell gas flow channels and the conservation equations for momentum, mass and energy can be applied to the fluid flow. These transport phenomena have been numerically modelled by various researchers using the following forms of the governing equations [6, 62, 78]:

Continuity Equation (Conservation of Mass)

$$\frac{\partial(\rho u)}{\partial x} + \frac{\partial(\rho v)}{\partial y} + \frac{\partial(\rho w)}{\partial z} = 0 \qquad\qquad (2\text{-}1)$$

Navier Stokes Equations (Conservation of Momentum)

$$\frac{\partial(\rho u u)}{\partial x}+\frac{\partial(\rho u v)}{\partial y}+\frac{\partial(\rho u w)}{\partial z}=-\frac{\partial P}{\partial x}+\frac{\partial}{\partial x}\left(\mu\frac{\partial u}{\partial x}\right)+\frac{\partial}{\partial y}\left(\mu\frac{\partial u}{\partial y}\right)+\frac{\partial}{\partial z}\left(\mu\frac{\partial u}{\partial z}\right)$$

$$\frac{\partial(\rho v u)}{\partial x}+\frac{\partial(\rho v v)}{\partial y}+\frac{\partial(\rho v w)}{\partial z}=-\frac{\partial P}{\partial y}+\frac{\partial}{\partial x}\left(\mu\frac{\partial v}{\partial x}\right)+\frac{\partial}{\partial y}\left(\mu\frac{\partial v}{\partial y}\right)+\frac{\partial}{\partial z}\left(\mu\frac{\partial v}{\partial z}\right) \qquad (2\text{-}2)$$

$$\frac{\partial(\rho w u)}{\partial x}+\frac{\partial(\rho w v)}{\partial y}+\frac{\partial(\rho w w)}{\partial z}=-\frac{\partial P}{\partial z}+\frac{\partial}{\partial x}\left(\mu\frac{\partial w}{\partial x}\right)+\frac{\partial}{\partial y}\left(\mu\frac{\partial w}{\partial y}\right)+\frac{\partial}{\partial z}\left(\mu\frac{\partial w}{\partial z}\right)$$

Where ρ is the reactant flow mixture density and u, v, w, are the flow velocities in the $x, y,$ and z directions respectively. Density ρ of the mixture can be calculated using the following formula:

$$\rho=\frac{\sum x_i.MW_i}{RT}p \qquad (2\text{-}3)$$

Mass transport of the reactant species in the PEM fuel cell gas channel can be described by the divergence of mass flux through diffusion and convection using the following form of the steady state species transport equation:

$$\nabla\left[-\rho w_i\sum_{j=1}^{N}D_{ij}\left\{\frac{\nabla M}{M_j}\left(\nabla w_j+w_j\frac{\nabla M}{M}\right)+\left(x_j-w_j\right)\frac{\nabla p}{p}\right\}+w_j\rho u\right]=0 \qquad (2\text{-}4)$$

Here, i represent the oxygen at the cathode and hydrogen at the anode sides, while j is the water vapour on both sides of the PEM fuel cell. D_{ij} is the binary-diffusion coefficient of the reactant species and can be calculated using Maxwell-Stefan diffusivity relation, which is a good approximation for multi-component diffusion in gases at low density [79].

$$D_{ij}=\frac{T^{1.75}(1/M_i+1/M_j)^{1/2}}{\rho((\sum_k V_{ki})^{1/3}+(\sum_k V_{kj})^{1/3})^2} \qquad (2\text{-}5)$$

V_{ij} is the atomic diffusion volume of reactant species and its quantity can be obtained from work done by Cussler [80]. The molar fraction of each species in the PEM fuel cell gas channel is calculated using the following relation [81]:

27

$$x_i = \frac{w_i / M_i}{\sum_{j=1}^{n} w_j / M_j}$$

(2-6)

Where w_i is the mass fraction of species i, while M_i is the molecular weight of species i.

Temperature variation along the PEM fuel cell gas channel plays an important role in the behaviour of flow. Therefore, so as to increase the accuracy of a numerical analysis, variations in temperature must be taken into consideration. Due to the chemical reactions along the cathode membrane/catalyst layer interface, heat is generated and transported to the gas channel. A form of the energy equation based on the first law of thermodynamics is typically used to calculate the energy transfer in the gas flow channel in a PEM fuel cell. The following expression represents the energy conservation in the gas flow channel by conduction, species diffusion and viscous dissipation [78, 82]:

$$\nabla.(v(\rho E + p)) = \nabla\left(k_{eff} \nabla T - \sum_j h_j D_f + (\tau_{eff}.v) \right) + S_h$$

(2-7)

E is the total energy, k_{eff} is the effective thermal conductivity of the bipolar plate material, D_f is the diffusion flux of reactant species, h is the enthalpy, τ is the stress tensor and S_h is the source term per unit volume per unit time.

2.5.2 Gas Diffusion Layer (GDL)

The gas diffusion layer (GDL) of a PEM fuel cell consists of an anisotropic fibrous structure either in the form of paper or woven cloth that allows the distribution of the reactant gases through the porous structure and the collection of current through the fibres [3, 78]. Different researchers have investigated the numerical modelling of transport phenomena taking place inside the GDL of a PEM fuel cell.

William *et al.* [83] investigated the effect of cross-flow on fuel cell performance using a GDL with distinctively different gas permeability. Dohle *et al.* [84] examined flow homogeneity in the GDL using flow visualization to find the optimal permeability value. Benziger *et al.* [85] investigated the water flow in the GDL and their effects on fuel cell performance, while Inoue *et al.* [86] optimized the thickness of the GDL using the numerical modelling techniques. Lee *et al.* [87] and Jordan *et al.* [88] used these models to optimize the performance of fuel cells using different parameters such as GDL porosity, permeability and thickness. It was found that a thin GDL with a small porosity resulted in a good electrical conductivity; however, efficient mass transport required larger porous holes. Hontanon [12] investigated the effect of permeability of the gas diffusion layer on the consumption of reactant gases in the electrodes. Rismanchi *et al.* [89] presented a three dimensional model of a PEM fuel cell where they studied possible dead zones that can exist between the gas channel shoulder and the GDL, where the performance of the catalyst layer surface decreases to a minimum.

The governing equations that describe species transport in the gas diffusion layers are similar to those used for the gas flow channels, but with the addition of porosity effects. Numerical models of the porous media in PEM fuel cells consist of an extra momentum sink term that takes into account the loss terms for viscosity and inertia, which are added to the standard fluid flow equation. Inertial terms can typically be neglected because of the low velocity of the reactant species [62]. The following form of the steady state fluid flow equation can be used to numerically model the fluid flow in the porous gas diffusion layer of the PEM fuel cell [78]:

$$\frac{\partial(\varepsilon\rho uu)}{\partial x}+\frac{\partial(\varepsilon\rho uv)}{\partial y}+\frac{\partial(\varepsilon\rho uw)}{\partial z}=-\frac{\varepsilon\partial P}{\partial x}+\frac{\mu}{k_p}[\frac{\partial}{\partial x}\left(\mu\frac{\partial u}{\partial x}\right)+\frac{\partial}{\partial y}\left(\mu\frac{\partial u}{\partial y}\right)+\frac{\partial}{\partial z}\left(\mu\frac{\partial u}{\partial z}\right)]$$

$$\frac{\partial(\varepsilon\rho vu)}{\partial x}+\frac{\partial(\varepsilon\rho vv)}{\partial y}+\frac{\partial(\varepsilon\rho vw)}{\partial z}=-\frac{\varepsilon\partial P}{\partial y}+\frac{\mu}{k_p}[\frac{\partial}{\partial x}\left(\mu\frac{\partial v}{\partial x}\right)+\frac{\partial}{\partial y}\left(\mu\frac{\partial v}{\partial y}\right)+\frac{\partial}{\partial z}\left(\mu\frac{\partial v}{\partial z}\right)] \qquad (2\text{-}8)$$

$$\frac{\partial(\varepsilon\rho wu)}{\partial x}+\frac{\partial(\varepsilon\rho wv)}{\partial y}+\frac{\partial(\varepsilon\rho ww)}{\partial z}=-\frac{\varepsilon\partial P}{\partial z}+\frac{\mu}{k_p}[\frac{\partial}{\partial x}\left(\mu\frac{\partial w}{\partial x}\right)+\frac{\partial}{\partial y}\left(\mu\frac{\partial w}{\partial y}\right)+\frac{\partial}{\partial z}\left(\mu\frac{\partial w}{\partial z}\right)]$$

Where ε and k_p are the porosity and permeability of the GDL respectively. Darcy's law is used to model flow behaviour in a porous medium with a pressure gradient as the driving force. This law is based on the homogenization of porous and fluid media into a single medium and does not require a detailed geometrical description of the pore structure [65]. The velocity vector in the porous media using Darcy's law can be described as,

$$u = \frac{k_p}{\mu}\nabla p \qquad (2\text{-}9)$$

Similarly, for the species mass transport in porous media, the steady state species transport equation takes the following form, where D_{ij} can be calculated using the Maxwell Stefan relation [62, 78]:

$$\nabla\left[-\rho w_i \sum_{j=1}^{N} D_{ij}\left\{\frac{\nabla M}{M_j}\left(\nabla w_j + w_j \frac{\nabla M}{M}\right) + \left(x_j - w_j\right)\frac{\nabla p}{p}\right\} + w_j \rho u\right] = 0 \qquad (2\text{-}10)$$

$$D_{ij} = \frac{T^{1.75}(1/M_i + 1/M_j)^{1/2}}{\rho\left(\left(\sum_k V_{ki}\right)^{1/3} + \left(\sum_k V_{kj}\right)^{1/3}\right)^2} \qquad (2\text{-}11)$$

In order to account for the geometric construction of holes of the porous media, the diffusivities of reactant species can be corrected using the following form of the Bruggemann correction relation [52, 90].

$$D_{ij}^{eff} = D_{ij} \times \varepsilon^{1.5} \qquad (2\text{-}12)$$

D^{eff} is the effective binary diffusion coefficient of the reactant species that takes into account any additional drag by irregular shapes and the actual length of the pores in comparison to the bundle of straight parallel capillaries with a constant diameter [91]. The Maxwell-Stefan equation and Darcy's law are coupled through the velocity vector (u), and density (ρ) [65]. Energy transport in the porous media of

30

PEM fuel cells can be calculated using effective thermal conductivity that is the average conductivity of a fluid and solid assuming the thermodynamic equilibrium [78, 92]:

$$k_{s,eff} = (1 - \varepsilon) k_s \qquad \text{(2-13)}$$

K_s is the thermal conductivity of the solid media. The overall heat transfer in the gas diffusion layer of the PEM fuel cell can be calculated using the following relation [90];

$$\nabla.(\rho \varepsilon u h) - \nabla.(k_{s,eff} \varepsilon \nabla T) = \varepsilon S_q \qquad \text{(2-14)}$$

Here, S_q is the source term for heat exchange to and from the solid matrix of the porous media.

2.5.2.1 Effect of GDL Pore Design on Water Flooding

Water management is one of the most critical and widely studied issues in proton electrolyte membrane fuel cells. Excessive water flooding leads to fuel starvation and performance losses [93], while on the other hand, the polymer electrolyte membrane must be fully hydrated to ensure good proton conductivity [75]. Therefore, water management in the fuel cell is referred to as: *balancing membrane hydration while avoiding flooding* [49].

At the cathode side of the PEM fuel cell, water is generated by the electrochemical reactions along the membrane/catalyst layer interface. Water exists in both vapour and liquid form along the fuel cell domain and significantly hinders reactant flow access to the catalyst layer as water droplets block the pores of the GDL [94, 95]. Such clogging of porous holes in the GDL by water droplets can retard the electrochemical reaction along the cathode catalyst layer and consequently affect the overall performance of the fuel cell [96].

31

The gas diffusion layer of a PEM fuel cell is commonly treated with PTFE (*Teflon*®) to make the GDL hydrophobic and force water droplets to agglomerate at the free surface of the GDL. Hydrophobic *Nafion*-type electrolytic membranes adjacent to the catalyst layer absorb and retain liquid water. Water produced by the electrochemical reaction diffuses through the GDL to the gas channels of the fuel cell, where it is then evaporated by the excess air [97].

One major issue in the numerical modelling of this phenomenon is the necessity to rely on empirical correlations and experimental observations obtained from soil and sand sample-media with a structure that differs significantly from fibrous or woven GDLs. Djilali *et al.* [93] investigated dynamic liquid water transport through the GDL into the gas channel flow, with an ex-situ experimental setup. Kui and Biao [98] numerically investigated the water flooding problem by using three innovative GDLs. Wang [99] made a comprehensive overview of water management in a fuel cell. Coppa *et al.* [1] developed a three dimensional numerical model to describe liquid water removal from the GDL surface by advection due to the interaction of water droplets and the gas stream in the gas flow channel. This model was validated for a wide range of temperatures in order to study the effect of temperature-dependant parameter variations on fuel cell performance, and concluded that both liquid water transport within the GDL and liquid water removal from the surface of the GDL play a critical role in determining the variations in fuel cell performance.

To simplify the mathematical modelling of this process, a single phase (gas) model is used by most researchers. In the PEM fuel cell electrode, the capillary number (ratio of viscous and interfacial tension forces) is small and liquid transport is dominated by the capillary diffusion. Thus, the momentum equation for a single phase model is of the form [65]:

$$u = \frac{k_p}{\mu} \nabla p$$

(2-15)

32

Extending this single phase momentum equation for a two phase system yields the following:

$$u_g = -\frac{k_g}{\mu_g}\nabla p_g$$

$$u_l = -\frac{k_l}{\mu_l}\nabla p_l$$

(2-16)

In recent years, many two phase models of PEM fuel cells have been published by the researchers that accurately predict the amount of water flooding inside the fuel cell and the effect of liquid water on the performance of the fuel cell [100-102]. Most of these two phase models have not considered interface tracking between liquid water and gas. Jiao [98] investigated the effect of water management by considering three different micro structures (circular, cubic and trapezoidal) of the GDL by assuming serpentine shaped gas flow channel configuration. Analysis showed that a trapezoidal micro structure had a better water removal ability as it enhanced the airflow inside the catalyst layer and had a minimum area facing the gas channel. Results showed that in the case of U-shaped or serpentine shaped gas flow channels where a secondary flow exists at the corners, there was more chance of water flooding in those areas, but with an improved design of the GDL structure; better water draining was possible. The literature shows that keeping the maximum area of the porous holes facing the catalyst layer results in better water drainage [98].
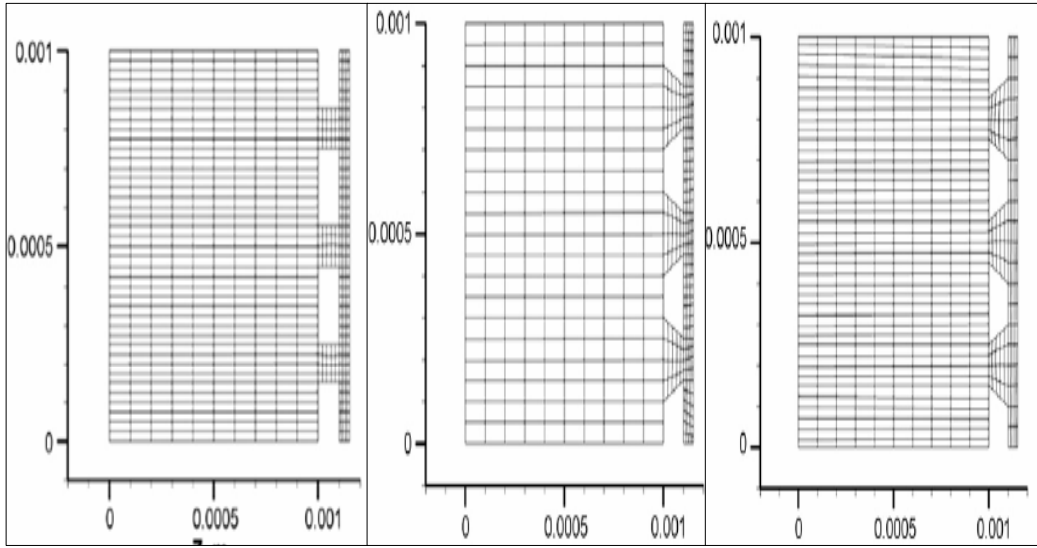
Figure 2-12: Shapes of GDL pores; a) cubes, b) holes, c) trapezoids [98]

2.5.3 The Catalyst Layer

A catalyst layer is treated as a thin porous interface between the GDL and the membrane where sink and source terms of the species are implemented. Due to the very small thickness of the catalyst layer, the source terms are actually implemented in the last grid cell of the porous media of the GDL for numerical modelling purposes[49]. Most researchers have assumed the catalyst layer as a thin boundary between the GDL and the membrane for the ease of numerical modelling.

Local volumetric sources and sink terms associated with the electrochemical reactions along the cathode catalyst layer are proportional to the local current density and can be described as: [62, 78]

$$
\begin{aligned}
S_{H2}(kg/sm^3) &= -\frac{M_{H2}}{2F}i_a \\
S_{O2}(kg/sm^3) &= -\frac{M_{O2}}{4F}i_c \\
S_{H2O}(kg/sm^3) &= \frac{M_{H2O}}{2F}i_c
\end{aligned}
\tag{2-17}
$$

The above mentioned source terms need to be included in the species mass transport equations for numerical modelling of the fuel cell current density calculation. The Butler-Volmer equation has been used by researchers for the calculation of current density along both anode and cathode catalyst layers [52, 53, 62]

$$i_c = i_{oc}^{ref} \left(\frac{C_{o2}}{C_{o2}^{ref}} \right) \left[\exp\left(\frac{\alpha_c F}{RT} \eta_{act,c} \right) - \exp\left(-\frac{\alpha_c F}{RT} \eta_{act,c} \right) \right]$$

$$i_a = i_{oa}^{ref} \left(\frac{C_{H2}}{C_{H2}^{ref}} \right)^{\frac{1}{2}} \left[\exp\left(\frac{\alpha_a F}{RT} \eta_{act,a} \right) - \exp\left(-\frac{\alpha_a F}{RT} \eta_{act,a} \right) \right]$$

(2-18)

Where ' i_o ' is the exchange current density, ' η ' is the local activation over-potential, ' R ' is the universal gas constant and ' α ' is the asymmetry parameter that is determined empirically to be between 0 and 1 [103]. The exchange current density depends on the cell temperature that can be described using the relation of Parthasarathy *et al.* [74]:

$$i_o = i_o (T_{ref}) \exp\left[\frac{\Delta E}{R} \left(\frac{1}{T_{ref}} - \frac{1}{T} \right) \right]$$

(2-19)

Where ' E ' is the activation energy ($E= 73.2$ $kjmol^{-1}$) and ' T_{ref} ' is the reference temperature. Activation overpotential needs to be taken into account when the electro-chemical reactions are not sufficiently fast to maintain equilibrium in the system. In most numerical models of PEM fuel cells, the local activation over-potentials at the cathode and the anode are calculated by [78]:

$$\eta_{act,cathode} = \phi_s - \phi_m - V_{oc}$$

$$\eta_{act,anode} = \phi_s - \phi_m$$

(2-20)

V_{oc} is the thermodynamic open circuit voltage and can be calculated using the following form of Nernst equation [104]:

$$V_{oc} = 1.229 - 0.9 \times 10^{-3}(T - 298.15) + 2.3\frac{RT}{4F}\log(p_{H2}^2 p_{O2}) \qquad \text{(2-21)}$$

This expression gives the thermodynamic potential for the hydrogen/oxygen fuel cell in terms of temperature and pressure of the reactant gases. For simplicity, this expression can be reduced to:

(2-22)

$$V_{OC} = 0.2329 + 0.0025T$$

Useful work from the fuel cell is obtained only when a current is drawn. Current is drawn due to the potential difference between the anode and cathode electrodes. Actual cell potential decreases from its equilibrium thermodynamic potential because of irreversibility. Such irreversibility occurs due to the activation, Ohmic and concentration potential losses. The following relation provides the value of actual operating cell potential:

$$E_{cell} = V_{oc} - \eta_{act,cathode} - \eta_{ohmic} - \eta_{membrane} - \eta_{concentration} \qquad \text{(2-23)}$$

The fuel cell potential E_{cell} drops below the reversible V_{oc} when the current starts flowing through the fuel cell. This potential drop is due to the several types of over-potentials including activation, Ohmic and concentration over-potentials described in equation 2-23. In addition to these typical electrochemical over-potentials, PEM fuel cells also suffer from other losses, such as internal currents and fuel crossover [6]. A brief description of these potential losses is given as follows:

1) Ohmic overpotential occurs due to the resistance to electron transport through the electrodes and proton transport through the electrolyte membrane. The magnitude of this potential loss depends upon the material properties of the electrodes and the membrane and operating conditions [6].

2) Activation overpotential occurs due to driving the electrochemical reaction from the equilibrium state. It depends upon the material properties of the electrodes, ion-ion interaction, ion-solvent interactions and characteristics of the electric double-layer at the electrode-electrolyte interface [6].

3) Concentration overpotential is due to the mass transport loss of reactant gases at the cathode and the anode when the fuel cell is operated at high current density. This loss is most significant at the cathode side in comparison to the anode side [6].

4) Crossover-potential is due to fuel cross-over from the anode to the cathode through the membrane without being oxidized at the anode catalyst layer. This loss has a low value and generally can be ignored.

Figure 2-13: Ideal and actual cell voltage/current characteristics of PEM fuel cells [105]

Figure 2.13 (the polarisation curve) shows the variation of operating fuel cell voltage with respect to the fuel cell current density. This figure shows that the open circuit voltage is less than the theoretical thermodynamic cell voltage (1.23 Volts), indicating that there is a loss in the fuel cell voltage even when no current is

drawn. This loss can be attributed to *'fuel cross over and internal currents through the electrolyte'*. The electrolyte membrane should only transport ions, but a small amount of the fuel and an even lesser amount of electrons will be conducted through the electrolyte membrane, which will have a reducing effect on the open circuit voltage.

As the current moves away from the zero current, a rapid initial drop in the cell voltage is observed. This drop is due to the slow rate of the electro-chemical reaction and is known as: *the activation overpotential*. Moving to the higher current densities, the voltage loss become more linear and falls very slowly. Such loss in the fuel cell potential is caused by resistance to the flow of electrons offered by the cell electrode. Such loss is known as the *'Ohmic overpotential'*. The final region of the above mentioned polarisation curve at higher current densities shows the potential drop due to mass transport limitations of the fuel cell. Such losses are known as '*concentration overpotential*'.

Heat generation in the PEM fuel cell is generally due to the entropy changes as well as irreversibility due to the activation overpotential. Both charged and uncharged species must be considered to calculate the heat generation in the fuel cell, which is caused by electrochemical reactions at the membrane/catalyst layer interface at the cathode side. Lampinen *et al.* [55] presented a numerical model for the calculation of heat generation due to the electrochemical reactions at the cathode catalyst layer of PEM fuel cells:

$$q^o = \left[\frac{T(-\Delta S)}{n_e F} + \eta_{act,c} \right] i_c \qquad (2\text{-}24)$$

Where T is the local temperature, ΔS is the entropy of the electrochemical reaction and n_e is the number of electrons transferred per mole of hydrogen. Djilali *et al.* [78] assumed the entropy changes at a standard state with platinum catalyst as $\Delta S = 0.104\ Jmol^{-1}K^{-1}$ for the anode and $\Delta S = -326.36\ Jmol^{-1}K^{-1}$ for the cathode [106, 107]. Heat generated by the chemical reaction at the catalyst layer is then

transferred to the GDL and to the gas channels, which can then be calculated using the following relation:

$$\nabla.\left(\rho \varepsilon C_p u T - k_{s,eff} \varepsilon \nabla T \right) = \varepsilon \beta \left(T_{solid} - T \right)$$

(2-25)

β is the heat transfer coefficient that accounts for the convective heat transfer, while C_p is the specific heat capacity of the fluid.

Figure 2-14: Transport of reactant and product species along a PEM fuel cell cathode[3]

2.5.4 Polymer Electrolyte Membranes (PEM)

The polymer electrolyte membrane provides a key function by conducting protons from the anode to the cathode, preventing any reactant cross over. It acts primarily as a gas barrier between the anode and cathode reactants. A polymer electrolyte membrane consists of a micro-phase separated structure that comprises hydrophobic polymer chains and hydrophilic-Sulphonic acid groups [3]. The most widely used numerical model to date for determining membrane conductivity in large scale fuel cell models was published by Springer *et al.* [51]. This model relies on empirical correlations obtained for *Nafion*-type electrolyte membranes only. In practice, this model does not perform well under low humidity conditions.

Theoretically, an electrolyte membrane in contact with either saturated vapour or liquid water should have the same water content. However, experimental studies reported different water absorption from liquid water in comparison to saturated water vapour [65]. This phenomena was first reported by Schroeder in 1903 and thus is called Schroeder's paradox [49]. The Ionic conductivity of the electrolyte membrane depends upon its water content. For a fully humidified membrane, values of membrane water content vary from 14 to 17 [108]. The water content λ in a membrane depends upon the water activity a, diffusion coefficient and electro-osmotic drag coefficient [31, 109]. A linear relation is assumed between the membrane water content and water activity in numerical modelling.

$$a = \frac{X_{H2O}P}{P_{sat}}$$
$$\lambda = A_1 + A_2 a - A_3 a^2 + A_4 a^3 \qquad \text{for } 0 < a \leq 1$$
$$= 14 + 1.4(a-1) \qquad \text{for } 1 \leq a \leq 3 \qquad (2\text{-}26)$$
$$A_1 = 0.043,\ A_2 = 17.18,\ A_3 = 39.85,\ A_4 = 36$$

$$\log_{10} P_{sat} = -2.1794 + 0.02953(T - 273.15) - 9.1837 \times 10^{-5}(T - 273.15)^2$$
$$n_d = B_1 \lambda + B_2 \lambda - B_3$$
$$\alpha = \frac{n_d I_k}{F} - D_w \nabla C_w \qquad (2\text{-}27)$$
$$B_1 = 0.0028,\ B_2 = 0.05,\ B_3 = 3.5 \times 10^{-19}$$

The above relations show that the molar flux of water in the membrane is a function of membrane water diffusivity D_w and water concentration C_w. These two parameters can be calculated using the following relations [110, 111]:

$$C_w = \frac{\rho_{mem,dry}}{M_{mem,dry}} \lambda$$

$$D_w = D_\lambda \exp\left[2416\left(\frac{1}{303} - \frac{1}{T}\right)\right]$$

where

$$
\begin{aligned}
D_\lambda &= 10^{-10} & \lambda < 2 \\
D_\lambda &= 10^{-10}(1 + 2(\lambda - 2)) & 2 \le \lambda \le 3 \\
D_\lambda &= 10^{-10}(3 - 1.67(\lambda - 3)) & 3 \le \lambda \le 4.5 \\
D_\lambda &= 1.25 \times 10^{-10} & \lambda > 4.5
\end{aligned}
$$

(2-28)

A potential difference exists between the anode and cathode sides of the membrane that can be computed using the following relation [52]:

$$-\nabla \cdot (\sigma_m \nabla \phi_m) = 0$$

(2-29)

φ_m is the membrane potential and σ_m is the membrane conductivity, which is a function of membrane water content λ. Membrane conductivity σ_m is a function of the local temperature that can be correlated as [65, 112]:

$$\sigma_m = \exp\left[1268\left(\frac{1}{303} - \frac{1}{T}\right)\right]\sigma_{30}$$

$$\sigma_{30} = 0.5139\lambda - 0.326$$

(2-30)

The above relation clearly indicates the strong dependence of the membrane ionic conductivity on water content. Several studies have been carried out to analyse the relation between membrane ionic conductivity and the water content [113-115]. Mass flux of water in an electrolyte membrane is governed by the electro-osmotic drag due to the flow of protons, diffusion due to the concentration gradient and convection due to the pressure gradient [78]. Numerically, these three processes can be described as [111]:

$$N_w = \frac{t_w.I.M_{H2O}}{F} - D_w \nabla c_w - c_w u_w$$

The balance between electro-osmotic drag of water from anode to cathode and back diffusion from cathode to anode yields the net water flux through the membrane. Variation of the water content and water activity 'a' affect the overall performance of the membrane. The permeability of the membrane for all species except water is assumed to be of the order of 10^{-30}, which is very low, and can be assumed to be zero [114]. The consumption of reactants and the formation of products due to electrochemical reactions at the cathode catalyst/membrane interface are obtained by coupling the flux of reactant species to the local current density. The current flux at the cathode boundary between the electrode and the membrane can be given by the following expressions [65];

$$n.(-\sigma_s \nabla \phi_s) = i_c$$
$$n.(-\sigma_m \nabla \phi_m) = -i_c$$

(2-32)

2.6   Material Characterization of a PEM Fuel Cell

Accurate characterization of PEM fuel cell materials used in numerical modelling cannot be over-emphasized because numerical predictions of a fuel cell model can only be as accurate as the initial material properties supplied to the model. The material properties of a PEM fuel cell can be organized as follows [49];

1) Electro-kinetic data for the catalyst layer;
2) Gas diffusion layer properties;
3) Bipolar plates properties.

Electro-kinetic data of the catalyst layer affects the rate of oxidation and reduction along the membrane/catalyst layer interface. This affects the rate of the electrochemical reaction. Platinum is mostly used as the catalyst layer although, due to its high cost, it is used sparingly.

The bipolar plate is one of the major components of a fuel cell both in terms of cost and weight, as it constitutes around 30% of the total cost and 60% of the total weight of a PEM fuel cell. Its material properties play an important role in terms of cost reduction and better performance of PEM fuel cells. It is the only part of a PEM fuel cell whose material can be chosen by the user or manufacturer, as material selection for other parts of the fuel cell are very limited. The major requirements for the bipolar/end plate material are: good electric and thermal conductivity, gas tightness, sufficient mechanical strength and chemical stability in both oxidizing and reducing conditions.

Several materials have been identified by the researchers that can be used for bipolar plates. The following are some common materials that are typically used in the manufacture of PEM fuel cell bipolar/end plates [116]:

Metals / Alloys	Stainless steel 316/L, nickel-chromium alloy, aluminium alloy
Coatings	Gold, nickel, tin, carbon
Composite Materials	*Cu* alloy with carbon fibres, graphite/carbon composites

Table 2.1: PEM fuel cell bipolar/endplate materials

Dense solid graphite is used as the typical material for PEM fuel cell bipolar plates. Graphite is porous, fragile and prone to damage during manufacturing and handling. Therefore, bipolar plates constructed from graphite are treated at high temperatures so as to make them denser, but this leads to porosity issues in these plates. These porosity effects can be minimized using special resins. However, the treatment with resins leads to higher manufacturing costs and forces designers to select graphite plates of greater thicknesses so that they can withstand the machining stresses and tightening torque in the fuel cell. Moreover, the flow channels on graphite bipolar plates are usually made by machining with different configurations that can increase the machining cost, depending upon the complexity of the topological design of the flow channel.

Use of metal as a bipolar plate material has several advantages over the commonly used graphite plates, such as reductions in cost, weight and manufacturing time. Steel alloys such as stainless steel can be a good alternative to standard graphite for bipolar plate material due to its low cost, high strength, ease of manufacture and improved power/volume ratio [117]. Bipolar plates constructed from stainless steel are mechanically durable and very thin in size when compared to typical graphite plates. Moreover, stainless steel is less expensive when compared to graphite, and is readily available in the market. The most commonly used stainless steel alloy for PEM fuel cells is SS316.

The main drawbacks of using stainless steel as a bipolar plate material include high contact resistance due to an oxide layer on the surface of the metal that can lead to possible corrosion in the long term. The effect of this oxide layer can be minimized by applying special coatings such as tin, chromium or nickel on the stainless steel bipolar plates [118]. Davies *et al.* [119] successfully tested the endurance of stainless steel bipolar plates for 3000 hours. Similarly, detailed performance analyses were carried out at the University of Alabama, using stainless steel SS316L as a fuel cell bipolar plate material, and the fuel cell stack was operated for over 1000 hours without any appreciable drop in the cell voltage [116].

2.7 Summary

This chapter reviewed the existing literature on PEM type fuel cells, mainly focusing upon the important components and mathematical models of the different transport phenomena taking place inside its domain. Numerical modelling of the PEM fuel cell is a complex process as it involves the coupling of flow in porous media, charge balance and electro-kinematics. In this chapter, mathematical models of these transport phenomena for each section of the PEM fuel cell have been discussed separately to provide a good understanding of the coupling of these transport phenomena. Different materials for bipolar/end plates were also discussed in this chapter. It was described that stainless steel is used as a material for the gas distributor and bipolar plates due to lower required thickness, good mechanical strength and cost effectiveness.

CHAPTER 3

3 Numerical Modelling Configuration

3.1 Introduction

This chapter describes the numerical modelling used for the analysis of a PEM fuel cell in this research work. To solve for multi-species transport, a numerical model of the PEM fuel cell coupled with the flows in porous media, charge balance, electrochemical kinetics and membrane water content, a finite element numerical modelling technique is used. It can also account for the distributed overpotential at the catalyst layer, as well as the convective and diffusive transport of reactant and product species in the PEM fuel cell domain. Results obtained from this numerical study have been compared with experimental data to validate the accuracy of the numerical model.

For experimental analysis of the PEM fuel cell with a perforated-type gas flow distributor, an experimental test facility (rig) was designed and assembled locally at the *Energy and Environmental Technology Applied Research Group (EETRG), Coventry University*. For the experimental study, a PEM fuel cell was constructed with an effective area of 25 cm^2, having the stainless steel perforated gas flow distributor and electrodes [120]. To validate the numerical model of the PEM fuel cell with the pulsating flow, performance trends obtained from the numerical analysis were compared with the experimental work done by Kim *et al.* [17].

3.2 Computational Fluid Dynamics (CFD)

Computational fluid dynamics (CFD) is *'The analysis of systems involving the fluid flow, heat transfer and associated phenomena such as chemical reactions by*

means of computer based numerical simulations' [121]. CFD numerical techniques have several unique advantages over experimental methods, such as:

i.   Substantial reduction of lead times and costs of new designs;

ii. The ability to study systems where controlled experiments are difficult to perform;

iii. The ability to study systems under hazardous conditions at and beyond their normal performance limits.

Aside from the above mentioned advantages of CFD, numerically modelling of the transport phenomena using CFD is not straightforward; a good understanding of the real problem and the underlying physics is vital.

3.2.1 Discretization Methods

The mathematical models describing the underlying physics of a physical problem is a core part of numerical modelling. The mathematical model describing fluid flow behaviour is a set of partial differential equations and their associated boundary conditions [122]. Selection of a suitable discretization method is essential to solve the mathematical model describing the underlying physics.

A discretization method can be defined as, *'A method of approximating the differential equations by a system of algebraic equations for a variable at some set of discrete locations in space and time'.* There are three main approaches of discretization, a) finite difference b) finite volume c) finite element. For this research work, a finite element based discretization technique is used for the numerical modelling of the coupled transport phenomena of the PEM fuel cell.

3.2.1.1 Finite Element Method

In the finite element discretization approach, the computational domain is divided into a set of discrete finite elements and the governing equations are multiplied by a weighting function before they are integrated over the flow domain [122]. The numerical solution in this approach is approximated by a linear shape-

function within each element in a way that guarantees continuity of the solution across element boundaries. Such shape-functions can be constructed from their values at the corners of the elements. The approximation is then substituted into the weighted integral of the conservation equation, and the equations to be solved are derived by setting the derivative of the integral with respect to each nodal value equal to zero. This corresponds to selecting the best solution within the set of allowed functions (the one with the minimum residual).

3.3   Multiphysics Numerical Modelling

Multiphysics numerical modelling involves the coupling of multiple physical models or multiple simultaneous physical phenomena. Traditional computer aided analyses are based upon different continuum phenomena such as computational fluid dynamics (CFD), computational structural mechanics (CSM), computational electro-mechanics (CEM) and computational acoustics (CA). Multiphysics numerical analyses involve and closely couple all phenomena under study. There is no generic approach to model the complex physical interactions in multiphysics modelling as the level and nature of the physical coupling required to accurately model such processes is problem dependant, and may range from relatively straightforward multidisciplinary processes requiring low coupling to strong two way coupling requiring mesh compatibility [123].

To numerically model the coupled transport phenomena of the PEM fuel cell during this research work, a commercial finite element multiphysics numerical solver (COMSOL v 3.4) was used. COMSOL Multiphysics has an integrated modelling environment by linking well known 'application modes' transparently. Its extended multiphysics capability provides coupling between logically distinct domains and models that permit simultaneous solutions of the complex physical problems [124]. COMSOL Multiphysics is fully compatible with the MATLAB which enables user defined programming for advanced modelling.

3.4   Numerical Model Description

The numerical modelling of coupled transport phenomena taking place inside the PEM fuel cell involves species transport, heat transfer, charge balance

47

and electrochemical kinetics. All these transport phenomena are coupled with each other. Governing equations for mass, momentum and energy conservation and charge balance are used to numerically solve the flow in porous media and electro chemical kinetics. The following section briefly describes the set of governing transport equations used for the numerical modelling of the PEM in this work.

3.4.1 Governing Equations

The set of governing transport equations used for the numerical modelling of coupled transport phenomena are given below. This form of governing transport equations were selected after examining the work done by different researchers which was reviewed in chapter 2.

The fluid flow in the gas channel is laminar and is assumed to be incompressible, giving a constant density. Reactant fluid flow behaviour in the PEM fuel cell gas channel is governed by the continuity equation to ensure mass conservation and to numerically describe the momentum conservation of Newtonian fluids, the following form of the incompressible Navier Stokes equation is used in the PEM fuel cell gas channels [62]:

$$\rho \, \frac{\partial u}{\partial t} - \nabla \cdot \eta \, (\nabla u + (\nabla u)^T) + \rho \, (u \cdot \nabla) u + \nabla p = 0 \qquad \text{(3-1)}$$

Momentum conservation in the gas diffusion layer (GDL) is described using the Brinkman equation, which is an extension of the Darcy's law and couples the flow in free and porous media by taking into account viscous effects. The following form of the Navier Stokes equation, coupled with the Darcy's law is used to study the flow behaviour in the porous gas diffusion layer of the PEM fuel cell [125]:

$$\frac{\rho}{\varepsilon} \frac{\partial u}{\partial t} + \nabla \cdot \frac{\eta}{\varepsilon} (\nabla u + (\nabla u)^T) + \frac{\eta}{k_p} u + \nabla p = 0 \qquad \text{(3-2)}$$

k_p denotes the permeability of the porous medium and ε is the GDL porosity. Reactant species transport in the PEM fuel cell domain is described by the

divergence of mass flux through diffusion and convection of the reactant species using the following form of the Maxwell-Stefan convection and diffusion equation [49]:

$$\nabla\left[-\rho w_i \sum_{j=1}^{N} D_{ij} \left\{\frac{\nabla M}{M_j}\left(\nabla w_j + w_j \frac{\nabla M}{M}\right) + \left(x_j - w_j\right)\frac{\nabla p}{p}\right\} + w_j \rho u\right] = R_i \qquad (3\text{-}3)$$

Subscript i denote the oxygen concentration at the cathode and hydrogen at the anode sides, while j is the water vapour at both sides. D_{ij} is the binary diffusion coefficient and R_i is the reaction rate. The reaction rate is zero for the gas flow channel and gas diffusion layer, whereas along the cathode catalyst layer the rate of electrochemical reaction is quite high. The mixture density ρ is the function of mixture components and is described by the following equation:

$$\rho = \frac{\sum x_i.MW_i}{RT} p \qquad (3\text{-}4)$$

Here, x_i is the mole fraction, R is the universal gas constant, M is the molecular weight and w_i is the mass fraction. At the cathode side, the species transport equation is solved only for two species as the third species can be obtained from the following form of the mass balance equation:

$$w_{N_2} = 1 - w_{O_2} - w_{H2O} \qquad (3\text{-}5)$$

On the other side, the hydrogen mass transport equation is solved first and then the mass fraction of water is calculated using the following form:

$$w_{H2O} = 1 - w_{H_2} \qquad (3\text{-}6)$$

Binary diffusion coefficients of the reactant species are important for species mass transport. The binary diffusion coefficients for the gas channel are calculated using the following empirical relation based on the kinetic theory of gases [62]:

49

$$D_{ij} = \frac{T^{1.75}(1/M_i + 1/M_j)^{1/2}}{\rho((\sum_k V_{ki})^{1/3} + (\sum_k V_{kj})^{1/3})^2} \qquad (3\text{-}7)$$

In order to account for the geometric constraints of the porous media in the gas diffusion layer, the binary diffusion coefficients of the reactant species are corrected using the following form of the Bruggemann correction formula [15, 62]:

$$D_{ij}^{eff} = D_{ij} \times \varepsilon^{1.5} \qquad (3\text{-}8)$$

Water management in the PEM fuel cell is critical and plays a vital role in its performance. In addition to the molecular diffusion and electro-osmotic drag in the electrolyte membrane, water is also generated due to oxygen reduction reactions at the cathode catalyst layer of the PEM fuel cell. For these analyses, a fully humidified *Nafion*-117 membrane is used. Water transport and charge balances are the major transport phenomena taking place inside the electrolyte membrane.

Water transport depends upon the membrane water activity and the water content. The molar flux of water α of a PEM fuel cell membrane is based upon the electro-osmotic drag coefficient n_d, the water content λ and the water activity a of the electrolyte membrane. Membrane water content λ depends on the water activity a and can be numerically modelled using the following relation [90, 126]:

$$a = \frac{X_{H2O}P}{P_{sat}}$$

$$\lambda = A_1 + A_2 a - A_3 a^2 + A_4 a^3 \qquad \text{for } 0 < a \leq 1$$
$$\quad = 14 + 1.4(a\text{-}1) \qquad\qquad\qquad \text{for } 1 \leq a \leq 3 \qquad (3\text{-}9)$$
$$A_1 = 0.043\,, A_2 = 17.18\,, A_3 = 39.85\,, A_4 = 36$$

Saturated vapour pressure P_{sat}, the electro-osmotic drag coefficient n_d and the molar flux of water α along the electrolyte membrane depends on the membrane water content and can be numerically modelled using the following relations [109]:

$$\log_{10} P_{sat} = -2.1794 + 0.02953(T - 273.15) - 9.1837 \times 10^{-5}(T - 273.15)^2$$

$$n_d = B_1 \lambda + B_2 \lambda - B_3$$

$$B_1 = 0.0028 \, , \, B_2 = 0.05 \, , \, B_3 = 3.5 \times 10^{-19}$$

(3-10)

$$\alpha = \frac{n_d I_k}{F} - D_w \nabla C_w$$

The membrane water diffusivity D_w and water concentration C_w across the membrane can be calculated by [110, 111]:

$$C_w = \frac{\rho_{mem,dry}}{M_{mem,dry}} \lambda$$

$$D_w = D_\lambda \exp\left[2416\left(\frac{1}{303} - \frac{1}{T} \right) \right]$$

$where$

$$D_\lambda = 10^{-10} \qquad\qquad\qquad \lambda < 2$$
$$D_\lambda = 10^{-10}(1 + 2(\lambda - 2)) \qquad 2 \le \lambda \le 3$$
$$D_\lambda = 10^{-10}(3 - 1.67(\lambda - 3)) \qquad 3 \le \lambda \le 4.5$$
$$D_\lambda = 1.25 \times 10^{-10} \qquad\qquad \lambda > 4.5$$

(3-11)

The charge balance in the membrane causes the movement of protons from anode to cathode and is calculated by the following form of the continuity relation [65]:

$$-\nabla.(\sigma_m \nabla \phi_m) = 0$$

(3-12)

Where φ_m is the membrane potential and σ_m is the membrane ionic conductivity. The membrane ionic conductivity depends upon the membrane water content and is calculated by the following empirical expression:

$$\sigma_m = \exp\left[1268\left(\frac{1}{303} - \frac{1}{T} \right) \right] \sigma_{30}$$

$$\sigma_{30} = 0.5139\lambda - 0.326$$

(3-13)

A potential difference exists between the anode and cathode side of the PEM fuel cell that causes the movement of electrons and proton ions from anode to cathode [127]. The current flux at the cathode boundary between the electrode and the membrane is calculated using the following equation of charge conservation [65]:

$$n.\left(-\sigma_{s,eff}\nabla\phi_s\right)=i_c$$
$$n.\left(-\sigma_{m,eff}\nabla\phi_s\right)=-i_c$$

(3-14)

At the anode side, this current flux is calculated by:

$$n.\left(-\sigma_{s,eff}\nabla\phi_s\right)=-i_a$$
$$n.\left(-\sigma_{m,eff}\nabla\phi_s\right)=i_a$$

(3-15)

The following form of the Butler-Volmer equation is used to express the relation between the local transfer current densities (i), the reactant concentrations (c_i) and the phase potentials along the membrane/catalyst layer interface at both anode and cathode sides of the PEM fuel cell [53]:

$$i_c=i_{oc}^{ref}\left(\frac{C_{o2}}{C_{o2}^{ref}}\right)\left[\exp\left(\frac{\alpha_a F}{RT}\eta_{act,c}\right)-\exp\left(-\frac{\alpha_a F}{RT}\eta_{act,c}\right)\right]$$

$$i_a=i_{oa}^{ref}\left(\frac{C_{H2}}{C_{H2}^{ref}}\right)^{\frac{1}{2}}\left[\exp\left(\frac{\alpha_a F}{RT}\eta_{act,a}\right)-\exp\left(-\frac{\alpha_a F}{RT}\eta_{act,a}\right)\right]$$

(3-16)

For the above mentioned Butler-Volmer equation the activation overpotential η_{act} at the cathode and the anode are calculated by [83]:

$$\eta_{act,c} = \phi_s - \phi_m - V_{oc}$$

where

$$V_{oc} = 0.2329 + 0.0025T \qquad \text{(Reduces form of Nernst law)}$$

while

$$\eta_{act,a} = \phi_s - \phi_m$$

During these analyses, the catalyst layer is treated as a thin boundary interface, where sink and source terms for the reactants are implemented. Local volumetric sources and sink terms associated with the electrochemical reactions are proportional to the local current density [58, 62]. At the cathode catalyst layer, oxygen consumption is modelled as a sink term based on the cathode local current density:

$$S_{O2} = -\frac{M_{O2}}{4F} i \qquad (3\text{-}17)$$

The production of water is modelled as a source term based on the local current density:

$$S_{H2O} = \frac{M_{H2O}}{2F} i \qquad (3\text{-}18)$$

At the anode catalyst layer, hydrogen is oxidised to produce electrons and protons. Consumption of hydrogen is modelled as a sink term by the following relation:

$$S_{H2} = -\frac{M_{H2}}{2F} i \qquad (3\text{-}19)$$

The total potential loss in the PEM fuel cell is a function of activation, Ohmic and concentration over-potentials. For this research work, these three different potential losses are calculated using the following expressions:

$$\eta_{ohmic} \quad = \quad V_{CL} - V_{ref}$$

$$\eta_{Protonic} \quad = \quad V_{CL,\,c} - V_{CL,\,a} \qquad\qquad (3\text{-}20)$$

$$\eta_{act} \quad = \quad E_{rev} - E_{cell} - \eta_{ohmic} - \eta_{Protonic}$$

V_{CL} is the potential at the catalyst layer; V_{ref} is the reference potential set at the interface between gas diffusion layer and the bipolar plate. E_{rev} is the reversible cell potential and E_{cell} is the input parameter based on the desired loading condition.

Heat generation in the PEM fuel cell is due to entropy changes and irreversibility related to the phase changes in both charged and uncharged reactant species. During this research work when considering non-isothermal conditions, heat generation is assumed to be predominantly due to the electrochemical reactions, while heat generation due to Ohmic losses is neglected. Lampinen *et al.* [55] proved that the heat generation from the anode reaction is considerably smaller and can be ignored in comparison to the cathode reaction. Therefore, only cathodic heat generation is considered for non-isothermal numerical analyses [90]. For this study the entropy change at standard states with a platinum catalyst were taken as $\Delta S = 0.104$ J/mol-K for the anode side and $\Delta S = -326.36$ J/mol-K for the cathode side [78]:

$$q^o = \left[\frac{T(-\Delta S)}{n_e F} + \eta_{activation} \right] i_c \qquad\qquad (3\text{-}21)$$

Heat generated at the cathode membrane/catalyst layer interface is then transferred to the fuel cell domain by convection and conduction, increasing the overall operating temperature of the PEM fuel cell.
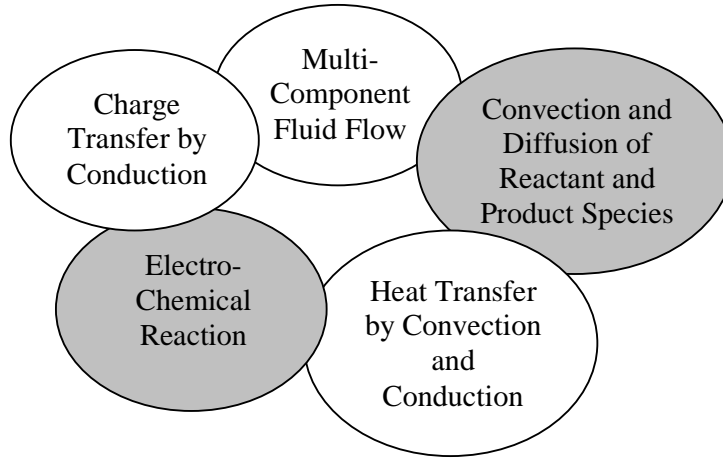
Figure 3-1: PEM fuel cell transport phenomena
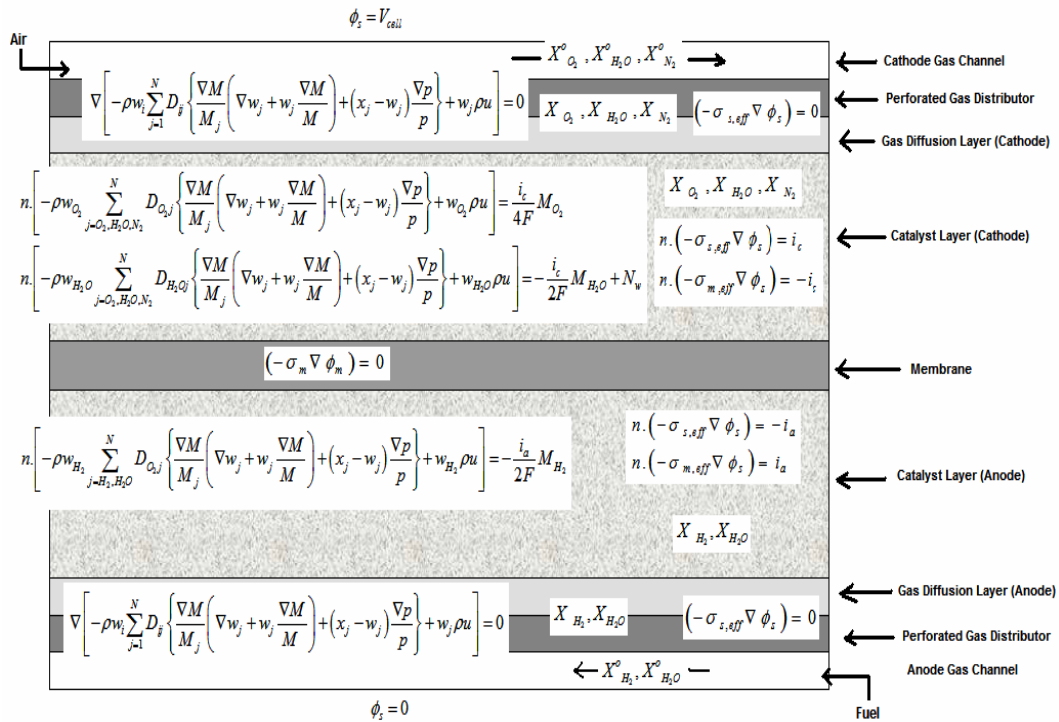
Figure 3-2: Cross sectional view of the PEM fuel cell domain highlighting the major governing equations involved in each section

55

3.4.2 Boundary Conditions

The boundary conditions for this numerical model are specified at all external boundaries, as well as boundaries for mass transport and the scalar equations inside the computational domain of the PEM fuel cell. The following points highlight the boundary conditions used for this numerical study:

- At the anode and cathode gas flow channel inlets, boundary conditions for velocity, temperature and species mass fractions are specified, whereas at the outlets, the atmospheric pressure and convective flux boundary conditions are specified for species and energy transport equations;
- A no-slip boundary condition is specified at the gas flow channel outer walls, which are also impervious to the species flow and thermally insulated;
- A continuous boundary is assumed between the gas flow channel and perforated gas flow distributor open channels. In the solid section of the perforated gas flow distributor, the wall is used as a boundary condition between the gas channel and the perforated gas flow distributor;
- At the gas diffusion\catalyst layer interface, continuity is assumed as a boundary condition;
- The flux of the reactant and product species is used as a boundary condition at the membrane\catalyst layer interface for both the anode and cathode sides due to the electro-chemical reactions;
- The solid phase potential is arbitrarily set to zero as a reference at the anode, while at the cathode side the cell potential is set to $E_{cell} - E_{rev}$, where E_{cell} is the desired cell potential and $E_{rev} = 1.14\ V$, which is the reversible cell potential. The cell potential gradient is set to be zero at both catalyst layer/membrane interfaces since there exists no solid phase current in the membrane.

3.4.3 Numerical Procedure

The numerical modelling of transport phenomena taking place inside a PEM fuel cell is not a straight forward process. It involves the coupling of non-linear systems of equations. A finite element based commercial multiphysics numerical

solver (COMSOL v 3.4) was used to solve the non-linear coupled transport equations describing the PEM fuel cell operation. The governing transport equations were discretized based upon the finite element method into a system of algebraic equations, which are then solved by an iterative algorithm. The PEM fuel cell computational domain is divided into a finite number of elements using a second order Lagrangian approach. The chemical engineering module of COMSOL is used for these analyses and the following physics application modes of the COMSOL chemical engineering module are used for solving the governing transport equations and respective dependant variables:

1. The incompressible Navier-Stokes application mode for simulating the Newtonian reactant fluid flow behaviour in free media of the fuel cell domain;

2. The incompressible Navier-Stokes mode coupled with Darcy's law (Brinkman Equation) for simulating the reactant fluid flow behaviour in the porous media;

3. The Maxwell-Stefan multi component diffusion and convection module for the species transport of reactants and products along the PEM fuel cell domain;

4. The conductive media DC application mode for charge balance in the fuel cell domain;

5. General heat transfer application mode for heat transfer in the fuel cell domain by convection and conduction.

A stationary non-linear numerical solver together with a direct linear solver (UMFPACK) was used, since the source terms of charge conservation make the problem non-linear. The relative tolerance for the error criteria was set at $1x10^{-4}$. For parametric analysis, the parametric solver of COMSOL was used, where the parametric variables were defined with a specific range of analyses. Performance polarisation curves were obtained by varying the cell potential using the parametric solver of COMSOL. The parametric solver uses an iteration loop to change the variable values in the specified range.

The convergence behaviour of this non-linear problem is highly sensitive to the initial estimation of the solution. Therefore, to accelerate the numerical convergence of this non-linear problem, the incompressible Navier-Stokes equations and the Brinkman equation are initially solved together to give a better initial estimation of the convective viscous properties of the reactant flow, before a fully coupled solution involving *all* the physics modes is solved using these values as an initial guess. This solution technique is used to avoid possible numerical instability of the convective terms in small channels of the gas flow distributor because numerical modelling of the flow behaviour in such small channels can lead to fluctuations near the walls, which can lead to numerical instabilities and result in a simulation crash.

To minimize the numerical instabilities in such small flow channels, the concept of artificial diffusion is used here. Streamline diffusion is used with a tuning parameter value of 0.25. Streamline diffusion introduces stabilizing terms into the incompressible Navier Stokes equations to reduce the numerical instabilities in the streamline direction of the fluid flow.

The results from the convective fluid flow model were also compared with the solution of the incompressible Navier Stokes equations using another commercial CFD solver called FLUENT. The incompressible Navier Stokes equations were solved in FLUENT at the same operating and geometric conditions, using different values of relaxation factors ranging from 0.4 to 0.8. The relaxation factors in FLUENT are used to stabilise the numerical solution. The main purpose of this small comparison study was to understand and analyse the numerical solution of the flow behaviour in such small flow channels with a focus on the numerical instabilities in the convective predictions of the reactant flow.

```
┌─────────────────────────────────┐
│         Initial Guessing        │
└─────────────────────────────────┘
                 ↓
┌─────────────────────────────────┐
│   Incompressible Navier Stokes  │
│  Equations and Brinkman Equation │
└─────────────────────────────────┘
                 ↓
┌─────────────────────────────────────────┐
│  Incompressible Navier Stokes Equations  │
│            Brinkman Equation             │
│  Maxwell-Stefan Diffusion and Convection │
│           Conductive Media DC            │
│           General Heat Transfer          │
└─────────────────────────────────────────┘
```
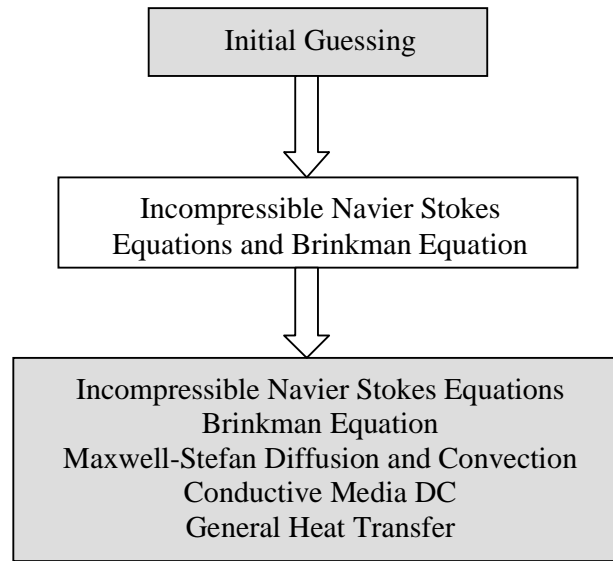
Figure 3-3: Solution Procedure used in COMSOL

3.4.4 Solution Algorithm

Most numerical models of the PEM fuel cell assume a constant activation overpotential for ease of the numerical procedure, but the numerical algorithm used for this research work calculates the activation overpotential for each cell voltage, as this method has the capability of calculating the current density from the input operating cell voltages.

The numerical solution begins by computing the reactant flow velocities and the pressure distribution along the free and porous media of the PEM fuel cell. Once the flow field is solved, the mass transport equations are then solved for the mass fraction of the species. Heat transfer and the charge balance equations are solved to calculate the temperature and cell potential distribution along the fuel cell domain. After solving the cell potential equations, the activation over-potential is obtained from the solution of equation 3.20. The local current density is then solved by the Butler-Volmer equation, which uses the activation over-potential and species concentration as inputs. The convergence criteria are then compared with the residual of each variable and the procedure is repeated until convergence is achieved.

Both 2D and 3D numerical simulations have been carried out for the detailed performance analyses. For the 2D numerical simulations, a computer with an AMD® 1.6 GHz CPU and 1.25 GHz RAM was used, whereas the 3D numerical simulations were carried out using an Intel Pentium® 2.6 G Hz quad core CPU with 8 GB RAM. Figure 3.4 is a flow chart showing the solution algorithm used for this research work. For the isothermal 2D numerical analyses, the computational time to solve each problem was approximately 18 minutes, while for 2D non-isothermal type numerical analyses the computational time was around 26 minutes. For the 3D full scale isothermal numerical analyses, the computational time was about 38 hours.

3.4.5 Modelling Assumptions

A PEM fuel cell system involves both macroscopic and microscopic geometric features, coupled transport processes and electrochemical reactions. Numerical models of the PEM fuel cell are usually based upon empirical relations and the experimental observations, requiring simplifying assumptions to be made. During this research work, both isothermal and non-isothermal analyses were carried out to consider the effect of the following modelling assumptions:

a) Ideal gas mixtures with incompressible laminar flow due to a low Reynolds number;

b) Single phase model where the water product was assumed to only exist in the vapour form;

c) Isotropic and homogenous electrodes and membranes;

d) Negligible contact resistance, whereby the spatial variation due to compression caused by the end plate structure was ignored;

e) Negligible membrane swelling;

f) Assumption of a thin reactive boundary layer on the catalyst layer;

g) Ohmic heating in the bipolar plates and in the gas diffusion electrodes is neglected due to the high conductivity values.
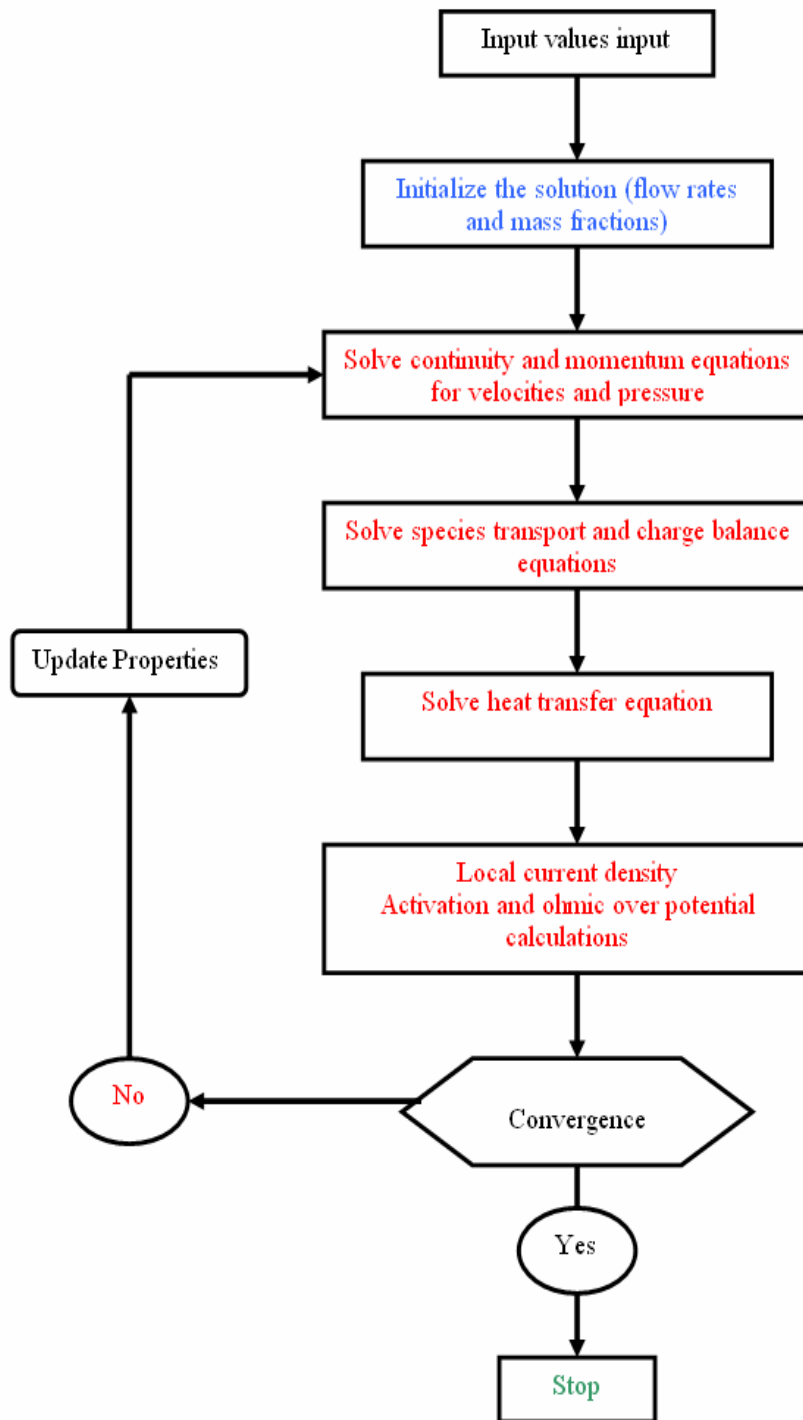
Figure 3-4: Solution Algorithm used in COMSOL

3.4.6 Modelling Parameters

The selection of correct modelling parameters is important in establishing the validation case of the numerical model in comparison to the experimental results. During this research work, two different design configurations of the PEM fuel cell were analysed. For the PEM fuel cell with the perforated gas flow distributor, the numerical results were validated with the experimental data obtained from work carried out by Mustafa [120] using a stainless steel perforated gas flow distributor, whereas the numerical model results of the PEM fuel cell with the cathode flow pulsations were validated with the experimental work performed by Kim [17].

To validate the numerical model with the experimental data, the PEM fuel cell with a stainless steel perforated gas flow distributor is used as a base-case. The modelling parameters used in the experiments by Mustafa [120] are used for the numerical modelling of the base case.

Parameter	Value	Unit
Gas Channel length	0.05	m
Gas Channel width	0.05	m
Gas Channel Height	0.005	m
Perforated sheet Thickness	0.00055	m
Perforated Hole Diameter	0.003	m
GDL Thickness	0.0002	m
Membrane Thickness	0.00018	m

Table 3-1: Geometric Properties of the PEM fuel cell computational domain

Parameters	Value	Unit	Reference
Oxygen Inlet Mass Fraction	0.226		[65]
Water Inlet Mass Fraction	0.0934		[65]
Hydrogen Inlet Mass Fraction	0.844		[65]
Operating Temperature	333	K	[120]
Inlet Pressure	101325	Pa	[120]
Relative Humidity, Air	70%		[120]
Relative Humidity, H2	92%		[120]

Table 3-2: Operating conditions for the base case

Parameter	Value	Unit	Reference
Electrode electronic conductivity	120	S/m	[65]
Membrane ionic conductivity (Nafion 117)	17.69	S/m	[48]
Transfer Coefficient, cathode side	0.5		[77]
Transfer Coefficient, anode side	0.5		[77]
Cathode reference exchange current density	1.0E-02	A/cm2	
Anode reference exchange current density	1.00E+04	A/cm2	
Gas diffusion layer (GDL) porosity	50%		
GDL Hydraulic Permeability	1.79e-11	m^2	[65]

Table 3-3: Electrode properties for the base-case

Parameter	Value	Unit
Electrical Receptivity	7.493e-7	Ω-m
Thermal Conductivity	15	W/m-K
Heat Capacity	502	J/Kg-K
Co-efficient of thermal expansion	1.6e-5	1/K
Density	7889	Kg/m^3

Table 3-4: Material properties of stainless steel, SS316L

3.5   Summary

This chapter described the numerical modelling configuration and the governing transport equations used for this research work. These governing equations were selected on the basis of the literature review of the work done by different researchers. A finite element based commercial multiphysics numerical solver (COMSOL v 3.4) was used to numerically model and solve the governing transport equations. Numerical modelling techniques, solution procedure and the algorithm used for this research work were discussed in detail.

CHAPTER 4

4   Model Validation and Performance Analyses of Perforated type PEM Fuel Cell

4.1   Introduction

This chapter describes the base case model validation with the experimental data and the performance analysis of a PEM fuel cell with a perforated gas flow distributor. The main purpose of analyzing this new design approach is to improve the performance of the PEM fuel cell by optimizing the reactant flow behaviour along its domain. Among the different parts of the PEM fuel cell, the bipolar/end plate is important both in terms of performance and cost. The effective weight and cost of a PEM fuel cell can be reduced significantly by simplifying the gas flow channel design configuration. The gas flow channels stamped on the bipolar/end plates play a vital role towards improving the distribution of reactant species and the overall performance of the PEM fuel cell. Different design topologies of the fuel cell gas flow channels such as straight, serpentine or spiral-shaped have been studied by the researchers to achieve the aforementioned functions efficiently with the aim of obtaining high performance and economic advantages. A 50% increase in the PEM fuel cell performance has been reported just by improving the distribution of the reactant species along its domain [44].

This chapter describes the design validation and performance analysis of a new design of PEM fuel cell which has a stainless steel (SS316L) perforated gas flow distributor instead of the more conventional graphite electrode plates. The experimental setup used for this research work [120] is briefly discussed here to highlight important assemblies and the working principles. Figure 4.1 shows a 3D CAD model of the perforated plate used as the gas flow distributor in this new design of the PEM fuel cell.
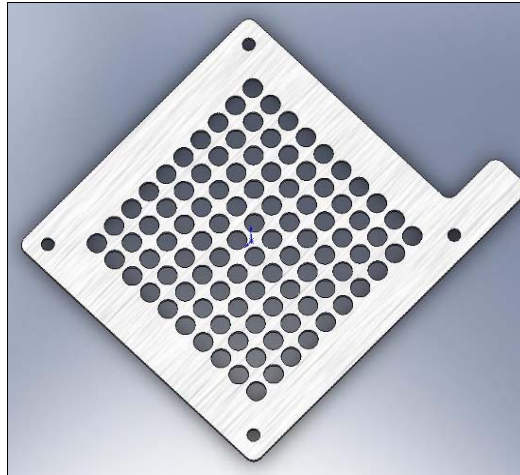
Figure 4-1: 3D CAD model of the perforated gas flow distributor

This new design approach is more compact than the standard graphite electrode fuel cell due to the lower thickness and greater robustness of the stainless steel plates. In this design approach, the membrane and stainless steel electrodes can be assembled as a single sealed unit which facilitates easier replacement.
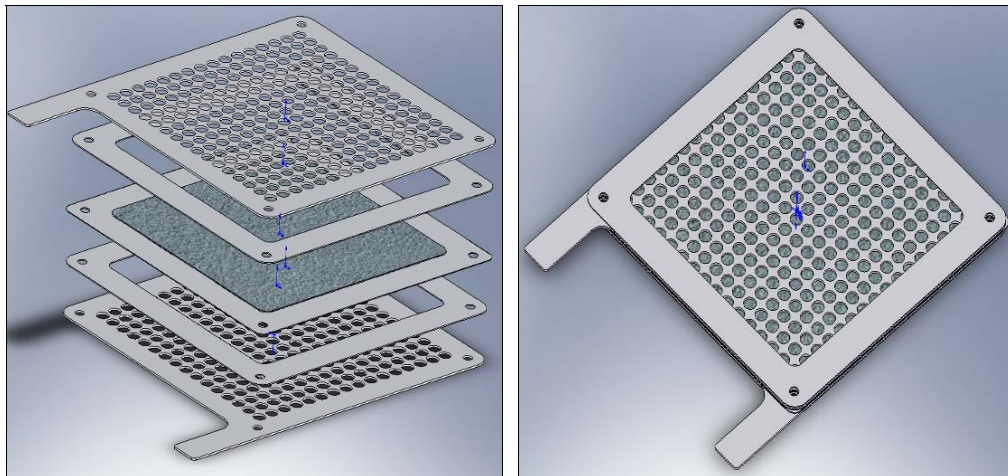
Figure 4-2:3D CAD model of the membrane electrode assembly (MEA) with perforated stainless steel gas flow distributors
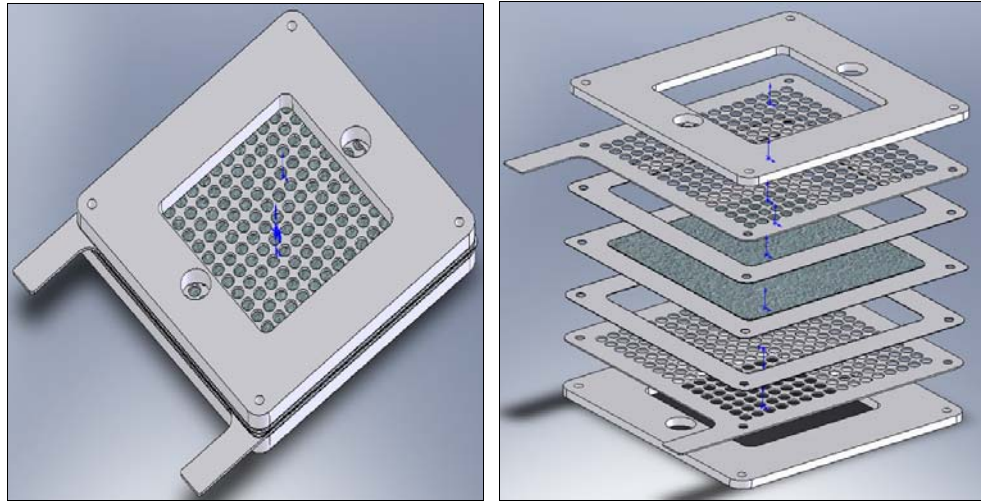
Figure 4-3: 3D full scale CAD model of the perforated type PEM fuel Cell

4.2 Experimental Setup

The basic operating principle of a PEM fuel cell is simple, but the experimental configuration required estimating its performance is complex. The major problems in PEM fuel cell operation, particularly when testing a fuel cell stack, is the control of membrane humidity and the reactant flow rates. The reactant flow of a PEM fuel cell is a function of temperature, pressure and humidification. The experimental setup used for this research work was initially designed by Mustafa [120] to perform the following main tasks:

- To provide a controllable apparatus for the conditioning of reactant gases in terms of flow rate, temperature, pressure and humidity;
- To measure the output conditions of the PEM fuel cell such as voltage, current, outflow rates and humidity of the gases at the outlet.

4.2.1 Experimental Test Rig

The PEM fuel cell system used for the experimental rig comprises two functionally identical, but independent gas flow circuits; one for the anode (hydrogen) and the other for the cathode (air). Each one of these circuits is composed of measurement and control apparatus. Figure 4.4 shows a schematic view of the test rig designed and used for this research work.
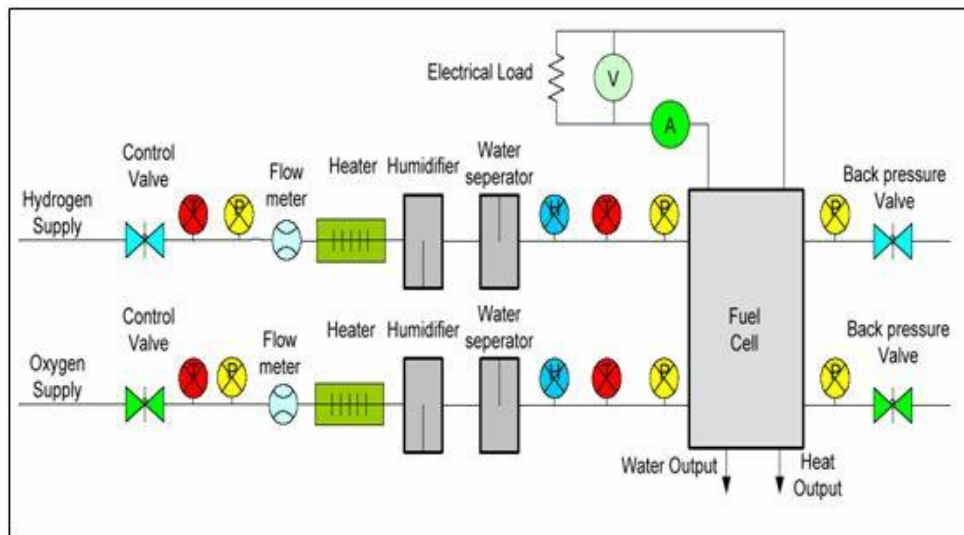
Figure 4-4: Schematic view of the experimental test rig [120]

The schematic diagram shows the different components of the test rig. Hydrogen, which is supplied from a compressed gas cylinder, enters at the hydrogen supply point where the flow is controlled by the flow control valve. Temperature, pressure and the volumetric flow rate of the hydrogen gas are recorded at this stage to calculate the mass flow rate. Hydrogen gas then enters a heating process where heat is added using a rope heater and a heating coil. The flow of gas is then routed to the humidifier.

In the case of hydrogen, the gas is by default bubbled through distilled water in the humidifier continuously; however, more moisture can be added to the flow when the ultrasonic vaporiser is on. For the air supply, the flow passes through the humidifier without bubbling and passes over the distilled water in the humidifier

where it can carry a slight amount of moisture. Humidity, temperature and pressure of the flow are recorded at this point. The gases are then directed to the PEM fuel cell where they react and the excess gases are vented out through a back pressure valve to control the pressure of the cathode and anode. The PEM fuel cell is treated as a 'black box' where only the external measurements are considered.

Major components of this experimental test rig include the flow measurement equipment, sensors and the data acquisition system, which are described briefly below:

Flow Measurement

Two standard floating ball flow meters are used for each of the reactant gases to measure the inflow and outflow rates. The difference between the two measurements indicates the amount consumed by the PEM fuel cell, including the fuel cross-over in the membrane.

Temperature Measurement

A set of K-type thermocouples is used to measure the temperature at the inlet and outlet sections. These thermocouples are used together with a four channel K-type thermocouple amplifier unit, specially designed to interface with the data acquisition systems.

Humidity Control and Measurements

A stainless steel cylinder equipped with an ultrasonic vaporiser powered by a 24V DC and a water level float sensor is used as a humidification chamber. Reactant gases pass through the chamber and carry water vapour as they go through. In the case of hydrogen, the gas stream is forced to bubble through the distilled water by default, while air just passes through the chamber without bubbling. Humidity measurement is performed using an electronic sensor.

Pressure Measurement

The experimental test rig is equipped with a pressure transducer which can measure pressure in the range1-5 atmospheric pressures. This records the inlet and outlet gas pressures for both hydrogen and air. Pressure control is achieved via

check valves at the outlet ports of the PEM fuel cell and by adjusting the flow control valves on the gas cylinders themselves.

Data Acquisition System

The data acquisition system used for the test rig comprises a data logger and the associated software. A USB analogue and a digital input/output unit (Labjack U12) was used for data logging, data acquisition, measurement and control. The LabView application represents virtually the experimental setup and displays the test results to aid the understanding of the performance of this experimental test rig under different conditions. Figure 4.5 shows the front panel of the LabView application highlighting the main measurements at different points.
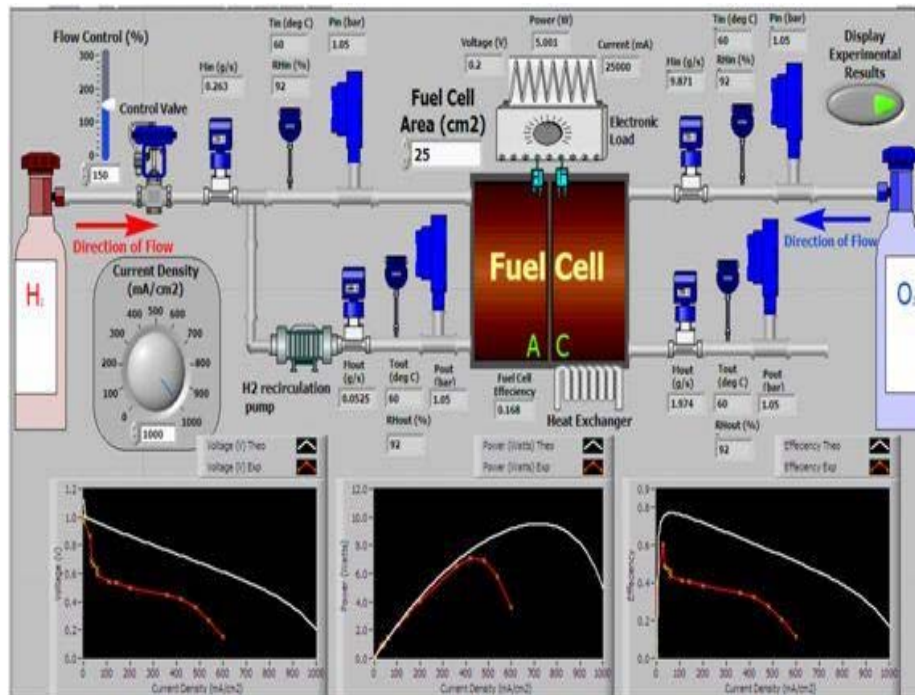
Figure 4-5: Front panel of the LabView application [120]

Figure 4-6: Experimental test rig
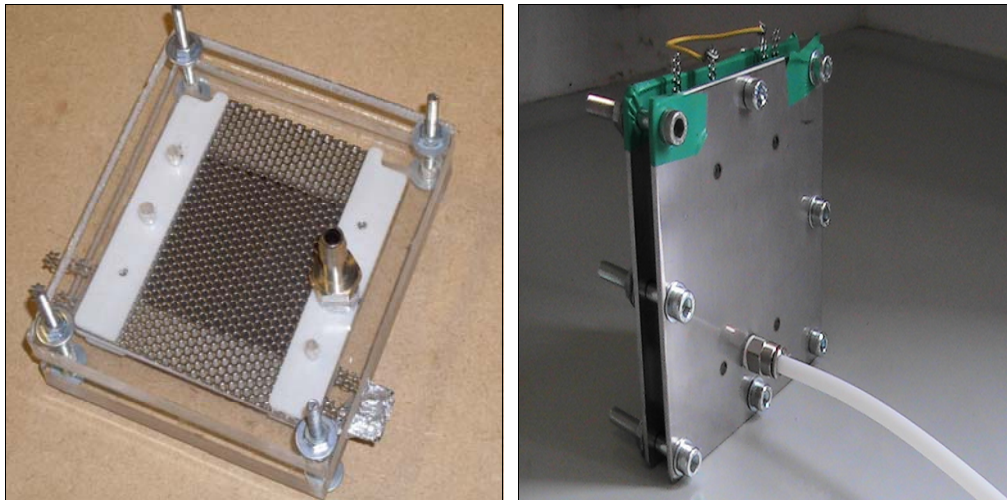
Figure 4-7: Experimental models of the perforated stainless steel electrodes PEM fuel cell

4.2.2 Experimental Procedure

For the experimental analysis, the perforated-type PEM fuel cell module was connected to the test rig and the data acquisition system. Humidified hydrogen was supplied to the anode side of the PEM fuel cell by bubbling the hydrogen gas in the humidification chamber through distilled water, which is a built-in feature of the test rig. In order to achieve the required level of performance, the reactant gases were preheated to the desired temperature (T = 333K) and then passed to the perforated PEM fuel cell for some time to remove the air residues from the PEM fuel cell channel and to give the fuel cell enough time to reach the desired operating temperature.

The PEM fuel cell was run open ended at atmospheric pressure. After this initial stage, the fuel cell was connected to the variable resistive load and voltage readings for different resistances were recorded by the data acquisition system. The current output of the PEM fuel cell was calculated using Ohm's law as the resistance and voltage were both known values. A standard technique was followed in the recording of the readings. The PEM fuel cell was given a few minutes to stabilize at open circuit voltage each time the resistive load was varied. A group of readings were logged to the data acquisition system each time the resistive load was changed. The average voltage reading was then taken and recorded against the respective resistance value and then a simple function of Ohm's law was used to calculate the current output.

4.3 Model Validation

This section presents the results of three dimensional, base-case numerical model validation in comparison with the experimental results provided by Mustafa [120]. Both numerical and experimental studies were carried out at operating and geometric conditions specified in Tables 3.1 to 3.4. The experimental setup used for this comparison study was described in the section 4.2.

At this point it should be noted that the polarisation curve is the most commonly used way of comparison between experimental and numerical data. Strict validation would require detailed comparison of data including the local distributions of current densities and the species concentrations along the fuel cell domain, but such data is very difficult to obtain from experiments. Therefore, for comparing the results obtained form the numerical and experimental study, the polarisation curve is used in this work. For the base-case numerical model, the 3D computational domain of the PEM fuel cell is divided into seven sections: the gas channel, the perforated gas flow channel and the gas diffusion layer for both anode and cathode, and finally a sandwiched membrane between anode and cathode. Figure 4.8 shows the computational domains used for this base case study.
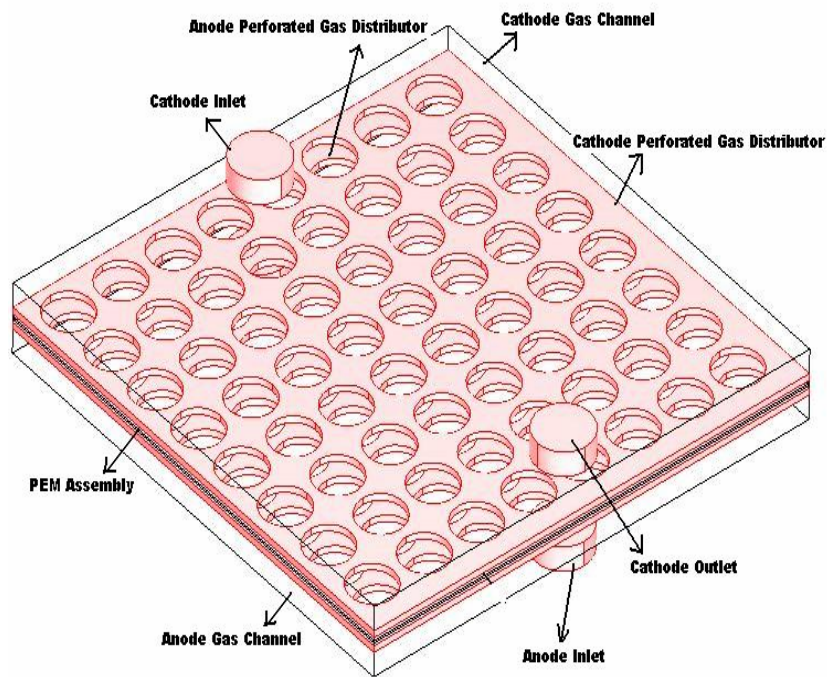
Figure 4-8: 3D computational domain of the perforated type PEM fuel cell
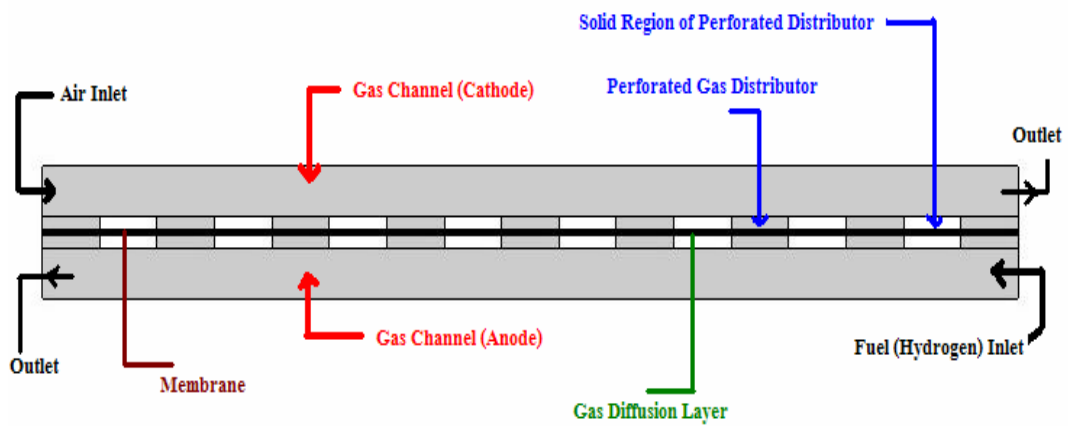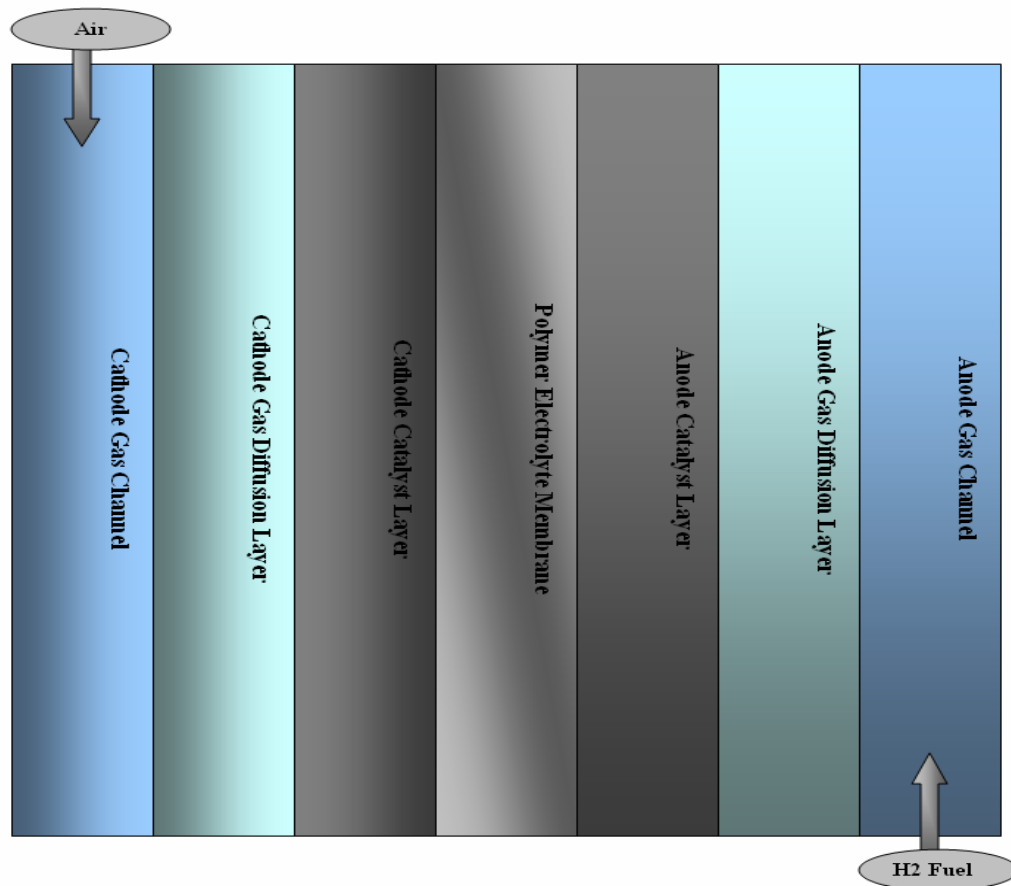
Figure 4-9: Cross sectional view of the perforated-type PEM fuel cell domain

The polarisation curves of the fuel cell potential versus fuel cell current density, for both numerical and experimental models of the perforated PEM fuel cell, showed good agreement. The Isothermal numerical analyses were carried out assuming T= 333K as the operating temperature of the PEM fuel cell.
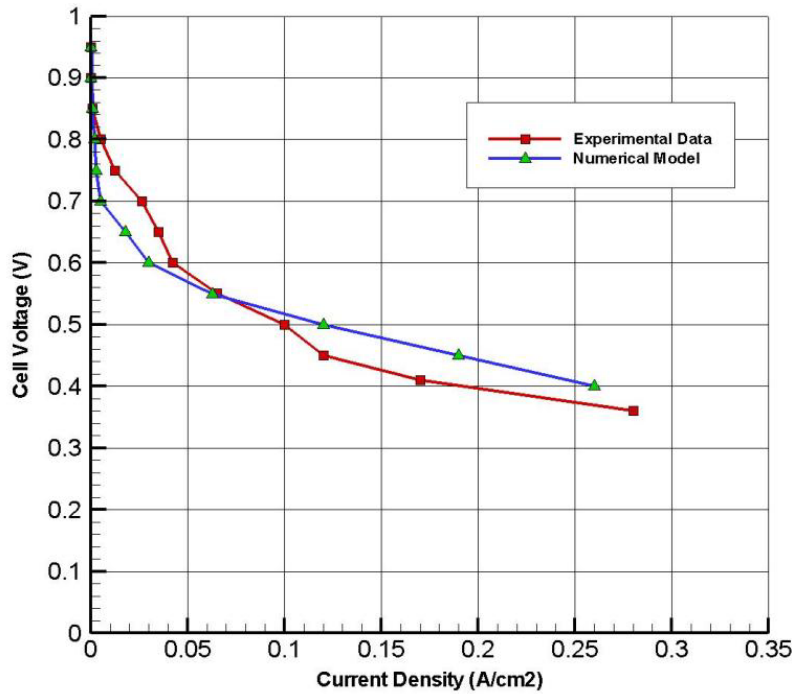
Figure 4-10: Comparison of numerical model and experimental polarisation curves at T = 333K

Figure 4.10 shows a small difference in the values at low and high current densities. This difference in current density values is mainly due to limitations in defining the electrochemical properties of the catalyst layer and the single phase assumption used for the numerical modelling. The results show high values of activation potential loss in the numerical results at low current densities. This is mainly due to the limited knowledge of the electrochemical material properties used in the numerical analysis. With better knowledge and definition of the electro-chemical material properties, it is expected that the numerical results can be improved.

The low concentration potential losses in the numerical results at higher current densities are mainly because of the single phase assumption. For the numerical modelling during this research work, the water content in the fuel cell domain is assumed to be in the vapour phase, whereas in actual fact water exists in both liquid and vapour forms. At higher current densities, due to the higher electrochemical reaction rates, the production of water as a by-product of the electrochemical reaction is high and leads to possible flooding of the cell. Such water flooding causes the blockage of the GDL pores and reduces the permeability of the reactant and product species through the pores of the GDL. This increases the concentration potential losses. Due to the single phase assumption, the numerical model does not accurately calculate the concentration losses due to the blockage of GDL pores, resulting in numerical predictions showing low values of concentration losses at the higher current densities.

Overall, these assumptions do not significantly affect the results, which is why they are used by most researchers for the numerical modelling of transport phenomena taking place inside PEM fuel cells. In comparison to the above mentioned polarisation curve, the predicted numerical model power density curve shows a good agreement with the experimental data. At high current densities, the predicted numerical values are higher than the experimental values as expected. Overall, a good agreement is found between the experimental and numerical results. Figure 4.11 shows the power density curve of the perforated-type PEM fuel cell for both numerical and experimental results, again demonstrating good agreement between the numerical model and the experimental results.
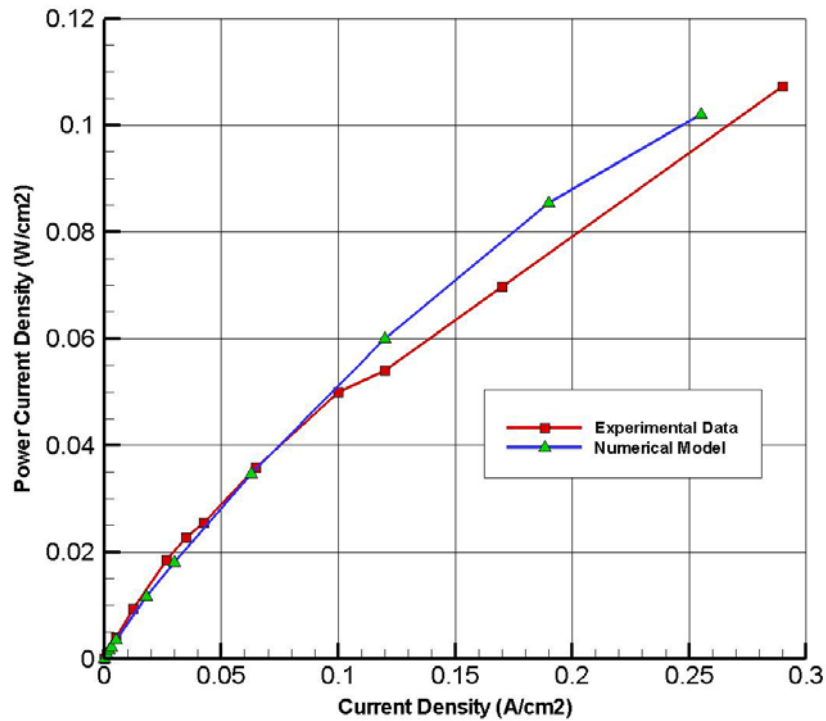
Figure 4-11: Power density curves for experimental and numerical models T = 333K

4.4 Base Case Numerical Results

In addition to the performance polarisation curve, the numerical study also provides important information and a detailed picture of the transport phenomena taking place inside the domain of the perforated-type PEM fuel cell, which is not possible with the experimental study. The distribution of reactants and product species concentrations, local current densities and over-potentials along the PEM fuel cell domain can be seen in the numerical study. The following sections provide a comprehensive overview of the variation of these transport phenomena along the perforated PEM fuel cell domain at isothermal conditions, i.e. T =333K.

4.4.1 Velocity Profile

The numerical analysis of the velocity distribution along a perforated PEM fuel cell shows that fuel and oxidant follow the shortest possible path from inlet to outlet in the PEM fuel cell gas channel. Results show a high velocity magnitude in the centre of the fuel cell gas channel, whereas a low velocity magnitude is

observed at the corners of the gas channel, possibly leading to dead zones at the corners of the fuel cell domain. The following figures show the velocity streamlines and velocity vectors along the perforated type PEM fuel cell domain.
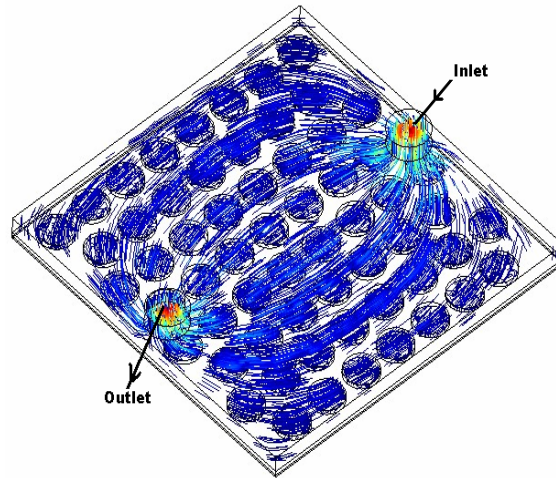
Figure 4-12: Streamline velocity profile along the fuel cell domain

(Near Outlet)   (Near Inlet)
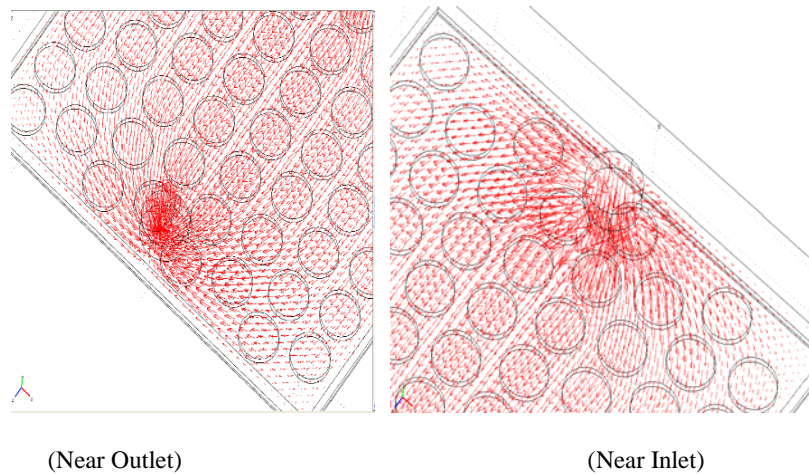
Figure 4-13: Velocity vectors near the inlet and outlet sections of the PEM fuel cell

The velocity profile affects the distribution of reactant and product species in the fuel cell domain; therefore, further investigations were carried out to understand and analyse the velocity variation along the gas channel and the perforated plate in the fuel cell. For these analyses, the velocity distribution is studied along a cross-section at the centre of the perforated PEM fuel cell domain.
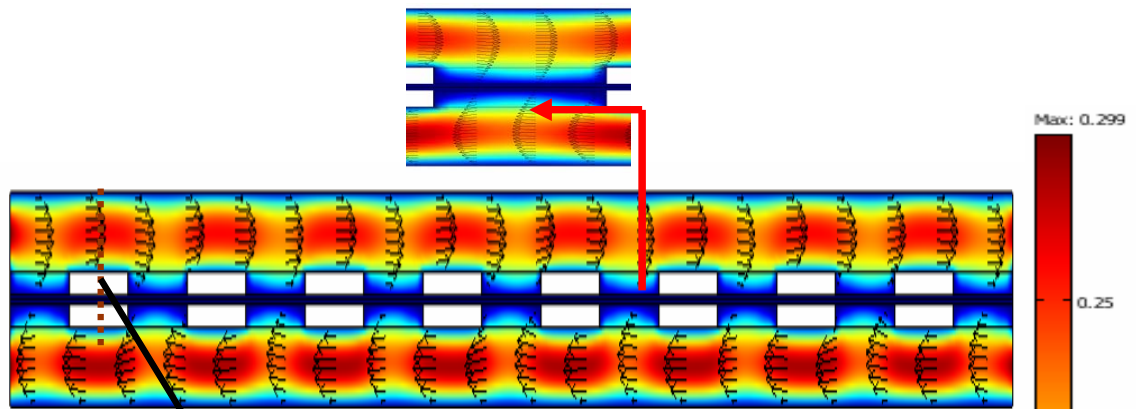
Figure 4-14: Velocity distribution along a cross section of the perforated type PEM fuel cell
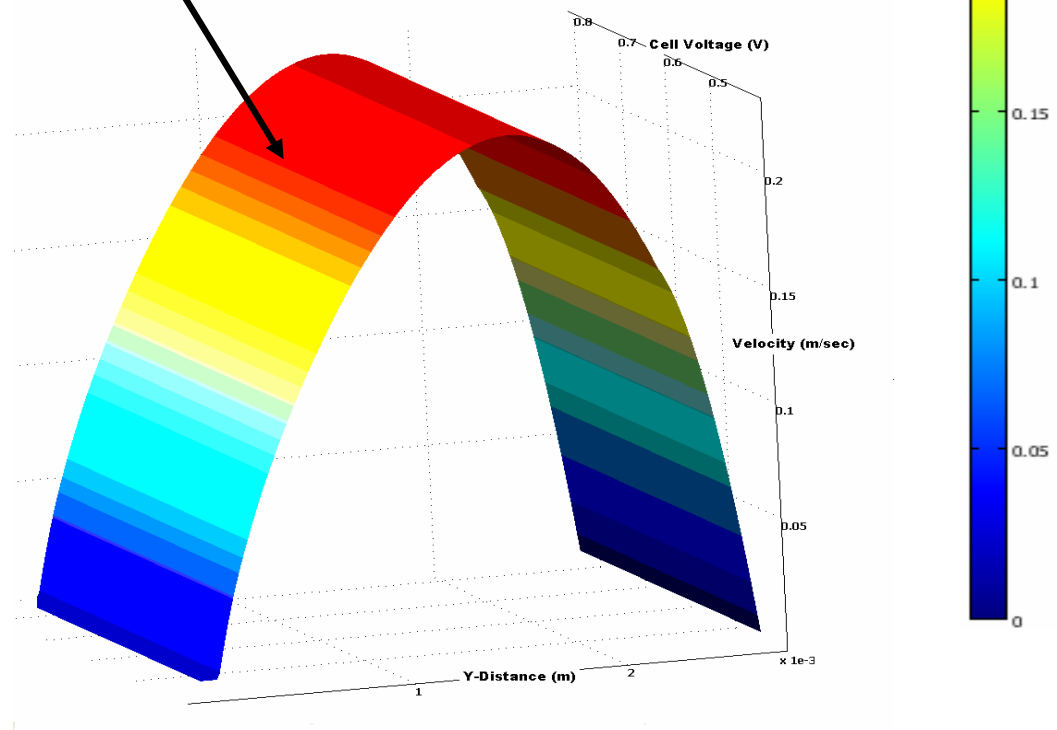
Figure 4-15: Velocity Profile at a cross section near the inlet of the PEM fuel cell gas channel

The analysis shows a parabolic velocity profile along the cross section, leading to a higher velocity at the centre of the gas channel. The parabolic velocity profile leads to a thick wall boundary layer that increases the residence time of the reactant species along the flow channel, passively forcing the fuel and oxidant to pass through the perforated holes of the gas distributor. Analysis also shows that the perforated holes of the gas distributor result in some frictional losses in the flow. To analyse the effects of the perforated holes size and shape, a detailed parametric study is carried out, which is presented in section 5.4.

4.4.2 Oxygen and Water Distribution along the Cathode Side

Oxygen and water distributions along the cathode side of the perforated-type PEM fuel cell domain have significant effect on the overall performance. Therefore, it is important to study and analyse the distribution of oxygen and water. The species distribution along the fuel cell domain depends upon the design configuration. In the perforated PEM fuel cell, the oxidant enters the straight rectangular gas channel and freely moves from the inlet to the outlet. Meanwhile, the oxidant passively passes through the holes of the perforated gas distributor attached to the gas channel and then diffuses through the pores of the GDL towards the catalyst layer where it chemically reduces at the membrane/catalyst interface and then chemically reacts with the protons and electrons travelling through the electrolyte membrane, generating heat and water.

The water generated by the electrochemical reaction moves from the catalyst layer to the gas channel where it evaporates in the excess reactant air. Transportation of water from the catalyst layer region to the gas channel takes place through the gas diffusion layer. This results in the blockage of the GDL pores during high rates of electro-chemical reactions, leading to possible water flooding. Such water flooding can be minimised by optimising the design of the PEM fuel cell in order to maximise the availability of reactant air to enhance water evaporation. In the case of the perforated type gas flow distributor, the passive diffusion of the reacting oxidant and removal of water product depends also upon the perforated holes diameter and shape.

Analysis of oxygen and water mass fraction distributions along the cathode side of the perforated type PEM fuel cell at different operating cell voltages show high values of oxygen mass fraction just below the inlet section that reduces near the outlet section due to its consumption through the fuel cell domain. Such a low value of oxygen mass fraction near the outlet section leads to a high water mass fraction near the outlet section, which is mainly due to the blockage of GDL pores and the reduced availability of reactant air to evaporate the water produced by the electrochemical reaction. Figure 4.16 and 4.17 show the distribution of oxygen and water mass fractions along the cathode side of the PEM fuel cell domain at two different operating cell voltages.

(V = 0.5 Volts)   (V=0.4 Volts)
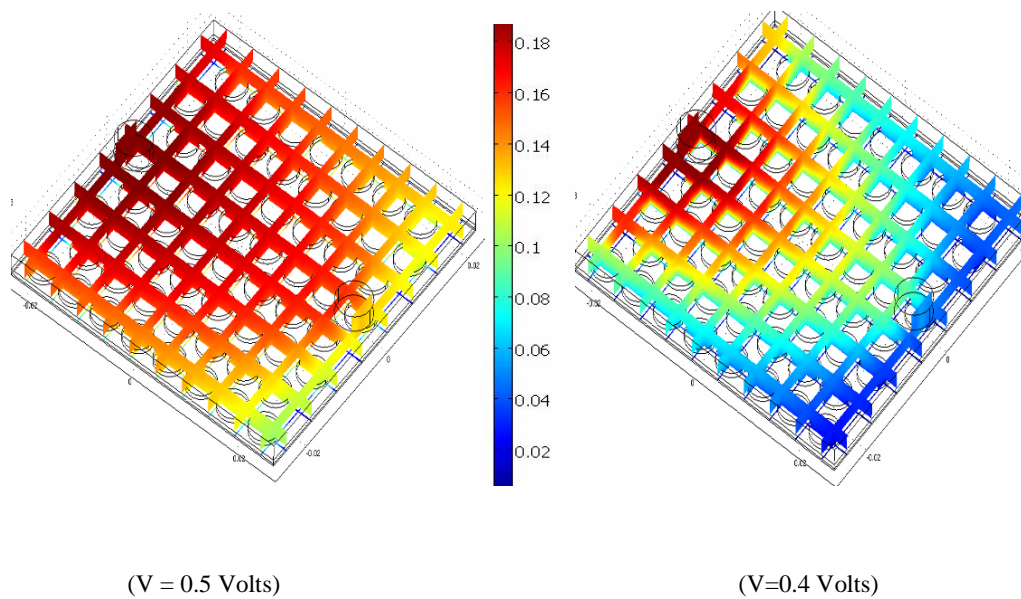
Figure 4-16: Oxygen mass fraction distributions along the cathode side at different load conditions

(V = 0.5 Volts)   (V=0.4 Volts)
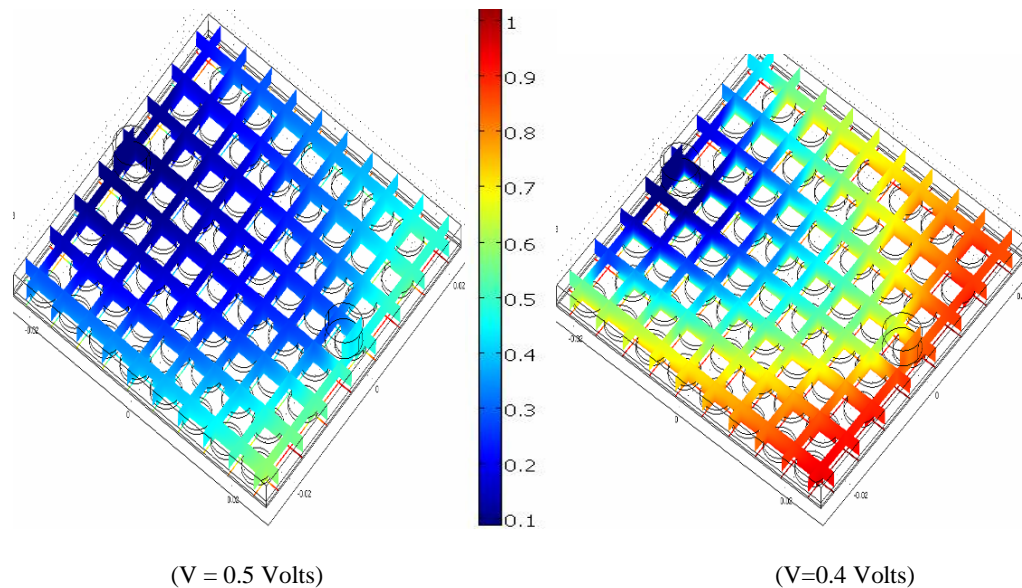
Figure 4-17: Water mass fraction distributions along the cathode side at different load conditions

Results show that the oxygen mass fraction decreases gradually from inlet to outlet due to its consumption along the cathode catalyst layer. The consumption of oxygen is high at low cell voltages because of the high electrochemical reaction rate. This behaviour is quite clear in figure 4.16 where the consumption of oxygen is low at V = 0.5 volts while at V = 0.4 volts the consumption of oxygen is high. There are also some concentration losses when the oxidant passes through the GDL along the cathode side of the PEM fuel cell. These concentration losses are more prominent at low cell voltages and high current densities due to the blockage of the GDL pores, caused by high water flooding at these load conditions.

Figure 4.18 and 4.19 show the distribution of oxygen and water mass fractions above and below the GDL surface at the cathode side. Results show that the maximum value of the oxygen mass fraction above the GDL surface is 0.14 and reduces to 0.1 below the GDL surface. Similarly, the minimum value of the water mass fraction above the GDL surface is 0.4 and increases to 0.5 below the GDL surface. This decrease in the oxygen mass fraction and increase in the water mass fraction is mainly because of the concentration losses due to blockage of the GDL pores.

(Above GDL Surface)   (Below GDL Surface)
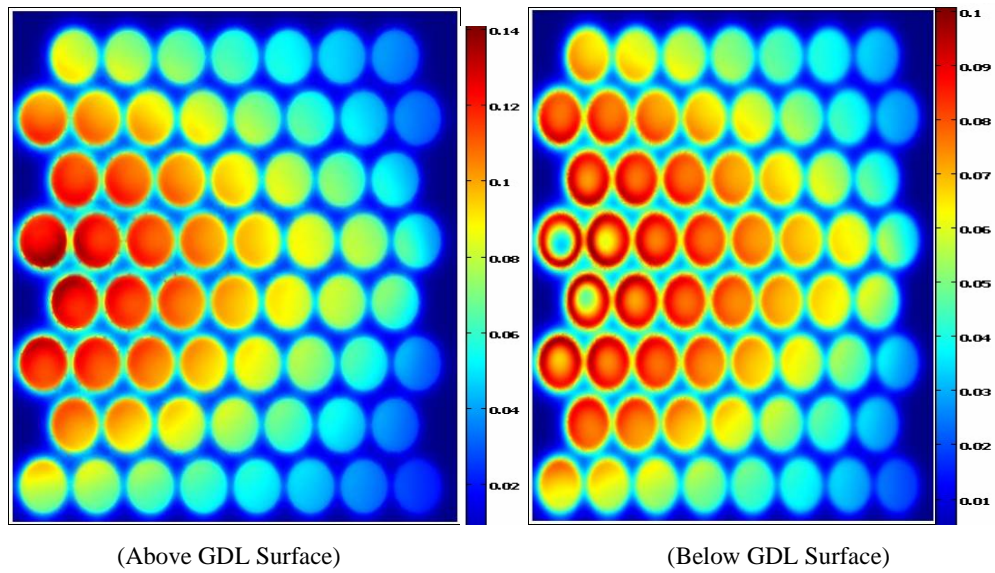
Figure 4-18: Distributions of oxygen mass fractions above and below the GDL, V = 0.5 volts

(Above GDL Surface)   (Below GDL Surface)
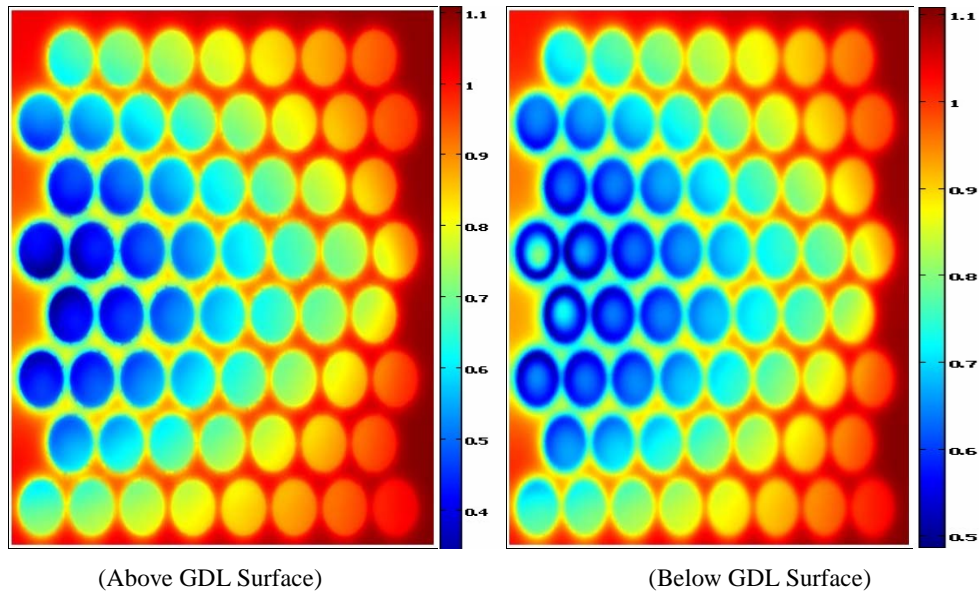
Figure 4-19: Distributions of water mass fractions above and below the GDL, V = 0.5 volts

The analysis shows that at the corners of the perforated PEM fuel cell domain, the rate of water removal is quite low due to the presence of less reactant air. This leads to water flooding in these areas. Similarly, below the solid regions of the perforated plate, the oxygen mass fraction is observed to be quite low, due to high amounts of water flooding below these solid areas.

The meshed area of the perforated gas distributor is an important factor that can improve gas distribution in these areas. For this study, a perforated plate with a 55% open area is used, meaning that 45 % of the area is not accessible for the reactant species in the gas channel to reach the porous media. Therefore, oxygen is not present below these solid areas of the perforated plate. This leads to the presence of excess water in these areas. Although increasing the meshed plate open area increases the chances of reactant species reaching the catalyst layer, it also affects the membrane life, as the membrane can rupture due to lower structural support from the electrode.

To study the distribution of oxygen and water along the perforated plate, detailed numerical analyses have been carried out at a cross-section of the perforated PEM fuel cell. These analyses provide a broader picture of the distribution of oxygen and water mass fractions along the cathode catalyst layer and their resultant effects on the PEM fuel cell performance. Figures 4.20 and 4.21 shows the distribution of oxygen and water mass fractions along the cathode catalyst layer in the cross-section of the PEM fuel cell at different cell voltages.
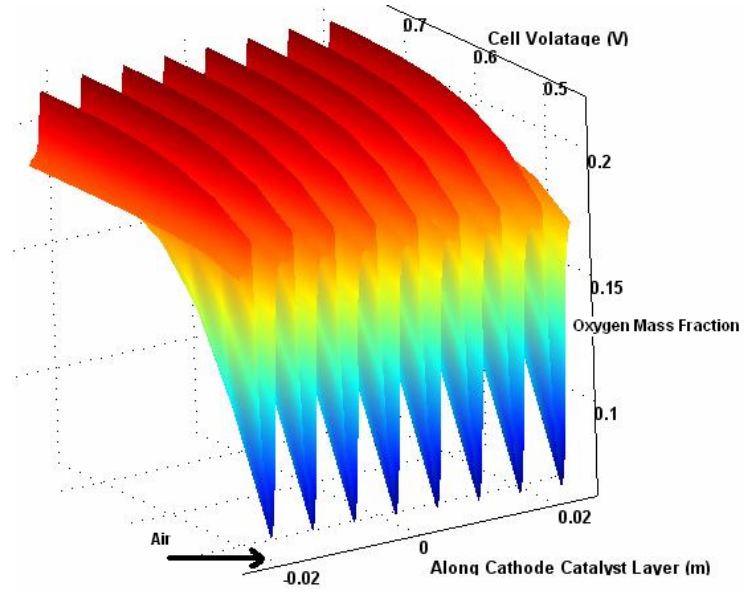
Figure 4-20: Oxygen mass fraction distribution in a cross section of the fuel cell along the cathode catalyst layer at different cell voltages
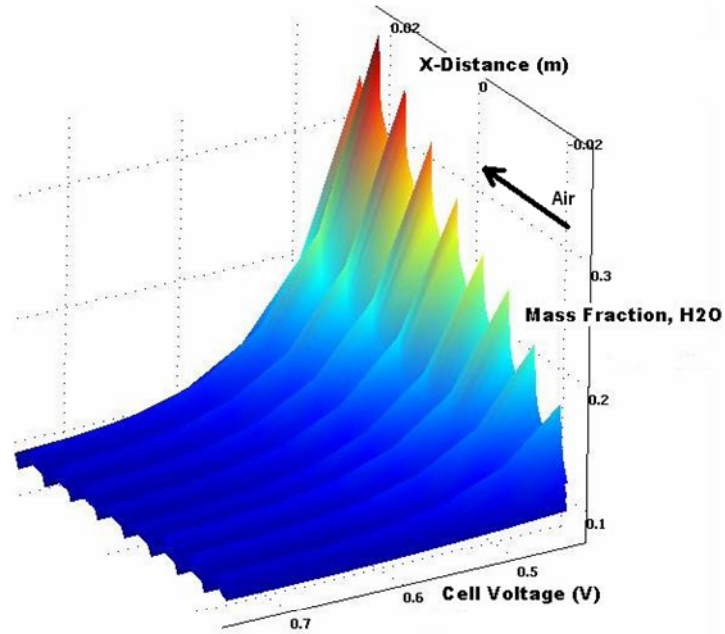
Figure 4-21: Water mass fraction distribution in a cross section of the fuel cell along the cathode catalyst layer at different cell voltages

4.4.3 Hydrogen Distribution along the Anode Side

The distribution of hydrogen along the anode side of the PEM fuel cell is important to study in order to improve the performance. Humidified hydrogen is used at the anode side of the PEM fuel cell to keep the electrolyte membrane wet. The water content at the anode side diffuses to the electrolyte membrane. 3D numerical analyses studying the distribution of hydrogen and water along the anode side of the perforated PEM fuel cell show a decrease in hydrogen and water mass fraction from the inlet to the outlet section. Figure 4.22 shows the distribution of hydrogen mass fraction along the anode side of the perforated PEM fuel cell at V = 0.5 volts.
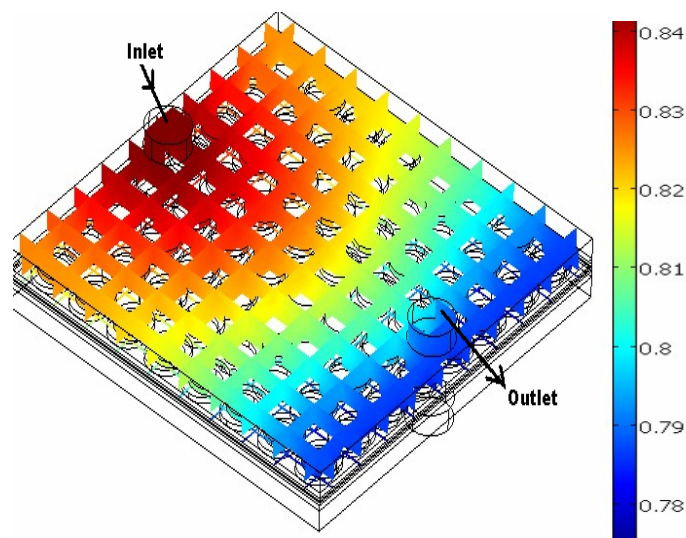
Figure 4-22: Hydrogen mass fraction distribution along the anode side at T = 333 K, V = 0.5 volts

Results show that the high consumption of hydrogen and water at the anode side of the PEM fuel cell at low cell voltages leads to a need for more water to diffuse to the electrolyte membrane to keep it wet. To analyse the distribution of hydrogen and diffusion of water to the electrolyte membrane, detailed numerical analyses have been carried out through a cross-section of the PEM fuel cell domain at the anode side. Figure 4.23 shows the distribution of hydrogen mass fraction along the anode catalyst layer in the cross section of the PEM fuel cell.

86
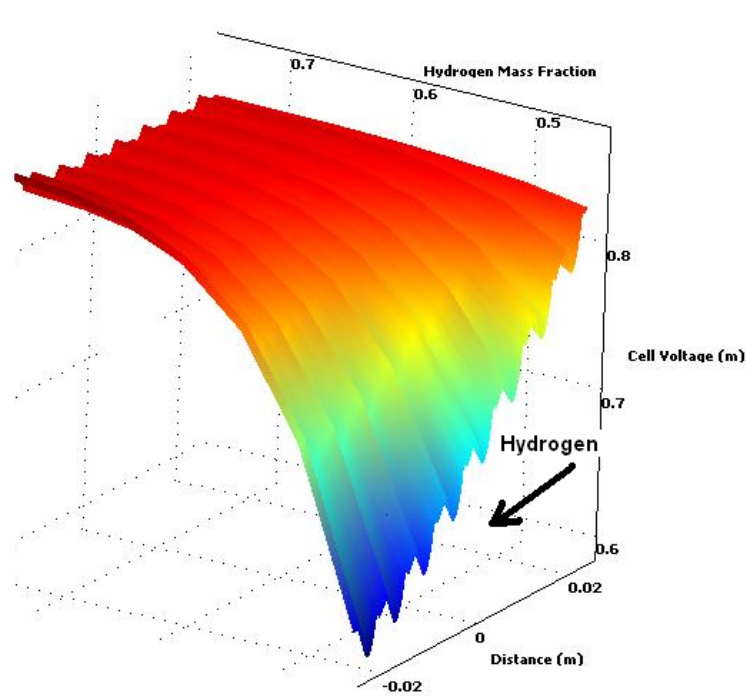
Figure 4-23: Hydrogen mass fraction distribution along the anode catalyst layer in a cross section of the fuel cell, T = 333K

Analyses show a high consumption of hydrogen at low cell voltages; this means that higher amounts of water are absorbed at low cell voltages to keep the membrane wet. At low cell voltages; electrochemical reaction rates at the cathode side are high, meaning that more protons are required to pass through the electrolyte membrane. Each proton carries some membrane water molecules with it (approximately one to three water molecules accompany each proton) as it passes through the membrane. This can lead to the possible membrane dryness at these low cell voltages. Therefore, humidified hydrogen is used at the anode side to keep the membrane wet. Detailed numerical analyses were carried out to explore the behaviour of the membrane water content at different cell voltages. Figure 4.24 and 4.25 show the variation of water activity and membrane water content along the cathode catalyst layer at different cell voltages.
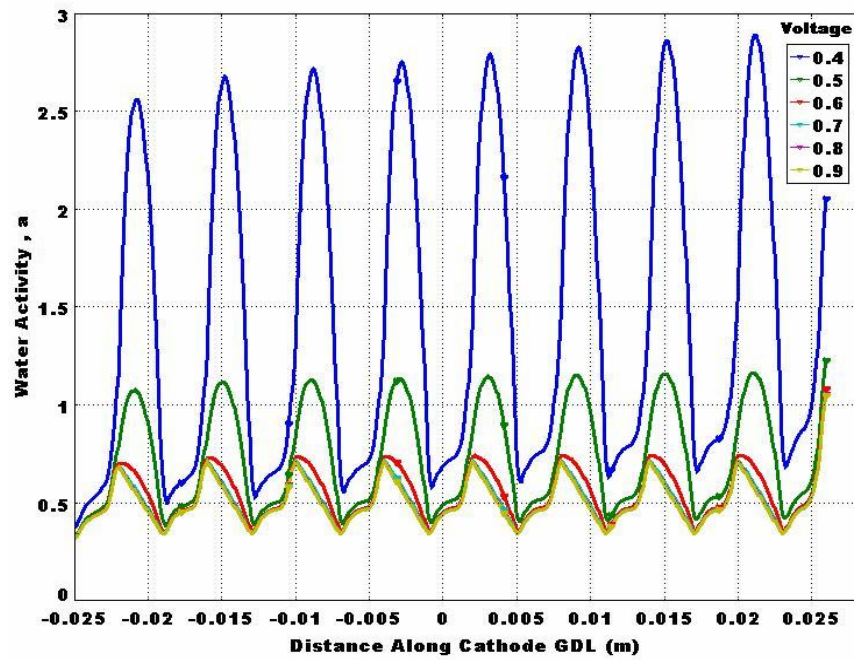
Figure 4-24: Membrane water activity along a cross-section of the perforated PEM fuel cell at different cell voltages, T = 333K
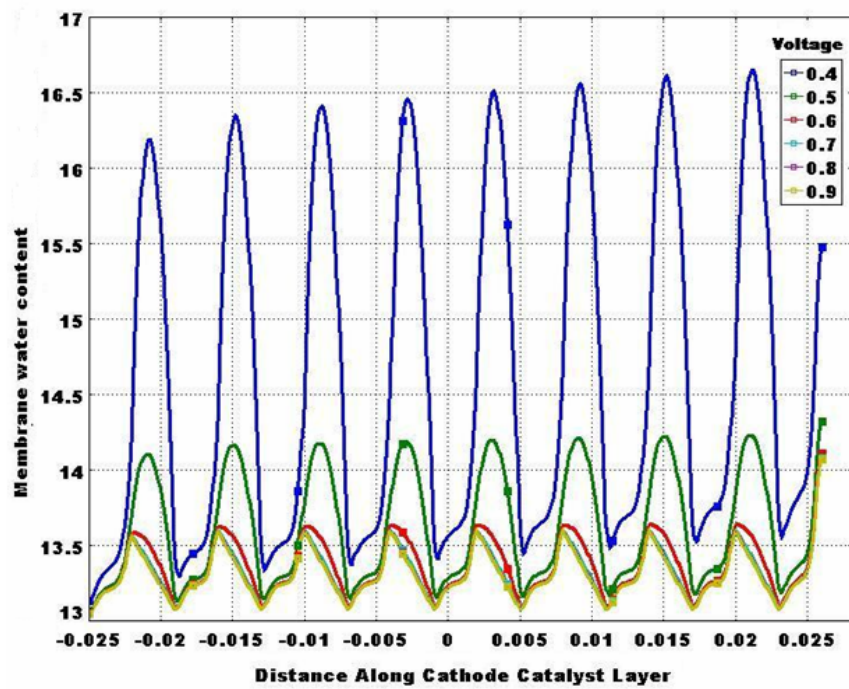
Figure 4-25: Membrane water contents along a cross-section of the perforated PEM fuel cell at different cell voltages, T = 333K

88

4.4.4 Ohmic Over-potential Distribution along the Cathode Side

The Ohmic over-potential is the potential loss caused by the resistance to electron transport in the PEM fuel cell electrode and gas diffusion layer. For a given load condition, the magnitude of the Ohmic over-potential depends upon the path travelled by the electrons. The longer the path, the larger the potential drop. In the perforated gas flow channel design configuration, numerical analysis shows that Ohmic losses are considerably higher below the open holes of the perforated plate while underneath the solid area of the perforated plate, the losses are low. Figure 4.26 shows the ohmic over-potential distribution along cathode side of the PEM fuel cell at V = 0.5 volts.

(Along Cathode Side of Fuel Cell)

(Along Cathode Catalyst Layer)
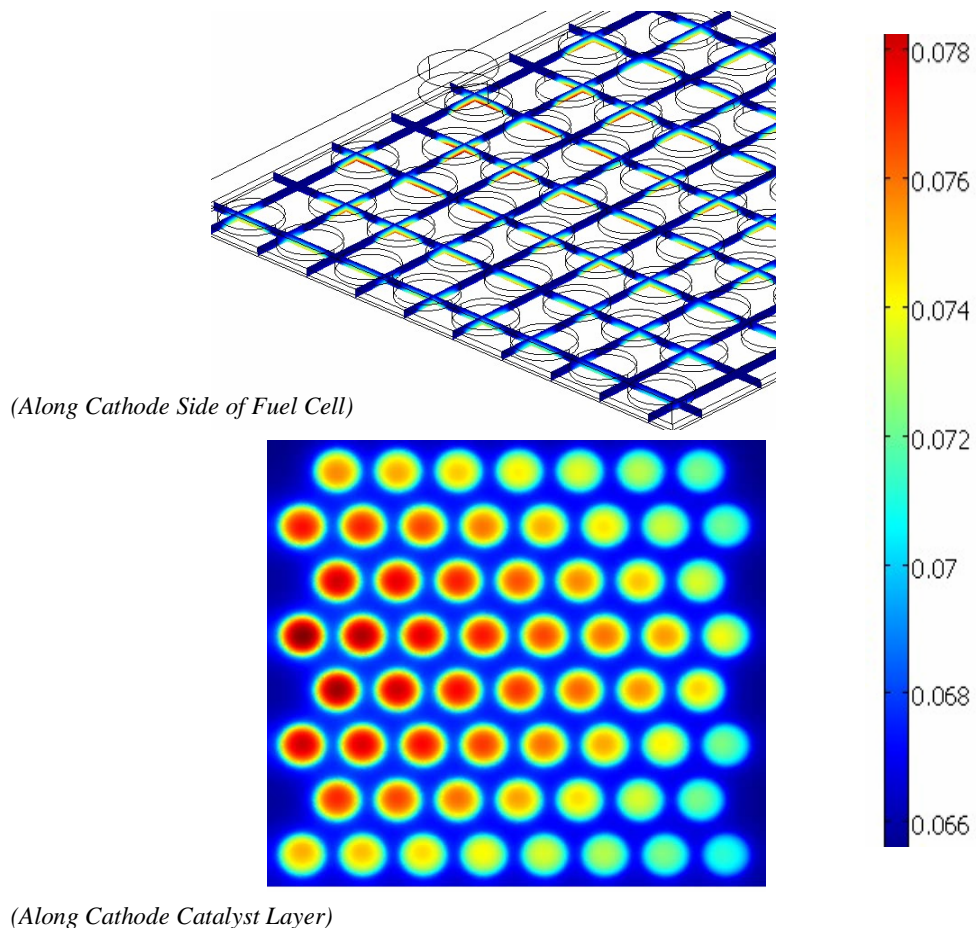
Figure 4-26: Variation of Ohmic over-potential along the cathode side of the fuel cell, V = 0.5 volts

4.4.5 Activation over-potential Distribution along the Cathode Side

The activation over-potential is due to driving the electrochemical reaction from an equilibrium state. It mainly depends upon the material properties and the availability of reactant species along the cathode catalyst layer. For this particular design configuration, the distribution of the activation over-potential is uneven along the fuel cell domain; it has a high value below the solid region of the perforated plate, while a low value of activation over-potential is observed below the open channels. This is mainly due to the availability of reactant oxygen just below the open channels, whereas under the solid area of the perforated plate, the electro-chemical reaction is low due to limited access of reactant species, leading to high activation over-potential. Figure 4.27 shows the distribution of activation over-potential along the cathode side of the perforated-type PEM fuel cell.
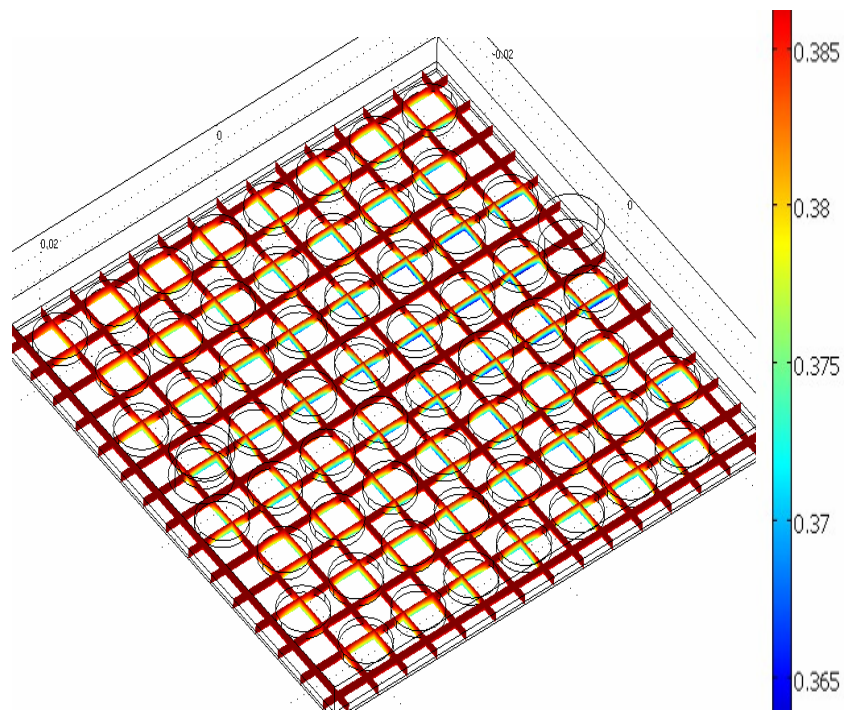
Figure 4-27: Variation of activation over-potential (volt) along the cathode side of the PEM fuel cell at V = 0.5 volts

4.4.6 Current Density Distribution along the Cathode Catalyst Layer

Current density is a function of oxygen concentration and activation over-potential along the cathode catalyst layer. The value of activation over-potential varies with the operating cell voltages; therefore, the value of current density is different at different cell voltages. Figure 4.28 shows the current density distribution along the cathode catalyst layer of the perforated type PEM fuel cell at two different load conditions.

(V = 0.4 Volts)   (V = 0.5 Volts)
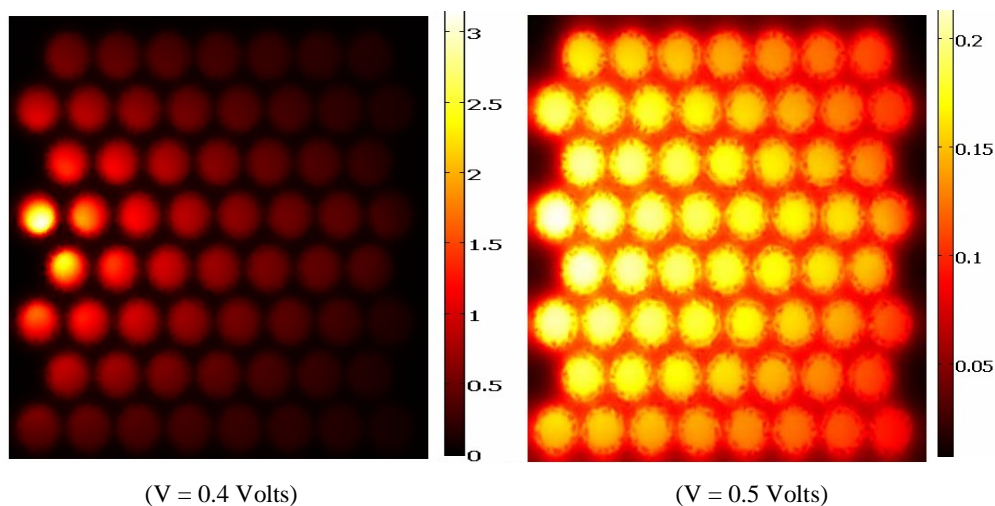
Figure 4-28: Current density distribution along the cathode catalyst layer at different load conditions

Results show that with the decrease of operating cell voltage, the overall value of current density increases along the cathode catalyst layer. There is no significant variation in the current density along the cathode catalyst layer at high cell voltages, which is mainly due to the low consumption of oxygen at these load conditions and high activation over-potential. For the perforated-type design configuration, analyses show that the value of current density is higher beneath the open areas of the perforated plate, whereas below the solid area of the perforated plate the value of current density is quite low.

4.5   Non-Isothermal Analysis

The actual operating principle of a PEM fuel cell is non-isothermal due to the heat generated as a by-product of the electrochemical reactions along the cathode catalyst layer. This heat is transferred to the PEM fuel cell domain and increases the overall operating temperature. Such increase in the operating temperature affects the overall performance of the PEM fuel cell. On one hand, it increases the rate of electrochemical reaction, but on the other hand it increases the chances of membrane dehydration which consequently affect the proton conductivity of the electrolytic membrane. Non-isothermal analyses of the performance of the PEM fuel cell provide a broader picture as these analyses can be used to find methods to counter the effect of temperature variation and its distribution along the fuel cell domain.

The temperature distribution along the fuel cell domain depends upon its material properties and design. The material properties can affect the thermal conductivity, whereas the design of the PEM fuel cell affects the distribution of reactants along the fuel cell domain, consequently affecting the convective rate of heat transfer from the fuel cell domain to the excess reactant air. The PEM-type fuel cell is well known for its low operating temperature range (293 - 363 K), therefore, a better fuel cell design is essential to improve the rate of heat removal from the PEM fuel cell domain to keep the operating temperature in the desired range.

This section presents the non-isothermal numerical analysis of the PEM fuel cell performance at different cell voltages. Two-dimensional steady state numerical analyses have been carried out in this regard. The temperature variation due to electrochemical reaction rates along the cathode catalyst layer and the resulting heat transfer to the fuel cell domain (gas channel) were studied closely to understand their effect on the overall performance. The effect of preheating the inlet air at the cathode side of the fuel cell was also analyzed to study its effect on the performance of the fuel cell in terms of water management and heat transfer.

The non-isothermal analysis shows a continuous increase in the PEM fuel cell operating temperature along its domain. In the case of a stainless steel gas flow distributor, the thermal conductivity of the stainless steel (SS316 L) is quite high, such that heat losses due to the thermal conductivity are not significant.

Results show that the solid areas of the perforated plate do not allow air to pass below them, resulting in the high operating temperatures observed in these solid regions. Moreover, frictional losses caused by the perforated holes are also noticeable in this design configuration. These effects vary the operating temperature along the domain of this perforated type PEM fuel cell. Figure 4.29 shows the temperature distribution along a cross section through the PEM fuel cell.
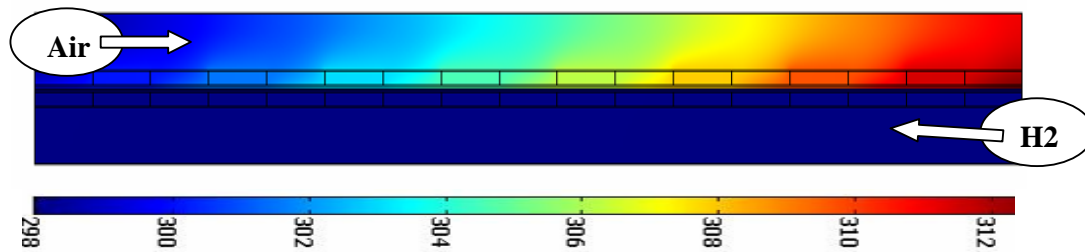
Figure 4-29: Temperature distribution along a cross section of the fuel cell at V = 0.45 and T_0 = 298 K
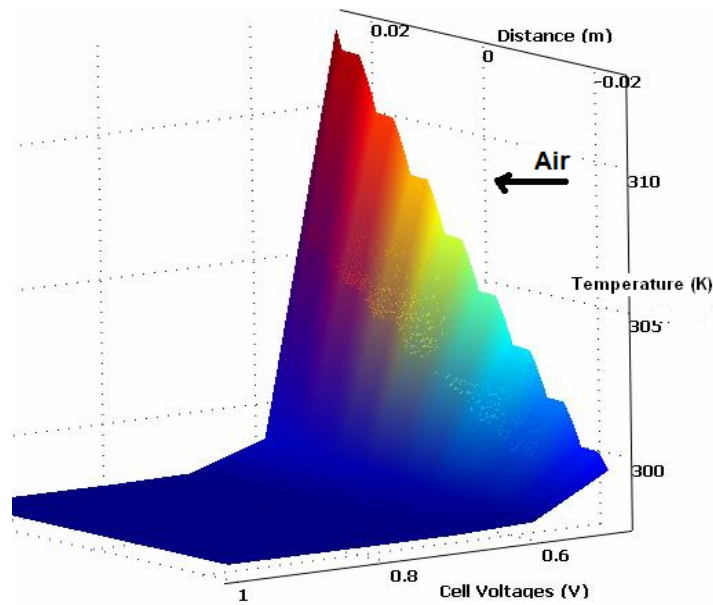
Figure 4-30: Temperature variation along the cathode catalyst layer at different voltages; $T_0 = 298$ K

The results show a continuous increase in temperature along the PEM fuel cell domain at all cell voltages. This increase in temperature is more prominent at low cell voltages because of high and stable electro-chemical reaction rates. The analysis shows high temperatures near the outlet section of the fuel cell which are mainly caused by the blockage of the GDL pores, leading to low permeability of the reactant species through the GDL.

The heat generated at the cathode catalyst layer is transferred to the electrodes and gas channels of the fuel cell, where the excess reactant air absorbs the heat and takes it away from the fuel cell domain. Heat transfer from the catalyst layer to the gas channel depends upon the heat transfer coefficient which is a function of fuel cell material (porous media and electrode). In this particular design configuration, the temperature distribution along the fuel cell domain is significantly influenced by the effective open area of the perforated gas distributor and its thermal conductivity. Figure 4.31 shows the non-isothermal performance polarisation curve of the fuel cell at an inlet temperature of 298 K.
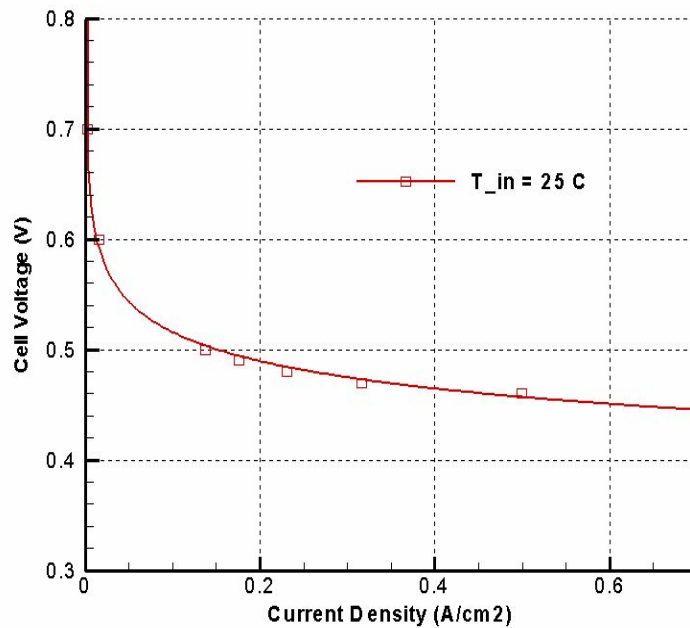
Figure 4-31: Performance polarisation curve along the cathode catalyst layer under non-isothermal conditions; $T_0 = 298$ K (25 C^o)

4.5.1 Effect of Preheating the Inlet Air

Pre-heating of the inlet air is a viable method to increase the reactant air moisture handling capacity. Although this increases the moisture handling capacity of the reactant air, it also raises the operating temperature of the PEM fuel cell. Such an increase in the operating temperature affects the membrane life and performance, as it can lead to dehydration of the membrane which could reduce its protonic conductivity, consequently affecting the overall performance of the PEM fuel cell. This section presents the non-isothermal numerical study concerning the effects of inlet temperature variation on the temperature distribution in the fuel cell domain and on the overall performance of the fuel cell.

Two-dimensional steady state numerical analyses were carried out at different inlet air temperatures ranging from 298 K to 313 K (25 to 40 °C) to study their effects. Results show an increase in fuel cell performance with the increase of inlet air temperature, but on the other hand it also increases the amount of heat generated due to higher electrochemical reaction rates which increase the operating

temperature of the fuel cell. Figure 4.32 shows the effect of preheating the inlet air on overall temperature distribution along the cathode catalyst layer at operating cell voltage = 0.5 V.
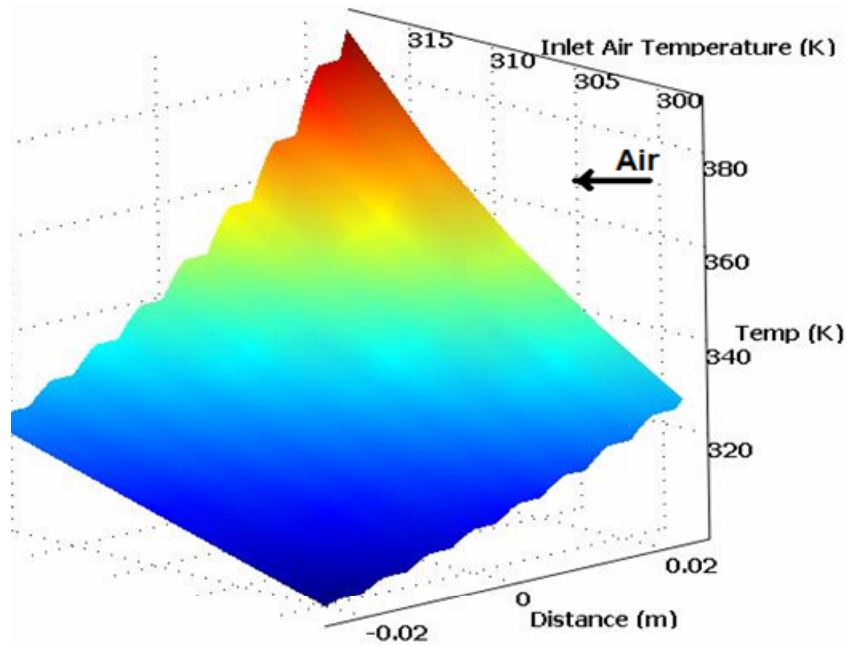
Figure 4-32: Effect of inlet temperature variation along the cathode catalyst layer at V = 0.5V

Analysis of the temperature variation shows an increase in the operating temperature along the cathode catalyst layer of the PEM fuel cell with increasing inlet air temperature. Preheating the inlet air increases the overall temperature of the fuel cell and speeds up the electrochemical reactions. Overall, the fuel cell performance increases with preheating the inlet air. Figure 4.33 shows the fuel cell polarisation curve for two different inlet air temperatures.
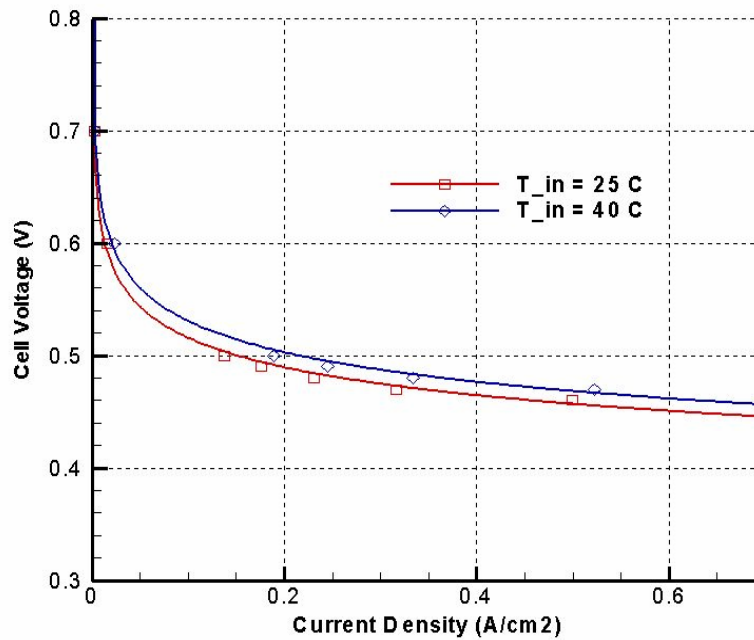
Figure 4-33: Effect of preheating the inlet air temperature on the overall performance of the PEM fuel cell

4.5.2 Findings

Following is a summary of the important findings based upon the two dimensional non-isothermal numerical study described previously:

i.   The analyses show that the perforated-type PEM fuel cell operating temperature variation is more prominent on the cathode side whereas at the anode side there is no significant variation in operating temperature and it remains almost constant.

ii. The fuel cell temperature reaches its maximum near the exit of the cathode side. Such an increase in temperature is mainly due to the blockage of GDL pores by product water.

iii. Preheating the inlet air improves the air moisture handling capacity, but on the other hand it increases the operating temperature of the PEM fuel cell due to the increased rate of electrochemical reaction.

4.6 Comparison Study of PEM Fuel Cell Performance with Perforated-Type and Serpentine Shaped Gas Flow Channels

This section presents a numerical comparison study of two different design configurations of the PEM fuel cell. Performance of the conventional PEM fuel cell with a serpentine shape is compared with the PEM fuel cell with a perforated-type gas flow distributor. Attention was focused primarily on the distribution of reactant species in both configurations. Steady state isothermal numerical analyses were carried out to compare their performances. A fuel cell with an effective area of 25 cm^2 is used in both cases. The operational and electrochemical properties used for this comparison study are similar as mentioned in Tables 3.2 and 3.3, while the geometric properties for both fuel cells are outlined below. The analysis was carried out under atmospheric pressure conditions.

Parameter	Perforated	Serpentine	Unit
Gas Channel length	0.05	0.05	m
Gas Channel width	0.05	0.05	m
Gas Channel Height	0.003	0.003	m
Perforated sheet Thickness	0.00055	-	m
Perforated Hole Diameter	0.003	-	m
Serpentine flow channel width	-	0.003	m
GDL Thickness	0.0002		m
Membrane Thickness	0.00018		m

Table 4-1: Geometric properties of perforated and serpentine PEM fuel cell domains

The main purpose of this study is to compare the performances of perforated PEM fuel cells with a conventional PEM fuel cell design. Detailed analyses were carried out to analyze the flow behaviour and the distribution of the reactant species along the PEM fuel cell domain in both design configurations. Figure 4.34 shows

vector presentations of the velocity distributions along the fuel cell domains in both design configurations.

(Serpentine Type)   (Perforated Type)
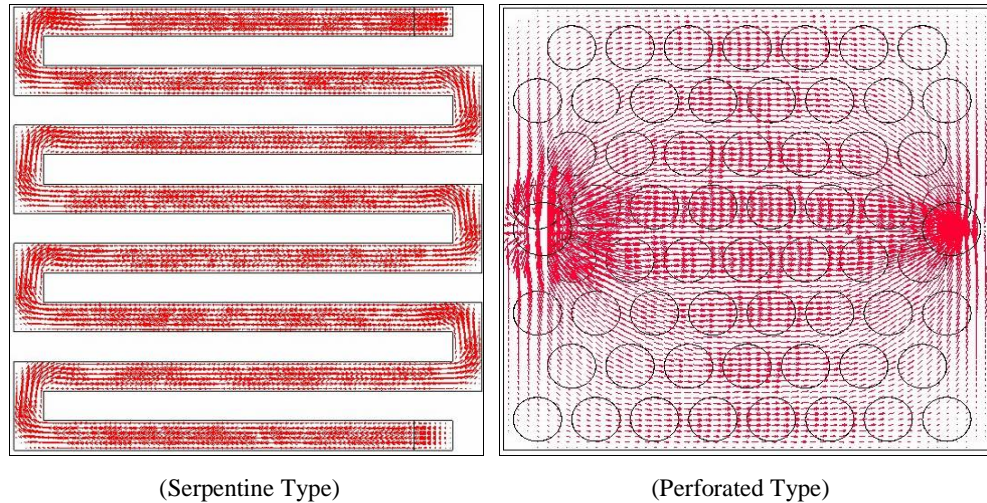
Figure 4-34: Vectors showing the velocity distribution along the fuel cell domain with serpentine and perforated gas flow channel configurations

Figure 4.34 shows a top view of the fuel cell domains for both design configurations. The results show that in the case of a serpentine shaped gas flow channel, a secondary flow exists at the corners of the flow channel that can lead to possible dead zones. In the case of the perforated-type gas flow distributors, it is observed that the velocity vectors are following the shortest possible path from the inlet to the outlet of the gas channel.

In the case of the perforated gas channel, the flow enters into the rectangular gas channel domain and is then allowed to move freely from the inlet to the outlet section. The reactant flow passively diffuses through the perforated holes while moving from the inlet to the outlet section. An examination of the velocity distribution shows secondary flows at the corners of the PEM fuel cell domain, but the effect of those secondary flows in the case of a perforated design configuration is not significant when compared with the serpentine type design configuration. At standard operating conditions, the overall distribution of velocity vectors along the fuel cell domain is better in the perforated type gas flow distributor than that of the serpentine shaped gas flow channel configuration.

The velocity distribution considerably influences the diffusion of reactant species along the gas diffusion layer. For perforated gas flow channels, the reactant flow enters from the inlet and spreads freely out along the gas channel and passes through the perforated holes, whereas in case of serpentine shaped gas channel, the flow is not free to move around. The flow moves through narrow gas channels where the side wall effects on the flow are considerable. These side wall effects do not allow the reactant flow to move smoothly from the inlet to the outlet section. Most of the reactant species get consumed near the inlet section when operating at atmospheric pressure conditions which leads to an uneven distribution of the reactant species along the serpentine PEM fuel cell domain. To overcome such issues, a high pressure flow can be used in a serpentine gas flow channel to move the reactants from the inlet to the outlet; another method is to increase the size of the gas channel, but this can add additional manufacturing costs.

Detailed numerical analyses were carried out during this comparison study to analyse the distribution of the reactant species. Analyses of the distribution of oxygen along both the fuel cell domains in both configurations indicated higher rates of oxygen consumption near the inlet section in the case of the serpentine design as compared to the perforated electrode design. This leads to reduced mass fractions of oxygen in the centre and outlet sections. Figure 4.35 shows the distribution of oxygen mass fraction along the cathode side of the fuel cell. In both cases, the operating cell voltage was $V = 0.5$ volts.
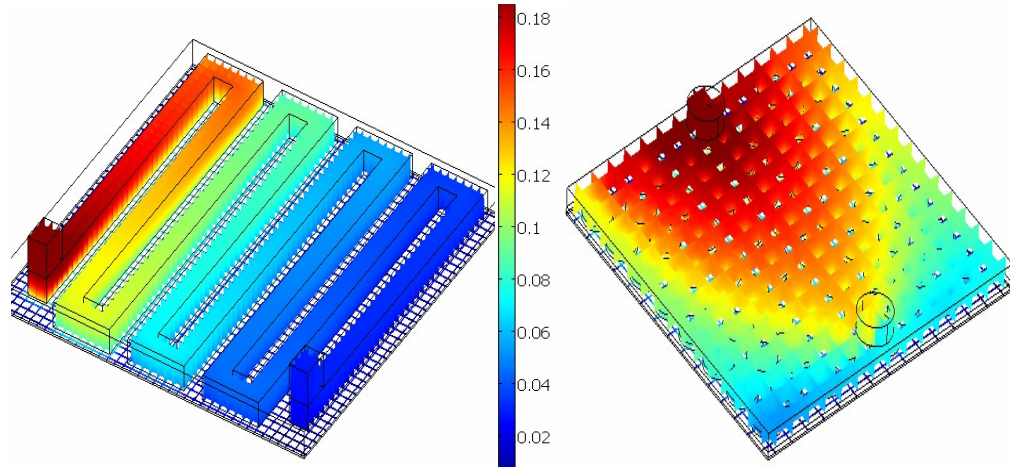
Figure 4-35: Oxygen mass fraction distributions along the cathode sides of the PEM fuel cell in serpentine and perforated gas flow channel configurations at V = 0.5 Volts, T = 333 K

The results show that in the case of a serpentine shaped gas channel, most of the oxygen is consumed near the inlet section of the fuel cell and very little oxygen reaches the outlet section, whereas in the case of the perforated gas distributor, a much better distribution of oxygen is observed. Such distributions of oxygen also significantly affect water management along the fuel cell domain. Figure 4.36 shows the distribution of water mass fractions along the cathode sides of the PEM fuel cell for both types of gas channel configurations.
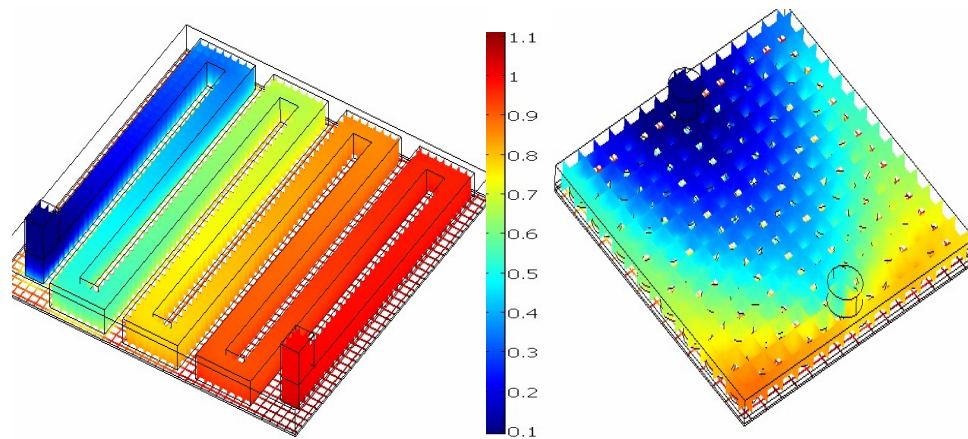
Figure 4-36: Water mass fraction distributions along the cathode sides of the PEM fuel cell in serpentine and perforated gas flow channel configurations at V = 0.5 Volts, T = 333 K

Figure 4.36 shows a high water mass fraction near the outlet section of the PEM fuel cell in the case of the serpentine shaped gas flow channel. This is mainly because of a lower availability of oxygen and reactant air near the outlet section, whereas in the case of the perforated-type gas flow distributor, a more even distribution of water mass fraction is observed.
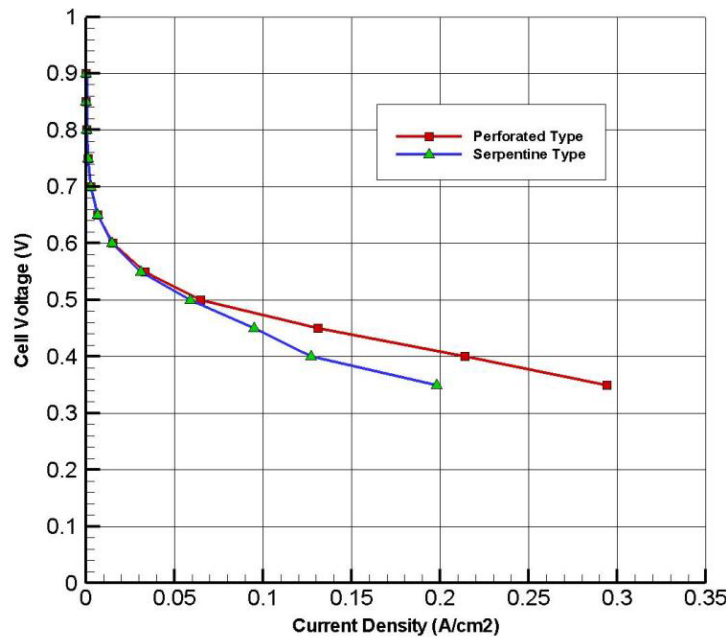
Figure 4-37: Performance comparison of PEM fuel cells with perforated and serpentine gas flow channels configurations at T = 333 K

The performance polarisation curves of the PEM fuel cell with both types of gas channel configurations show that the fuel cell with a perforated gas flow channel illustrated better performance in comparison to the fuel cell with a more conventional serpentine gas flow channel at standard atmospheric pressure. The main reason for such an improved performance in the case of the perforated gas distributor is the better distribution of reactant species along the fuel cell domain. Also, for the perforated gas flow channel, no high pressure flow is required to move the reactants along the fuel cell domain, whereas in the case of the serpentine shaped gas flow channels, a high pressure supply is required to move the reactants along the fuel cell domain. Moreover, the design configuration of the perforated-type fuel cell is simple when compared to the serpentine type, and no additional manufacturing efforts are required for the perforated gas flow channels. Overall, the

results show that the fuel cell with a perforated gas flow channel performs better than that with a serpentine shaped gas flow channel at atmospheric pressure conditions.

4.7 Summary

This chapter described the numerical modelling based performance analysis of a PEM fuel cell having a stainless steel perforated gas flow distributor. The fuel cell numerical design and experimental setup used for this novel configuration were discussed and explained. Results obtained from the base-case 3D numerical model were validated with the experimental data and a good agreement was found. Following the numerical modelling techniques used for the base-case model, detailed performance analyses of the perforated-type PEM fuel cell were carried out to gain an insight into the different transport phenomena taking place, such as species distribution, heat transfer and electrochemical kinetics.

Both isothermal and non-isothermal numerical analyses were carried out to understand the distribution of reactant and product species and their effect upon the electrochemical reaction rates along the domain of a PEM fuel cell with a perforated plate, something which is not easily possible with experimental techniques due to the reactive environment of the fuel cell domain. These performance analyses highlighted some design-related issues which can be examined to improve the performance of perforated PEM fuel cells, such as varying the effective open area of the perforated plate and the gas channel height. These issues are discussed in Section 5.4. A comparison study was also carried out to compare the distribution of species and the overall performance of the perforated PEM fuel cell with a standard fuel cell configuration that had a serpentine shaped gas flow distributor. Results showed that a perforated-type PEM fuel cell illustrated better performance at standard atmospheric pressure conditions.

CHAPTER 5

5 Parametric Performance Analysis of Perforated-Type PEM Fuel Cell

5.1 Introduction

This chapter describes the numerical base parametric study concerning the effect of different operating and design (geometric) parameters variation on the distribution of reactant/product species and the overall performance of the perforated PEM fuel cell. The numerical modelling techniques used for the validated base model at isothermal conditions were used for this parametric study. The PEM fuel cell performance at different operating and geometric conditions were compared using the polarisation curves and assessments of reactant/product species distribution along the perforated PEM fuel cell domain.

5.2 Selection of Parameters

PEM fuel cells are difficult to numerically model due to their complex non-linear multivariate nature. A large number of geometric and operating factors contribute to the performance and final output voltage of a PEM fuel cell. This motivates a 'Design of Experiment' (DOE) approach for the selection of such parameters to improve the performance of a PEM fuel cell [120]. The parameters that influence the performance of a PEM fuel cell can be grouped into two categories: geometric and operating parameters. It is not possible to change the geometry in real-life application of the PEM fuel cell without manufacturing multiple rigs, leaving the operating conditions as the only variable that can be changed. Nevertheless, the use of numerical modelling techniques allows the geometric variables to be changed easily to analyse their effects on the PEM fuel cell performance at different operating conditions.

The main concern of this research work is to improve the distribution of the reactant species and the performance of the PEM fuel cell by simplifying the gas flow channel design which will result in reducing the manufacturing cost. For this purpose, a detailed parametric study was carried out to analyse the performance of the perforated-type PEM fuel cell at different operating and geometric conditions. The operating and geometric parameters used for this parametric study were selected based on the literature review and analyses of the species distribution along different sections of the perforated fuel cell domain from the base case numerical model, discussed in the previous chapters of this thesis.

The operating parameters for this study were mostly selected from the literature review [1, 2, 6, 62, 65, 78, 92]. These parameters were selected based upon their effect on the flow behaviour and electrochemical reaction rates in the PEM fuel cell. The operating temperature, gas diffusion layer porosity and the exchange current density were selected as operating parameters to be analysed during this parametric study. The reactant flow behaviour and its distribution can be influenced by the operating temperature and GDL porosity, whereas the exchange current density directly influences the rate of oxidation and reduction along the catalyst layers.

The geometric parameters used for this parametric study were selected from the analyses of reactant and product species distribution. The base-case numerical model analysis provided an insight into the reactant/product species distribution along the perforated PEM fuel cell domain and highlighted some design issues that needed to be addressed in order to improve the distribution and the overall performance of the perforated PEM fuel cell. Perforation hole diameter, perforation hole shape, gas channel height, fuel cell inlet/outlet hole diameters and locations were selected as geometric parameters for this parametric study. The main criteria for the selection of the geometric parameters were to improve the distribution of species without requiring any major design changes.

Parameters	Tested Range (Units)	Reasons
Operating temperature	313 - 353 (Kelvin)	Affects the rate of water removal and electrochemical reaction
Cathode exchange current density	1×10^{-2} - 5×10^{-3} (A/cm^2)	Affects the rate of electrochemical reactions
Gas diffusion layer porosity	-	Affects the reactant and product species transport through GDL
Operating pressure	Analyses performed at atmospheric pressure conditions to avoid the extra cost of compression	
Mass flow rate	Due to the very small amounts of hydrogen needed which is difficult to measure accurately considering the available apparatus, this parameter was not analyzed	

Table 5-1: List of fuel cell operating parameters considered during the parametric study

Parameters	Reasons
Perforated hole diameter	Affects the diffusive transport of species and frictional losses
Perforated hole shape	Affects the species distribution
Gas channel height	Affects the residence time of reactant species and diffusive flux
Inlet/outlet hole diameter	Affects the mass flow rate and distribution of reactant species
Inlet/outlet hole location	Affects the distribution of reactant and product species

Table 5-2: List of fuel cell geometric parameters considered during the parametric study

(These parameters were selected on the basis of their cost effectiveness and likelihood of implementation without requiring a major design change for the perforated-type design approach)

5.3 Effect of Operating Parameter Variation

This section describes a two dimensional parametric study examining the impact of varying different operating parameters on the overall performance of the perforated-type PEM fuel cell. Detailed parametric analyses were carried out to explore the effects of GDL porosity, operating temperature and exchange current density on the overall performance of perforated-type PEM fuel cells.

5.3.1 Effect of Gas Diffusion Layer Porosity

The gas diffusion layer is a thin porous media that efficiently distributes the reactant species and collects the product species. Its performance depends upon the porosity and permeability values of the material. The porosity of the GDL is the ratio of pore volume to the total volume. Three different values of the GDL porosities were examined, ranging from 0.3 to 0.5 (30 % to 50%). Attention was focused on the analysis of their effects on the distribution of reactant species and the collection of product species along the PEM fuel cell domain.

With a decrease in GDL porosity, it becomes increasingly difficult for the reactant species to permeate through the GDL and reach the catalyst region. Therefore, GDL porosity considerably influences the concentration of the reactant species and water flooding characteristics in the PEM fuel cell. Increasing the GDL porosity improves the diffusion of the reactant air through the GDL, which improves the electrochemical reaction rates and the rate of water evaporation from the fuel cell domain. Figure 5.1 shows a comparison of the water mole fraction variation along the cathode catalyst layer at two different values of the GDL porosity.
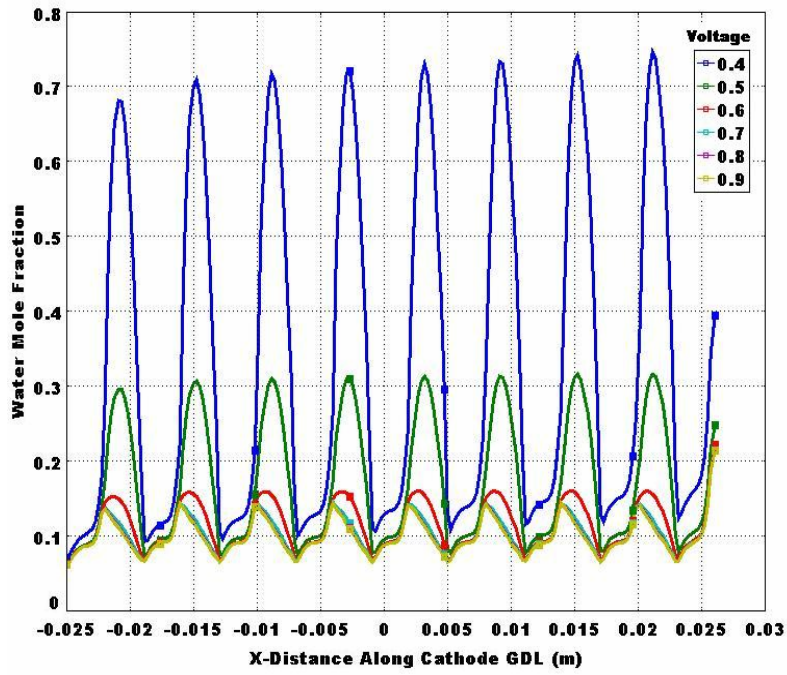
(a)
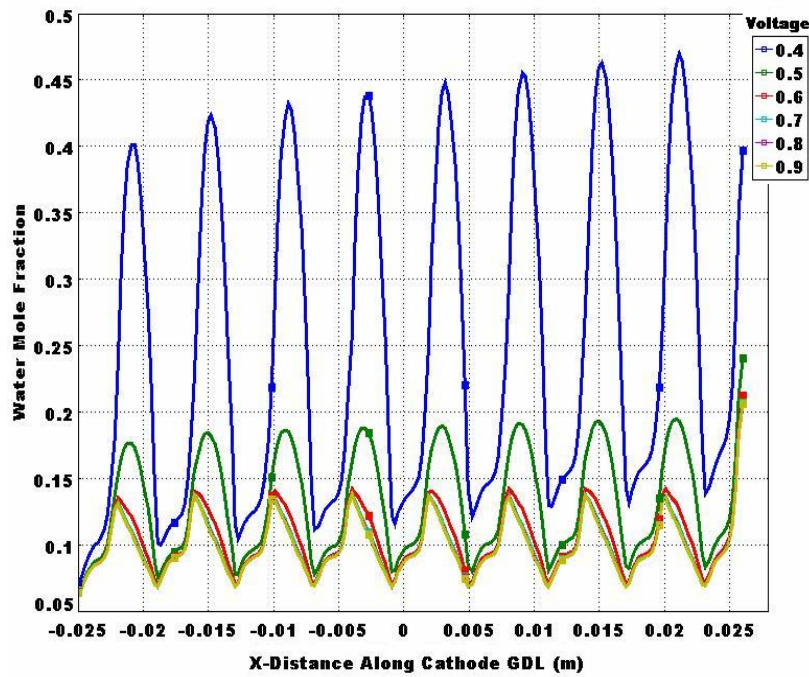
(b)

Figure 5.1: Variation of water mole fraction along the cathode/ GDL interface at two different values of GDL porosity a) 30 %, b) 70% at T = 333 K

Figure 5.1 indicates that there exists a considerable difference in the mole fraction of water along the cathode catalyst layer at two different values of GDL porosity. The excess water flooding at higher electro-chemical reaction rates blocks the GDL pores, which causes an additional obstruction which limits the reactant air from permeating through the GDL. This behaviour is not considerable at high values of GDL porosity, but at lower values, it is quite significant. Figure 5.1 also showed an uneven behaviour of the mole fraction variation at the GDL/catalyst layer interface, which is mainly due to the solid areas of the perforated gas distributor. Just below the solid areas of the perforated gas distributor, high values of water mole fractions were observed; those values are attributed to the limited access of air in these regions. This is a design problem which can be minimised by undertaking some design improvements such as changing the perforated holes diameter and/or shape.

Overall, variation in the GDL porosity affects the concentration losses along the PEM fuel cell domain. Results show that there is no significant influence of the GDL porosity variation on the activation and Ohmic losses. Figure 5.2 shows the performance polarisation curves of the PEM fuel cell at three different values of the GDL porosity at T = 333 K.
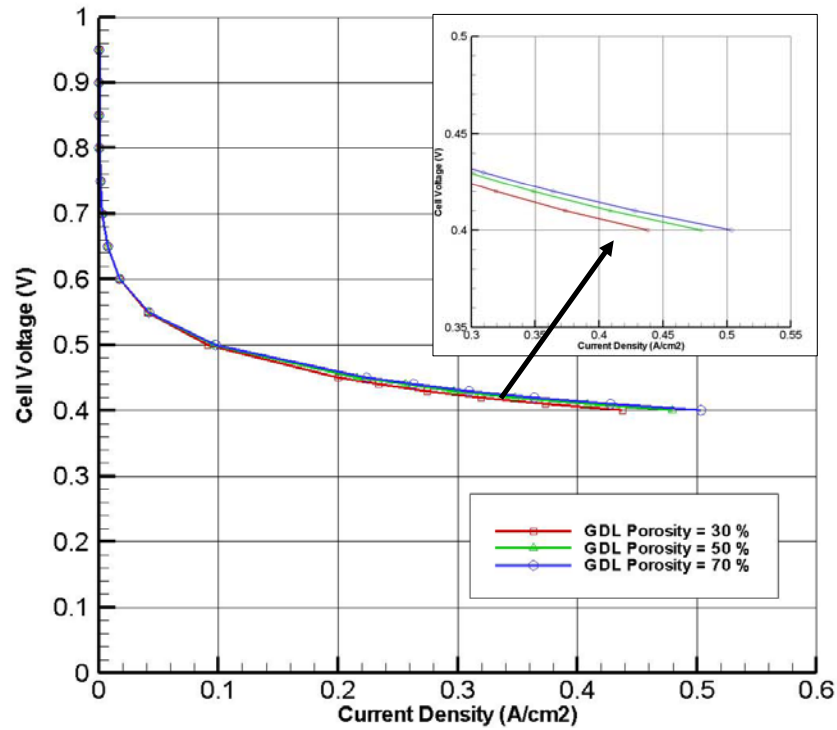
Figure 5.2: Perforated type PEM fuel cell polarisation curves at different values of GDL porosity. It is indicated that the activation and Ohmic losses are not significantly influenced due to GDL porosity variations

5.3.2 Effect of Operating Temperature Variation

The operating temperature can play an important role towards improving the performance of a PEM fuel cell. An increase in the PEM fuel cell operating temperature improves the rate of electrochemical reactions along the cathode catalyst layer and also increases the rate of product water removal from the fuel cell domain, as an increase in operating temperature improves the water handling capacity of the reactant air. Such increases in the fuel cell temperatures also affect the membrane performance and membrane life, as increases in temperature can result in membrane dryness and rupturing. Therefore, a comprehensive parametric study is essential to explore these effects and to find an optimum temperature for a particular design and operating condition of the PEM fuel cell. This section presents a parametric study examining the effect of operating temperature variation on the overall performance of the perforated type PEM fuel cell.

The numerical analyses show that an increase in PEM fuel cell operating temperature increases the consumption of oxygen along the cathode catalyst layer. This is an indicator of an increase in the rate of the electro-chemical reaction. With an increase in the electrochemical reaction rates, the amount of water generated as a by-product of the electro-chemical reaction also increases, which can lead to flooding. Some amount of this water diffuses back to the electrolyte membrane while most of it moves towards the gas channel and evaporates with the excess reactant air.

An increase in the operating temperature of the reactant species (air) leads to a change in the saturation pressure that consequently affects the heat absorbing capability of the reactant air. This affects the overall performance of the PEM fuel cell. To analyse this effect, a detailed parametric study was carried out at different operating temperatures ranging from 313 k to 353 K (40 ^{o}C to 80 ^{o}C). Figure 5.3 shows the polarisation curves of a perforated PEM fuel cell at different operating temperatures.
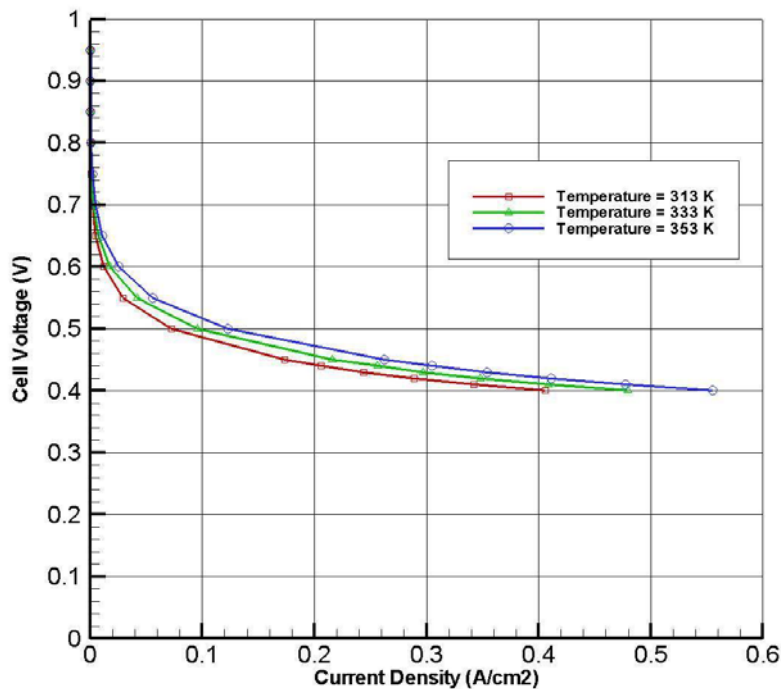
Figure 5.3: The polarisation curves of a perforated type PEM fuel cell at different operating temperatures

Figure 5.3 shows an increase in the performance of the PEM fuel cell as the operating temperature increases. Increases in the operating temperature mainly affect the activation potential losses. Results also show a decrease in the activation potential loss as the operating temperature is increased. Increasing the operating temperature also affects the concentration over-potential, as the increase of operating temperature improves the heat capacity of the reactant air, which in turn reduces the chances of water flooding and blockage of the GDL pores, consequently reducing the concentration losses and improving the performance of the PEM fuel cell.

5.3.3 Effect of Cathode Exchange Current Density Variation

The exchange current density defines the rate of oxidation and reduction at the electrode in terms of current. The magnitude of the exchange current density is a function of material composition, surface roughness and electrode surface impurities. In the case of the PEM fuel cell, exchange current density strongly depends upon the material properties of the electrode and the presence of the catalyst along the catalyst layer surface. The PEM fuel cell's performance can be influenced by the exchange current density. This section presents a parametric study about the effect of cathode exchange current density variation on the overall performance of the PEM fuel cell at T = 333K. For this study, perforated type PEM fuel cell performance at three different values of the exchange current density is analysed. No particular numerical modelling is carried out regarding surface roughness and the impurities on the electrode surface.

Results show that a change in exchange current density mainly affects the activation potential losses. An increase in the exchange current density reduces the activation losses by improving the rate of oxidation and reduction along the catalyst layer. Overall, the parametric analysis shows that increasing the cathode exchange current density results in a considerable increase in the PEM fuel cell performance. Figure 5.4 shows the effects of exchange current density variation on the overall performance of the PEM fuel cell.
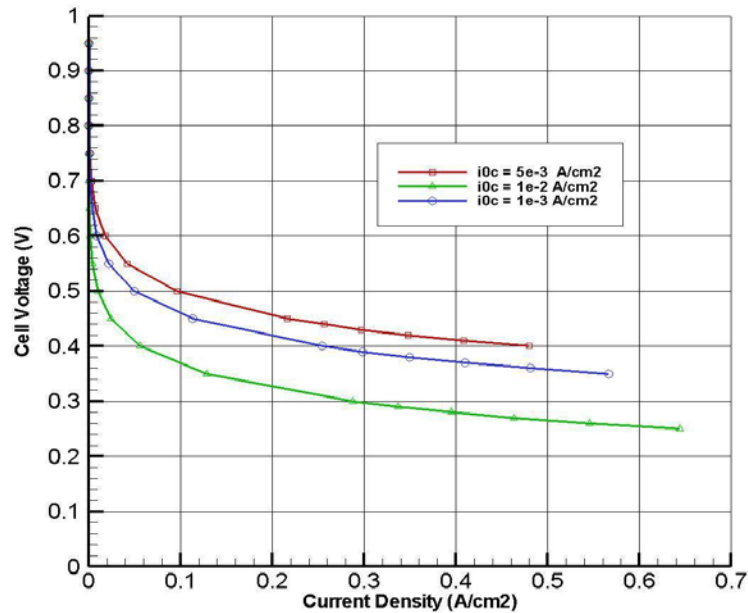
Figure 5.4: Effects of cathode exchange current density variation on the performance of the perforated PEM fuel cell, T = 333 K

5.3.4 Findings

The following are some important findings based upon the results obtained from the parametric study on the effect of varying different operating parameters on the overall performance of the perforated type PEM fuel cell:

i. An increase in the operating temperature improves the rate of electrochemical reaction and reduces the activation potential loss along the cathode catalyst layer. The parametric study shows an overall increase in PEM fuel cell performance with the increase in its operating cell temperature.

ii. An increase in the performance of the PEM fuel cell is observed in conjunction with an increase in the GDL porosity, as increasing the GDL porosity improves the efficiency with which the reactant species permeate through the GDL.

iii. An increase in exchange current density reduces the activation potential losses and improves the overall performance of the PEM fuel cell.

113

5.4   Geometric Parametric Study

This section presents a parametric study concerning the variation of different geometric parameters of the perforated-type PEM fuel cell, such as perforated hole diameter, perforated hole shape, gas channel height and the effect of inlet and outlet port locations on the distribution of reactant/product species and overall performance. These geometric parameters are selected on the basis of observations obtained from the base case numerical and experimental models about the distribution of reactant/product species. This parametric study is carried out using both numerical and experimental techniques, where numerical analyses are carried out at steady state isothermal conditions. The overall performances at these geometric conditions are compared using the polarisation curves and the assessment of the distribution of reactant species along the fuel cell domain. The following sections describe the results obtained from this parametric study.

5.4.1   Effect of Perforated hole Diameter Variation

The effect of perforation holes diameter was analysed to examine its effect on frictional losses and on the rate of diffusion of species through the holes. To study the effect, two different hole diameters (2.5 mm and 5 mm) were used with a constant gas channel (trough) height of 5 mm. For both cases, the effective open area of the perforated plate used was 55 % and 63% respectively. Results obtained from numerical analyses were compared with the experimental data and a good agreement was found.

The main purpose of increasing the perforation hole diameter is to improve the distribution of the reactant species along the fuel cell domain. An increase in the effective open area of the perforated plate generally enhances the reactant species concentration along the fuel cell domain, which was closely studied during the analysis. Figures 5.5 and 5.6 show the distribution of oxygen and water along the cathode catalyst layer for the two different hole-diameters.

114
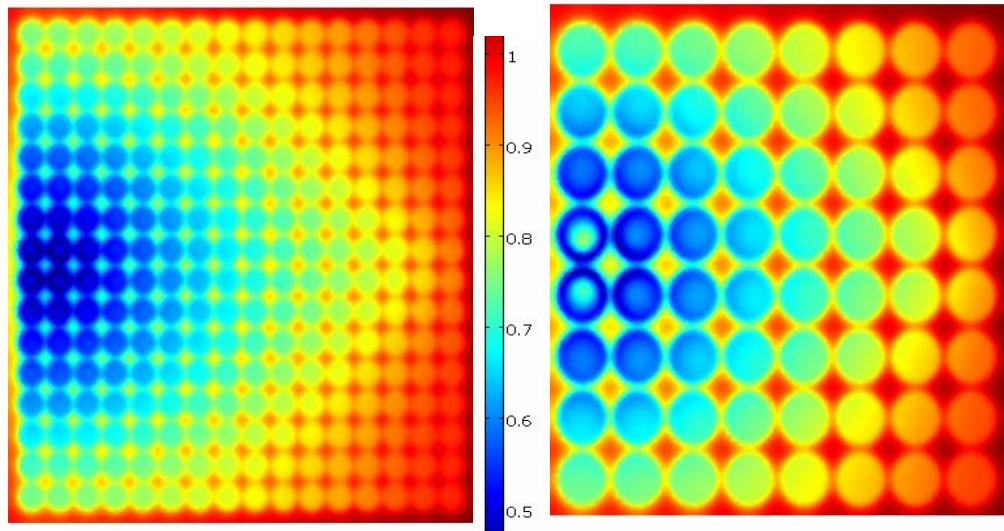
a) Diameter= 2.5 mm, Trough Height= 5 mm   b) Diameter= 5 mm, Trough Height= 5 mm

Figure 5.5: Effects of the perforated hole diameter variation on water mass fraction distribution along the cathode catalyst layer at V = 0.5V
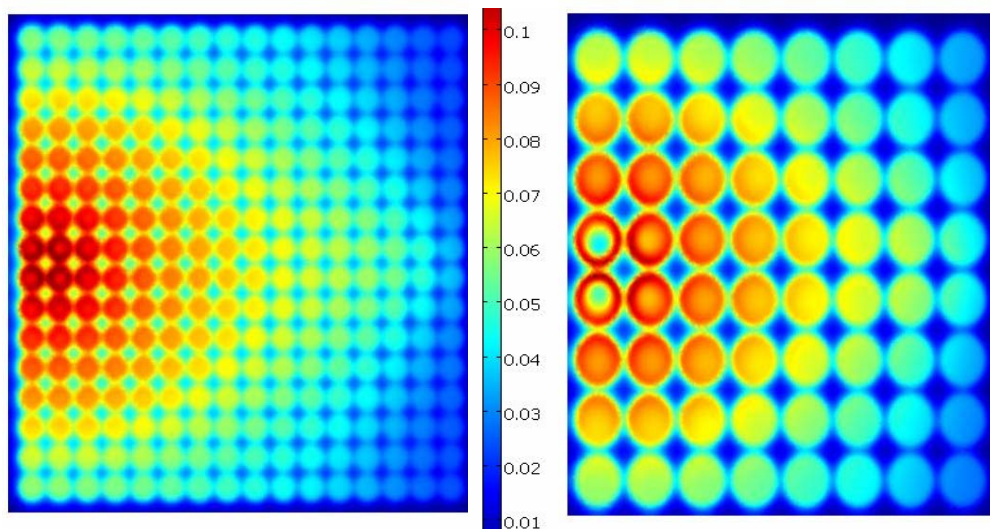
a) Diameter=2.5 mm, Trough Height= 5 mm   b) Diameter= 5 mm, Trough Height= 5 mm

Figure 5.6: Effects of the perforated hole diameter variation on oxygen mass fraction distribution along the cathode catalyst layer at V = 0.5 V

The above figures show a comparison of oxygen and water mass fraction distributions along the cathode catalyst layer for two different perforated hole diameters. Results show an increase in the oxygen mass fraction and a decrease in water mass fraction with an increase in perforated hole diameter. An increase in perforated hole diameter also reduces the frictional losses to flow while passing through the perforated holes as effects of perforated holes side wall shear stresses reduce to a certain extent with the increase in perforated hole diameter. All these factors lead to an improved distribution of oxygen mass fraction along the cathode catalyst layer that consequently improves the electrochemical reaction along the catalyst layer and reduces water flooding. Figure 5.7 shows the distribution of current density along the cathode catalyst layer of a perforated type PEM fuel cell at V = 0.5 volts.

a) Diameter= 2.5 mm, Trough height= 5 mm   b) Diameter= 5 mm, Trough height= 5 mm
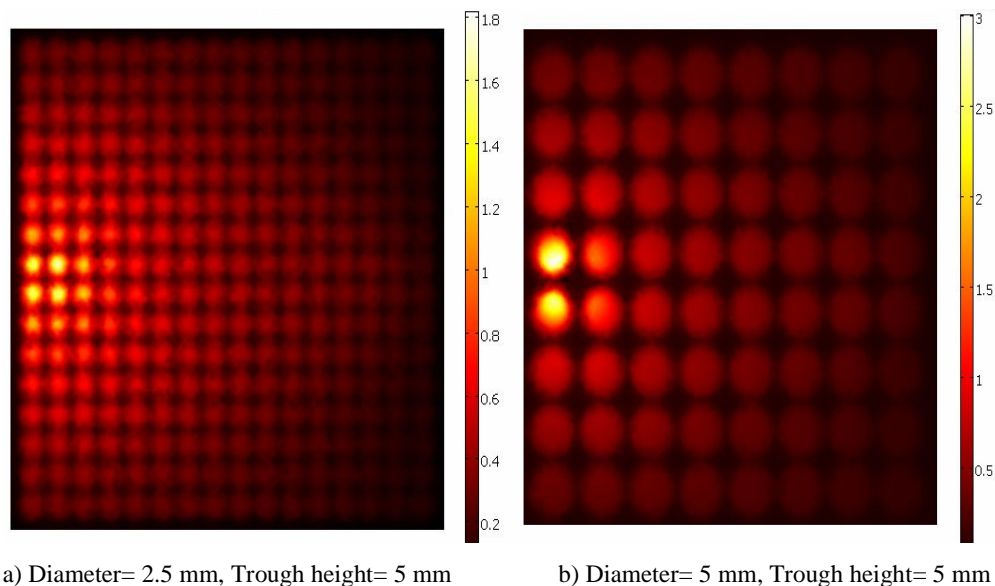
Figure 5.7: Effect of perforated hole diameter variation on the distribution of current density along the cathode catalyst layer at V = 0.5 volts

Figure 5.7 shows an increase in current density along the cathode catalyst layer when the perforated hole diameter is increased. This increase in the value of the current density is due to an improvement in the distribution of the reactant species along the cathode catalyst layer when the perforated hole diameter is increased.
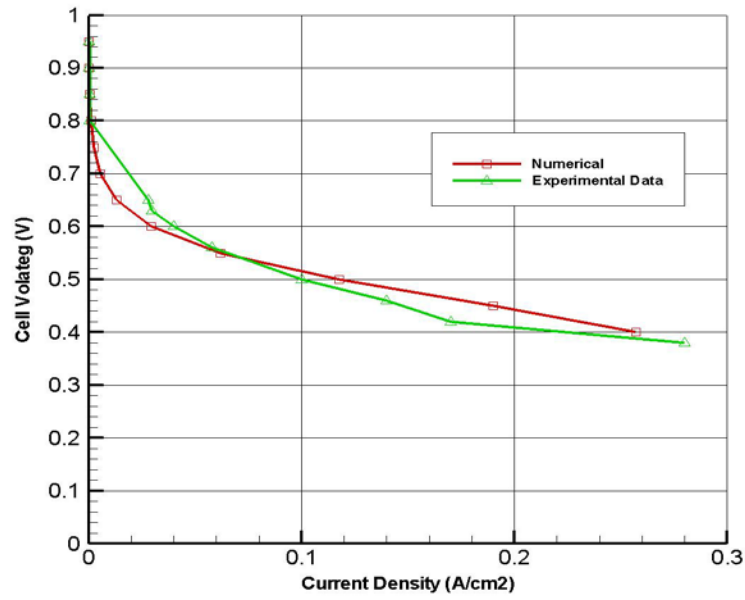
a) Perforated hole diameter = 2.5 mm; Gas trough height = 5 mm
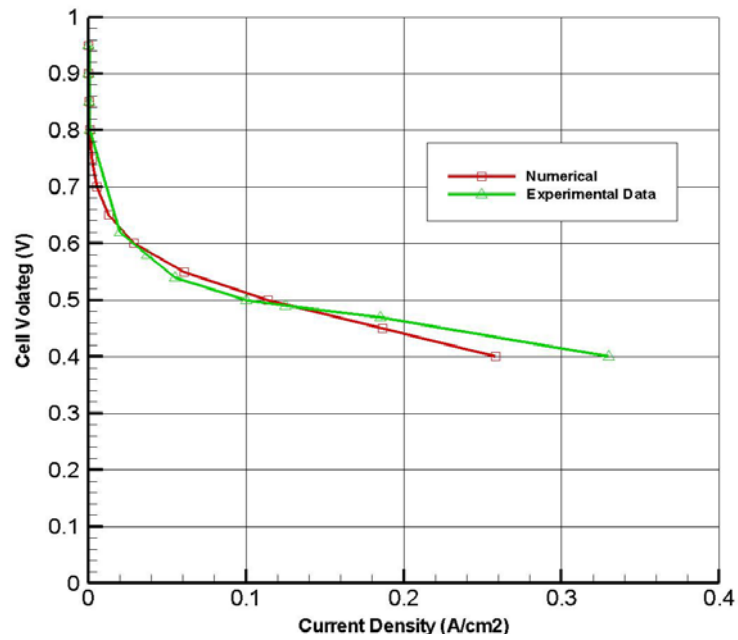
b) Perforated hole diameter = 5 mm; Gas trough height = 5 mm

Figure 5.8: The effects of perforation hole diameter on the performance of a PEM Fuel cell at T = 333 K. Comparison of the numerical and experimental results.

5.4.2 Effects of Perforated Hole Shape

The perforated hole shape is another interesting design feature that needs to be addressed to identify its influence on the distribution of the reactant species and the overall performance of the perforated-type PEM fuel cell. The perforated hole shape affects the frictional losses, but at low Reynolds numbers these frictional losses are not significant. Moreover, perforated hole shape also affects the diffusion of reactant species and the removal of product species from the membrane electrode assembly to the gas channel. To explore the effects of the hole shape, two different geometries (circular and trapezoidal) are considered. Figure 5.9 shows two cross sectional views of the velocity profile at the centre of the fuel cell domain for two different perforated hole shapes.

(Circular Holes)
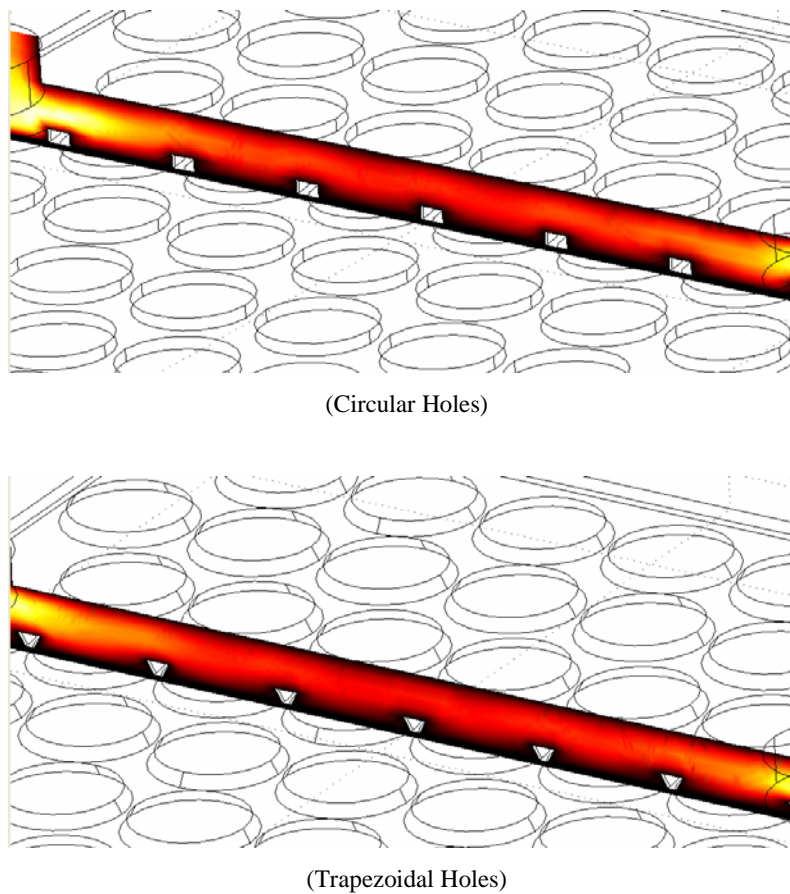
(Trapezoidal Holes)

Figure 5.9: Cross sectional views of the velocity profiles in the case of circular and trapezoidal holes

The trapezoidal shaped perforated holes have a larger open area facing the gas diffusion layer as compared to the circular holes. An increase in the open area facing the GDL improves the removal of product water consequently reducing the concentration losses. Results obtained from this study show that a small reduction in concentration losses was observed, while no change in the activation and Ohmic losses was observed when changing the geometry of the perforated holes from circular to trapezoidal shape. Overall, the results show a small increase in the performance of the PEM fuel cell in the case of trapezoidal shape perforated hole, but this change is not very significant. The polarisation curves are shown in Figure 5.10 below:
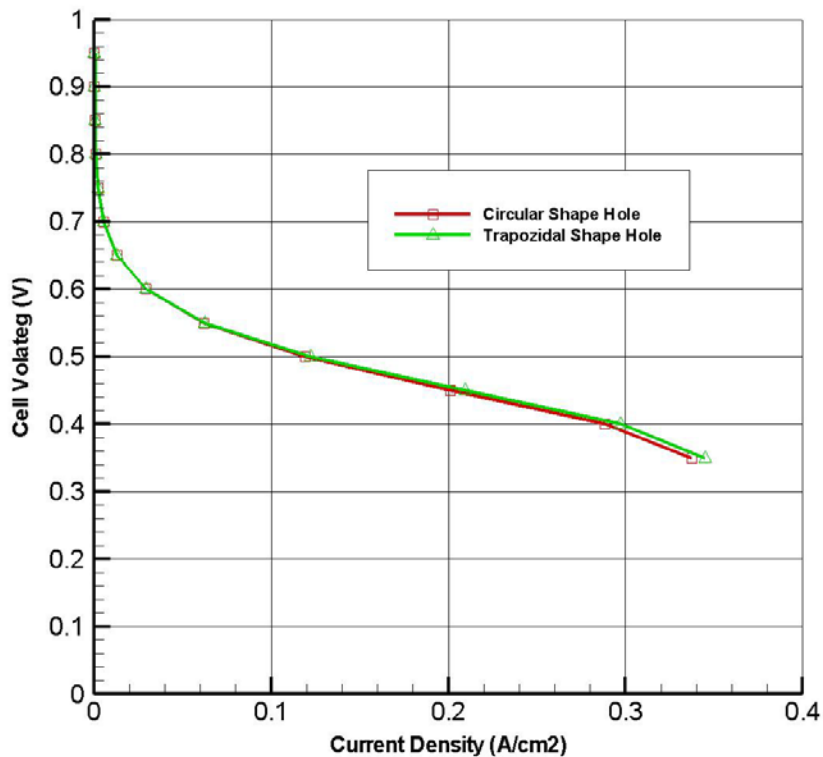
Figure 5.10: Polarisation curves for the perforated-type PEM fuel cell with two different perforated hole shapes at T = 333 K

119

5.4.3 Effect of Gas Channel Height Variation

The gas channel height is an important design parameter, as it can affect the flow behaviour along the fuel cell domain. In the perforated-type PEM fuel cell design configuration, the reactant flow enters into the gas channel and moves freely towards the outlet. The perforated plate is attached below the rectangular-shaped gas channel. A change in the gas channel height effects the passive diffusion and residence time of the reactant species along the fuel cell domain. Detailed parametric analyses were carried out to analyse the effect of gas channel height on the distribution of species and the overall performance of the perforated-type PEM fuel cell.

The gas channel height also affects the boundary layer characteristics and side-wall shear stresses that affect the residence time of the reactant gases; as well as the convective and diffusive fluxes of the reactant species along the fuel cell domain. This section presents a parametric study which examines the effect of gas channel height variation on the overall performance of the fuel cell. To study this effect, two different gas channel heights (2 mm and 5 mm) were taken into consideration and the distribution of the reactant species was closely studied during these analyses.

Results showed that with a decrease in gas channel height, the distribution of reactant species along the fuel cell domain improved. The increase in the performance was mainly attributed to a larger boundary layer thickness when smaller gas channel heights were used. Such an increase in the boundary layer thickness improves the diffusion rate and residence time of the reactant species and also passively forces the reactant species to pass through the perforated holes. Figure 5.11 shows the distribution of oxygen and water mass fraction along the cathode catalyst layer for two different gas channel (trough) heights.

120
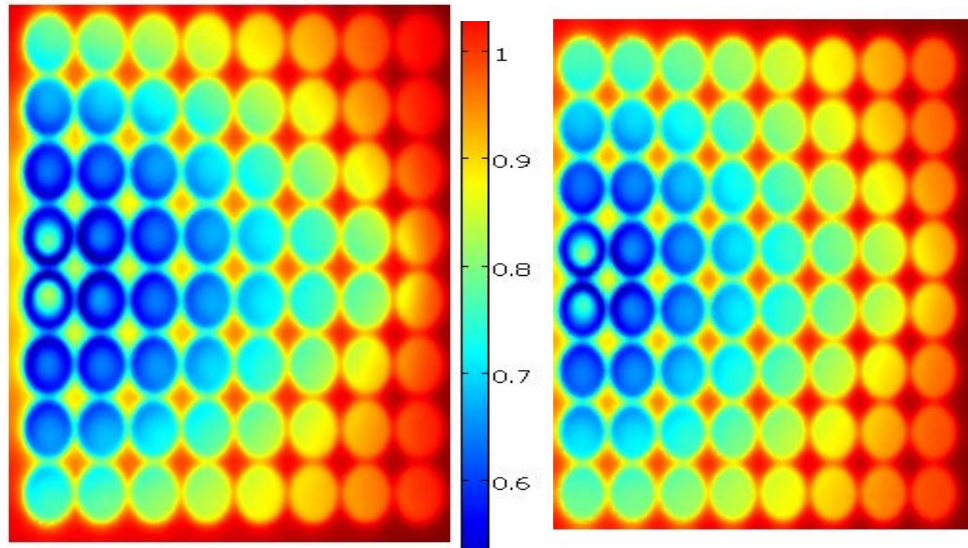
a) Diameter= 5 mm, Trough height= 2 mm   b) Diameter= 5 mm, Trough height= 5 mm

(Water mass fraction distribution)
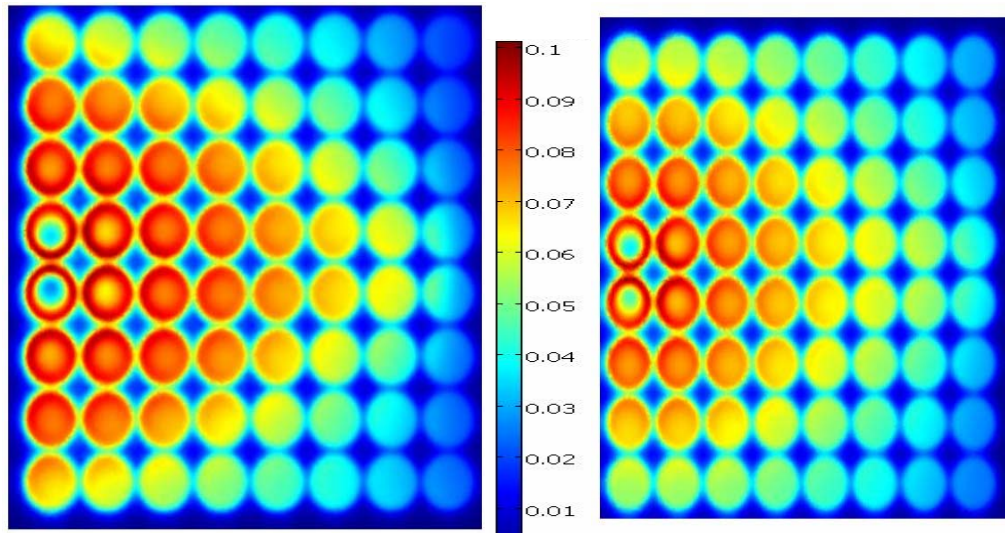
a) Diameter= 5 mm, Trough height= 2 mm   b) Diameter= 5 mm, Trough height= 5 mm

(Oxygen mass fraction distribution)

Figure 5.11: Effects of the variation of gas channel (trough) height on the oxygen and water mass fractions distribution along the cathode catalyst layer at V = 0.5V

121

Figure 5.11 shows an increase in the oxygen mass fraction and a decrease in the water mass fraction along the cathode catalyst layer when the gas channel height is reduced. Those changes are due to changes in the residence time and the diffusion rate of species. Overall, results show an increase in the performance of the PEM fuel cell with a reduction in gas channel height. Figure 5.12 shows the fuel cell polarisation curve for two different values of gas channel height.
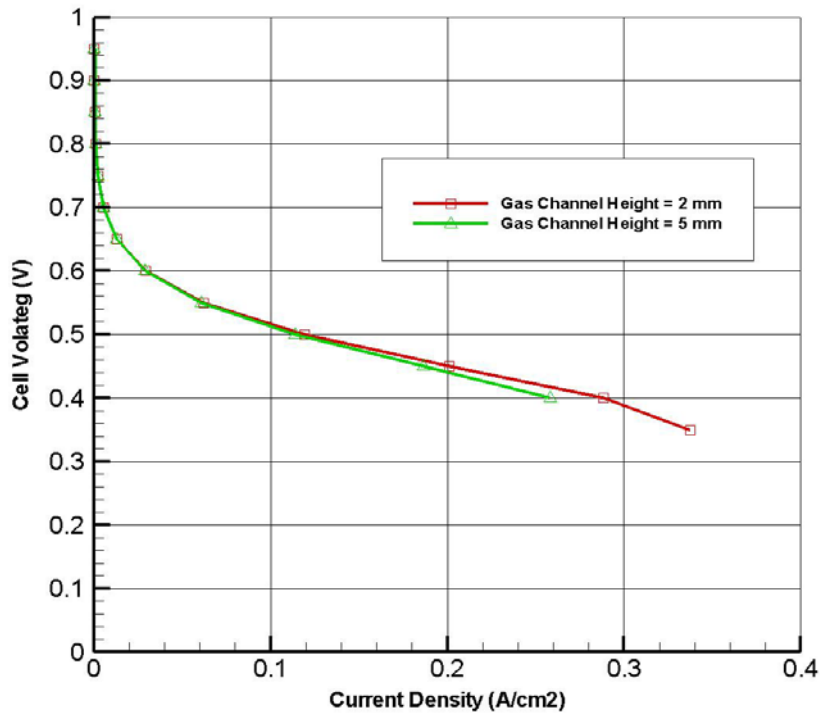
Figure 5.12: Effects of gas channel height variation on the fuel cell performance

5.4.4 Effect of Inlet Hole Diameter Variation

Changes in the inlet hole diameter generally affect the mass flow-rate of the reactant species in the fuel cell domain. Increase in the mass flow-rate improves the diffusive flux of the reactant species, which improves the water removal and heat carrying capacity of the excess reactant air along the PEM fuel cell domain. This section presents a numerical study addressing the effects of varying the inlet hole diameter on the performance of the PEM fuel cell.

Three different inlet hole diameters (6, 8 and 10 mm) are taken into consideration. The outlet diameter is kept constant (6 mm) to improve the residence time of the reactant flow in the fuel cell domain, so that an improved diffusive concentration of the reactant species can be obtained. For this parametric study, the perforated gas distributor with holes of 5 mm diameter and gas channel height of 2 mm was used.

The parametric results showed that when the inlet hole diameter was increased, there was a significant improvement in the reactant species distribution along the PEM fuel cell domain. If the inlet hole diameter is increased whilst keeping the outlet hole diameter constant, the residence time of the reactant flow in the PEM fuel cell gas channel increases. This increase in the residence time improves the passive diffusion of the reactant species through the perforated holes of the gas distributor, which also improves the diffusive flux of the reactant species through the gas diffusion layer. An increase in the diffusion of reactant species also improves water and heat removal from the PEM fuel cell domain. Figures 5.13 and 5.14 show the distribution of oxygen and water mass fractions along the cathode side of the PEM fuel cell for two different inlet hole diameters.

(a)   (b)

a) Inlet hole Diameter = 6 mm, b) Inlet hole Diameter = 10 mm
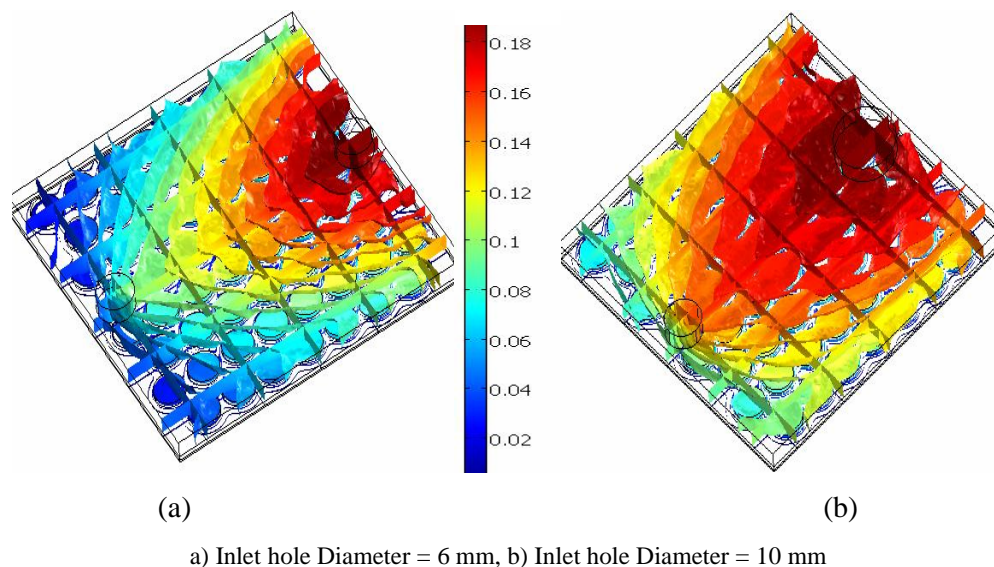
Figure 5.13: Effects of inlet hole diameter variation on oxygen mass fraction distribution along the perforated type PEM fuel cell domain; perforated hole diameter = 5 mm and trough height = 2 mm

(a)   (b)

a) Inlet hole Diameter = 6 mm, b) inlet Hole Diameter = 10 mm

Figure 5.14: Effects of inlet hole diameter variation on water mass fraction distribution along the perforated type PEM fuel cell domain; perforated hole diameter = 5 mm and trough height = 2 mm

Analyses showed an increase in the oxygen mass fraction distribution when the inlet hole diameter was increased. Such increases in the oxygen mass fraction corresponded with a decrease in water mass fraction along the domain. With the increase of inlet hole diameter, the effective wetted area of the perforated fuel cell domain covered by the reactant species was also improved, which minimised water flooding at the corners of the perforated-type PEM fuel cell domain. Although an increase in inlet hole diameter gives an improvement in the distribution of reactant/product species, one should also remember that excessive increases in the inlet hole diameter can lead to potential membrane dryness. As results of this study show; a decrease in water mass fraction along the PEM fuel cell domain occurs as the inlet hole diameter is increased as this causes the water evaporation rate to increase, which corresponds with an increase in mass flow rate. Overall, the results show that with an increase in inlet hole diameter, the fuel cell performance improves. Figure 5.15 shows the fuel cell polarisation curve for three different values of inlet hole diameters.

124

Figure 5.15: Effects of inlet hole diameter variation on the performance of the PEM fuel cell for a perforated hole diameter = 5 mm and trough height = 2 mm

5.4.5 Effect of Inlet Hole Location

The above discussed parametric analyses provided a detailed overview of the effect of various geometric parameters on the overall performance of a perforated-type PEM fuel cell. For all of these analyses, the inlet and outlet hole positions for the reactant gases (air and hydrogen) was assumed to be at the centre of the fuel cell gas flow channel domain. Fluid flow always tends to follow the shortest possible route. In the case of a centralised inlet/outlet port location, the reactant species follow the shortest possible way and subsequently do not cover the full domain area.

In this section the analysis of the effect of varying the inlet/outlet hole location on the distribution of reactant species and the overall performance of the perforated-type PEM fuel cell is presented. Two different design configurations are taken into consideration; in the first case, both the inlet and outlet ports are assumed to be at the centre of the gas channel domain; in the second case, the inlet and outlet

125

holes are assumed to be at opposite corners of the fuel cell domain at both cathode and anode sides. The diameters of the perforated holes were 5mm, and the gas channel height was 2 mm for these analyses. Both inlet/outlet hole diameters were set at 6 mm.

Results indicated improved distributions of reactant species and a small increase in the performance of the PEM fuel cell with the change of inlet/outlet hole locations from the central position to the corners of the fuel cell gas channel domain. Such an increase in performance is due to the increase in area covered by the reactant species at both sides of the fuel cell domain. The analyses also show that in the case of the inlet/outlet holes positioned at the corners, the distribution of oxygen is better as compared to the case where they were located at the centre, as the reactant species covered more surface area which improved the performance of the fuel cell. Figure 5.16 shows the oxygen mass fraction distribution along the cathode side of the PEM fuel cell in both configurations.
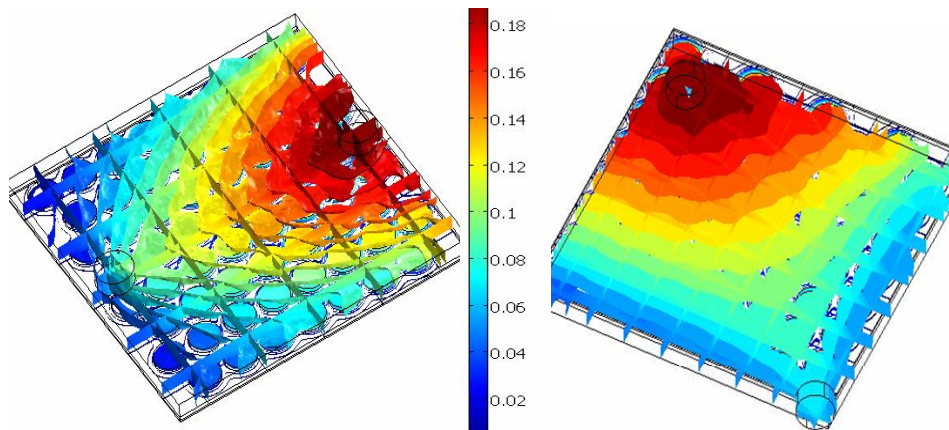
Figure 5.16: Effects of inlet\outlet hole locations on oxygen mass fraction distribution along the fuel cell domain; perforated hole diameter = 5 mm, trough height = 2 mm; inlet and outlet diameter = 6 mm. It is noted that the distribution of oxygen is better in the case where inlet and outlet holes are positioned at the corners

A change in the inlet/outlet hole locations affect the distribution of the reactant species, but generally they do not have a significant effect on the performance of the PEM fuel cell in the activation and Ohmic regions. A slight improvement is observed on the concentration losses when the holes are located at

the corners. Figure 5.17 shows the performance polarisation curve for both of these cases.
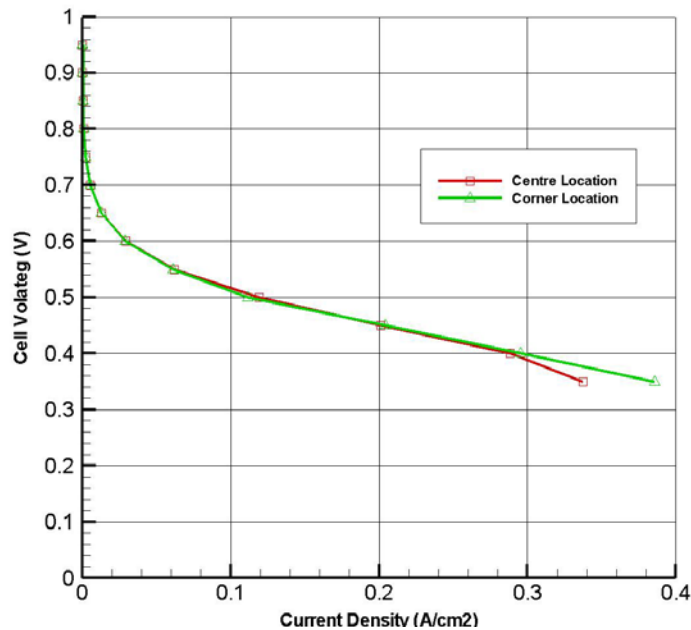
Figure 5.17: Effects of inlet and outlet hole locations on the PEM fuel cell performance; perforated hole diameter = 5 mm; Trough height = 2 mm; Inlet and outlet diameters = 6 mm

5.4.6 Findings

The following are some important findings resulting from this geometric parametric study:

i.   An increase in perforated hole diameter improves the diffusive flux of the reactant species and the overall performance of the PEM fuel cell;

ii. A change in the shape of perforation holes from circular to trapezoidal does not significantly affect the fuel cell performance;

iii. The performance of the PEM fuel cell is increased with a reduction in the gas channel (trough) height, as an increase in gas channel height affects the wall shear stresses and the thickness of the boundary layer in the gas channel domain.

iv. An increase in the inlet hole diameter improves the mass flow-rate of the reactant species, leading to an increase in the overall performance of the PEM fuel cell;

v. Changing the inlet/outlet port locations from the centre to the corner of the fuel cell domain improves the distribution of the reactant species along the fuel cell domain, effectively improving the performance of the fuel cell to some extent.

Parameter	Concentration Overpotential	Ohmic Over-potential	Activation Overpotential
Increase in gas diffusion layer porosity	Decrease	No effect	No significant effect
Increase in operating temperature	Decreased, but not significantly	No significant effect	Decrease
Increase in exchange current density	No significant effect	No significant effect	Significant decrease
Geometric parameters	The geometric parameters discussed in this research work mainly affected the concentration and activation over-potentials.		

Table 5-3: Qualitative effects of operating and geometric parameters on the fuel cell potential losses

5.5 Summary

This chapter described the numerical parametric studies performed to analyse the effects of varying different operating and geometric parameters on the distribution of species and the overall performance of a perforated-type PEM fuel cell. The operational and geometric parameters used for this study were selected from the literature review and the analyses of species distribution from the base-case model results. The main criterion for the selection of these parameters was to improve the performance of the fuel cell without any major design change requirements to limit extra manufacturing costs.

The parametric study examining the variation of the operating parameters showed an improvement in the performance of the perforated-type PEM fuel cell when the operating temperature, GDL porosity and the exchange current density was increased. Variation of the exchange current density on the performance of the fuel cell was found to be the most significant factor as it directly affects the rate of oxidation and reduction of the reactant species.

The parametric study of different geometric parameters showed that changes in perforation hole and inlet hole diameters had a significant effect on the distribution of the reactant species and thus the overall performance of this new design configuration. A decrease in the gas channel height improved the residence time and passive diffusion of the reactant species, whereas analysis showed that the effect of changes in the perforated hole shape and inlet/outlet port location on the overall performance of the perforated-type PEM fuel cell were not very significant.

CHAPTER 6

6 Effect of Cathode Flow Pulsations on the Performance of a PEM Fuel Cell

6.1 Introduction

The performance of a PEM fuel cell can be considerably influenced by customising the fluid flow behaviour along its domain. The gas flow channel design configuration affects the thermo-fluid parameters of the reactant flow, such as the flow-rates, operating pressure and temperature distributions along the PEM fuel cell domain [17, 128]. The flow behaviour in the PEM fuel cell gas channel can be disturbed by both passive and active methods. Active methods include the use of electro-kinematics' devices, whereas passive methods include geometric changes in the fuel cell design configuration, especially along the gas flow channel.

This chapter describes a new method to improve the performance of a PEM fuel cell by optimising the thermo-fluid properties of the reactant and product species. Pulsations are introduced to the flow at the cathode side to improve the diffusive properties and the overall performance of the PEM fuel cell. Research has been carried out by various researchers to study the effects of flow pulsation on the heat transfer and the fluid flow properties [17, 129, 130], and in general they showed that flow pulsation affects the fluid flow behaviour considerably. Based upon this idea, a comprehensive numerical study has been carried out here to analyse the effects of flow pulsation on the distribution of the reactant and product species along the cathode side and the resulting performance of the PEM fuel cell.

Both active and passive design approaches were used here to numerically analyse the effects of flow pulsations. For the active method, pulsations were generated by assuming a woofer system at the cathode inlet, whereas the passive

design configuration used rectangular-shaped obstacles, placed in the PEM fuel cell gas flow channel domain to generate the pulsating effect in the reactant flow. The following sections describe the results obtained from this numerical study.

6.2   Effect of Inlet Flow Pulsation: Active Approach

The diffusive properties of the reactant mixture significantly affect the performance of the PEM fuel cell. One way of improving the diffusion of the reactant species along the fuel cell domain is to increase the flow-rate in order to overcome the resistance of the gas diffusion layer, so that more reactants can pass through the GDL and chemically react along the catalyst layer. This approach can lead to possible dryness of the electrolytic membrane as the increased excess air flow can carry more water away from the membrane. Another way of improving the diffusive properties of the fluid along the fuel cell domain is to introduce pulsations into the reactant flow passing through the gas flow channels. It has been well reported by researchers that flow pulsation can increase the diffusion rate by up to three or four orders of magnitude between two reservoirs that have a concentration gradient, due to enhanced dispersion [131, 132].

For the active design approach, the pulsations are introduced by using a system having a signal generator, signal amplifier and a woofer system. The signal generator produces a signal that is then amplified. The amplified signal is then sent to the woofer system, which generates pulsations in the air flow. Researchers from University of Seoul, South Korea [17] used this active design approach to experimentally analyse the effect of cathode flow pulsations on the performance of the PEM fuel cell stack.

During the active design approach study, the same technique was followed and the results were compared with experimental trends. As the numerical analyses were carried out using a single PEM fuel cell in comparison to the experimental analyses [17] which were carried out using a stack of 10 PEM fuel cells, the experimental *trends* of different variables were compared instead of the experimental data itself. In the numerical analysis, it was not easy to model the

active pulsation generation system, so a mathematical relation describing the time-averaged pulsating velocity (Equation 6.1) was used to model the effects of the pulsation generation system. This relation was defined by researchers from the University of Seoul, South Korea [17] in their experimental work with the same active system.

The flow pulsations were introduced at the cathode side of the PEM fuel cell in the unidirectional reactant air flow. The magnitude of the flow pulsations was controlled by its amplitude and frequency. The time-averaged pulsating velocity of the reactant flow was defined at the cathode inlet. This is a function of the pulsation frequency and amplitude. The function defining the time average pulsating velocity was previously described by Kim *et al.* [17]:

$$U_i = U_m + ASin2\pi ft \qquad (6\text{-}1)$$

Where:

U_m	=	Time-averaged inlet flow velocity
A	=	Amplitude of velocity pulsation
f	=	Frequency
t	=	Time

A series of transient two dimensional numerical analyses were carried out assuming isothermal flow conditions (T = 333K) to study the effects of cathode flow pulsations on the diffusive properties and overall performance of the PEM fuel cell. A straight gas flow channel was assumed for this study instead of a perforated gas flow channel to further simplify the design configuration. These numerical analyses were carried out at the cathode side (i.e. the anode side was ignored) to reduce computational requirements.

To numerically model the woofer system at the cathode inlet, a mathematical function (Equation 6.1) was used to numerically control the pulsating flow behaviour, such as its frequency and amplitude. The role of the pulsation

frequency and amplitude were studied individually to analyse their effect on the overall flow behaviour. The following sections describe the results obtained from the numerical study of the effects of pulsation frequency and amplitude variation on the flow behaviour and the overall performance of the PEM fuel cell.

Parameter (Operating Condition)	Value	Unit
Oxygen inlet mass fraction	0.226	
Water inlet mass fraction	0.0934	
Hydrogen inlet mass fraction	0.844	
Operating temperature	333	K
Inlet pressure	101325	Pa
Average inlet flow velocity	0.35	m/s
Cathode reference exchange current density	1.0E-02	A/cm^2
Anode reference exchange current density	1.00E+04	A/cm^2
Electrode electric conductivity	120	S/m
Gas diffusion layer porosity	0.5	

Table 6-1: Operating conditions used for the pulsating flow analysis

Parameter	Value	Unit
Gas channel length	0.05	m
Gas channel width	0.005	m
GDL thickness	0.0002	m
Membrane thickness	0.00018	m

Table 6-2: Geometric parameters used for the pulsating flow analysis

133

6.2.1 Effect of Pulsation Frequency Variation

This section presents the numerical analysis of the effects of pulsation frequency variation on the diffusive properties and overall performance of the PEM fuel cell. Three different values of the pulsation frequencies ranging from 0 to 30 Hz are analysed at constant pulsating amplitude of 0.15 and an inlet flow velocity of 0.35 m/s. These analyses are carried out assuming the operating and geometric conditions specified in tables 6.1 and 6.2.

The results obtained from the 2D numerical study were compared with the steady state flow analyses. The oxygen and water mass fraction distributions along the fuel cell domain were analysed at different pulsating frequencies to study their effect on the oxygen and water mass fraction distributions along the PEM fuel cell domain. Figure 6.1 and 6.2 shows the distribution of oxygen and water mass fraction along the cathode side of the PEM fuel cell when under the influence of a variable frequency pulsating flow.

Pulsating Frequency = 0 Hz
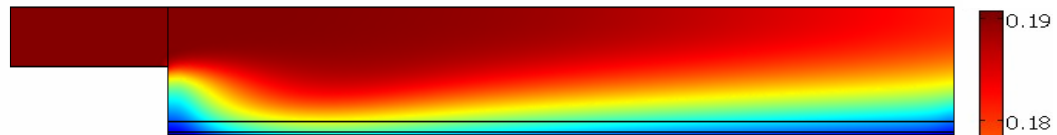
Pulsating Frequency = 10 Hz
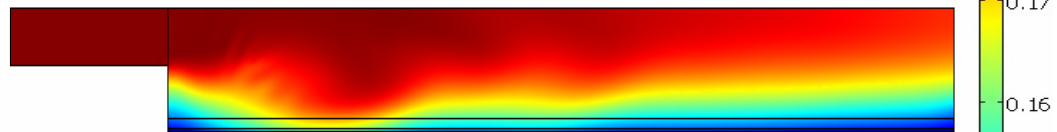
Pulsating Frequency = 30 Hz

Figure 6.1: Effects of pulsation frequency variation on oxygen mass fraction distributions along the cathode side of the PEM fuel cell; V = 0.4 Volts; T = 333 K; Inlet air velocity = 0.35 m/s; Pulsating amplitude = 0.1; t = 2 sec

134

Pulsating Frequency = 0 Hz
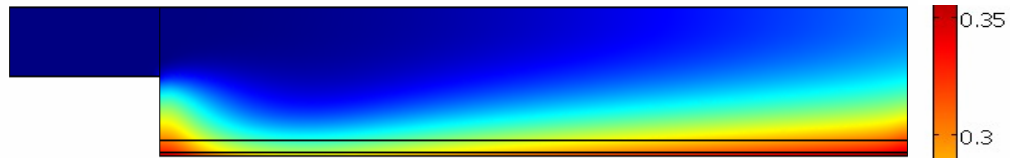
Pulsating Frequency = 10 Hz

Pulsating Frequency = 30 Hz

Figure 6.2: Effects of pulsating frequency variation on water mass fraction distribution along the cathode side of a PEM fuel cell; V = 0.4 Volts; T = 333 K; Inlet air velocity = 0.35 m/s; Pulsating amplitude = 0.1; t = 2 sec

Figures 6.1 and 6.2 show that the distributions of oxygen and water mass fractions along the fuel cell domain are improved with increasing pulsation frequency. This increase is not very significant, but it does have some influence on the overall performance. Generally, varying the pulsation frequency does not significantly influence the flow behaviour. Figure 6.3 shows the effects of pulsating flow frequency variation on the overall performance of the PEM fuel cell at T = 333K.
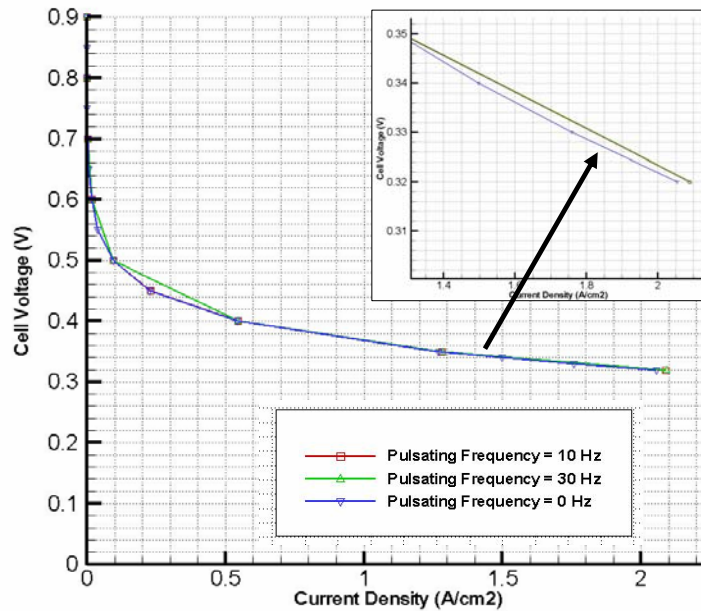
Figure 6.3: PEM fuel cell polarisation curve for three different values of pulsation frequency at T = 333K

Figure 6.3 shows that the overall performance of the PEM fuel cell increases by introducing the pulsations in the reactant air flow on the cathode side, but this increase is not very significant. Numerical results obtained from studies on the effect of pulsating frequency variation were compared with the experimental work of Kim *et al.* [17]; a good agreement was found between the trends obtained from both numerical and experimental studies. Kim *et al.* [17] performed experimental work using a fuel cell stack of 10 fuel cells, and also found that the effect of pulsating frequency variation is not significant on the PEM fuel cell performance.

6.2.2 Effect of Pulsating Amplitude Variation

This section describes the results obtained from the numerical study of the effects of pulsating amplitude variation on the flow behaviour in the PEM fuel cell domain. These analyses were carried out assuming the same operating and geometric conditions as specified in Tables 6.1 & 6.2. Three different values of the pulsating amplitude ranging from 0.5 to 2 at constant pulsating frequency (10 Hz), and average inlet velocity (0.35 m/s) were used. As reported in the literature [17, 132], the pulsating amplitude significantly influences the rate of diffusion across the

GDL; therefore, a parametric study was carried out to study the effects of pulsating amplitude variation on the diffusive flux of reactant oxygen across the GDL/gas channel interface. Figure 6.4 shows the results obtained from this numerical study.
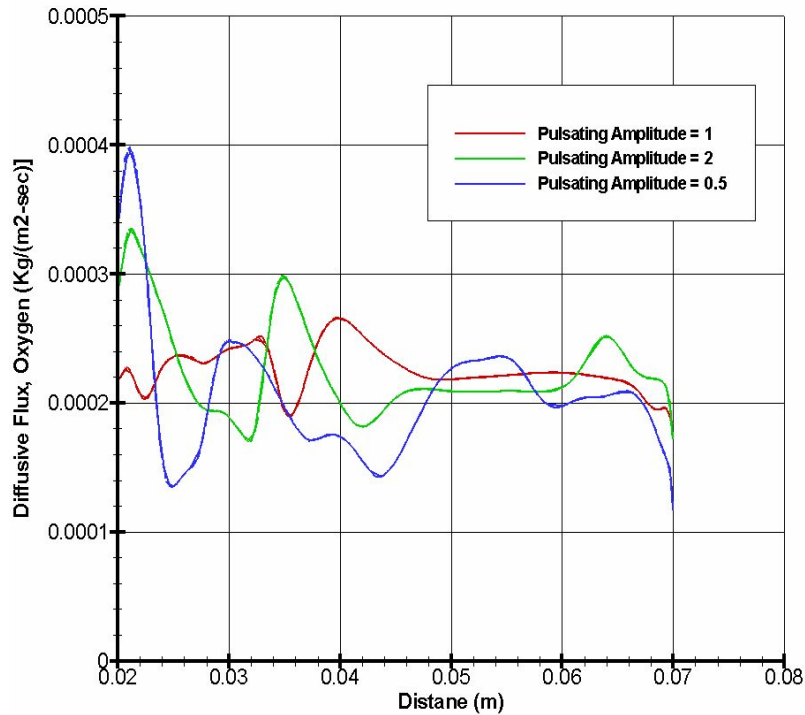
Figure 6.4: Effects of pulsating amplitude variations on the diffusive flux of oxygen along the gas channel/ GDL interface at f = 10 Hz and T = 333 K

Figure 6.4 shows that an increase in the pulsating amplitude gives an increase in the oxygen diffusion flux along the gas channel/GDL interface. This leads to an increase in the mass fraction of oxygen along the cathode catalyst layer, which consequently improves the electrochemical reaction rate. Figure 6.5 shows the distribution of oxygen mass fraction along the cathode side of the PEM fuel cell at different pulsating amplitudes.

Pulsation Amplitude = 0
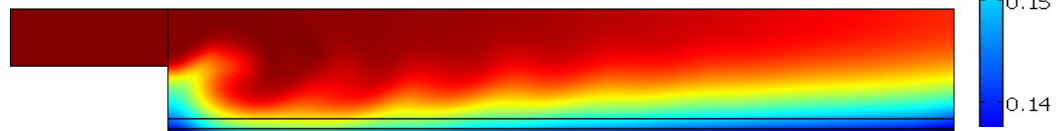
Pulsation Amplitude = 1

Pulsation Amplitude = 2
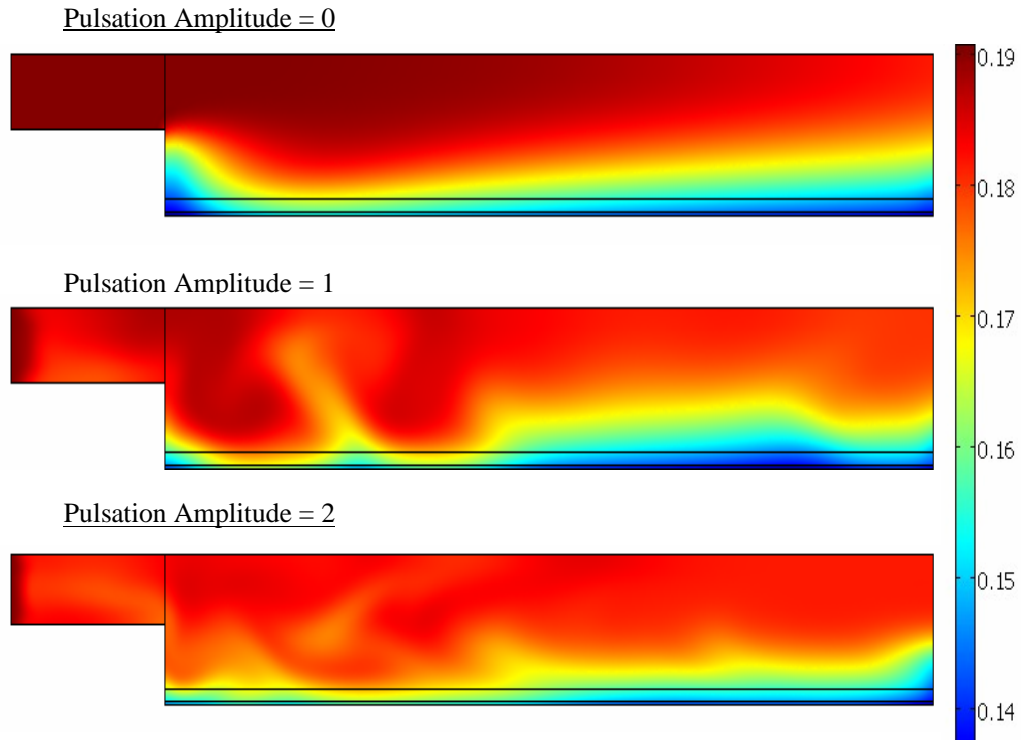
Figure 6.5: Effects of pulsating amplitude variation on the oxygen mass fraction distribution along the cathode side of PEM fuel cell at V = 0.4 volts; T = 333 K, inlet velocity = 0.35 m/s; pulsating frequency = 10 Hz
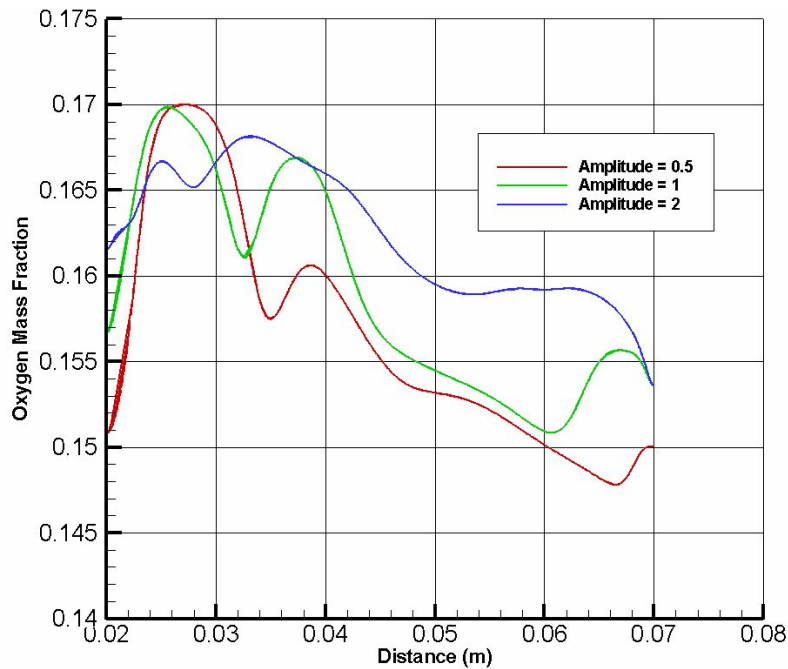
Figure 6.6: Variation of oxygen mass fraction along the cathode catalyst layer at different pulsating amplitudes

Figure 6.6 shows the distribution of oxygen mass fraction along the gas channel/GDL interface of the PEM fuel cell at three different pulsating amplitudes. Analysis shows a considerable increase in the oxygen mass fraction along the cathode catalyst layer when the pulsating amplitude is increased, which increases the rate of the electro-chemical reaction.

Such increases in the electro-chemical reaction rates lead to an increase in the water mass fraction along the cathode catalyst layer, however, this effect is counterbalanced by the diffusive flux of reactant air through the GDL, which increases the water carrying capacity of the excess reactant air so that the higher generation of water content is dissipated out with the excess air. Overall, low water content is observed at high values of pulsating amplitude. Figure 6.7 shows the variation of water mass fraction along the cathode side of the PEM fuel cell at three different pulsating amplitudes.

Pulsation Amplitude = 0
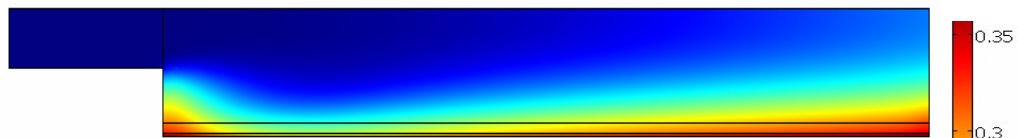
Pulsation Amplitude = 1
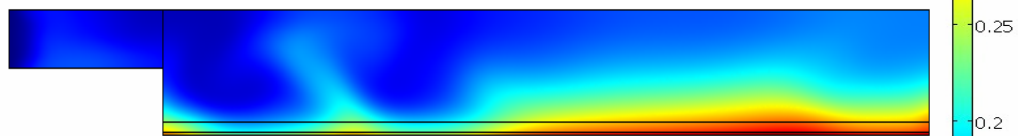
Pulsation Amplitude = 2

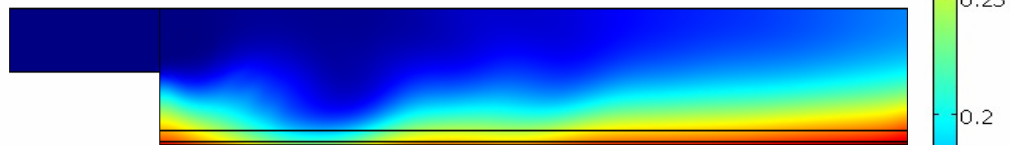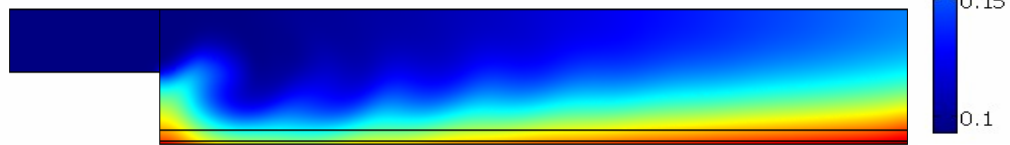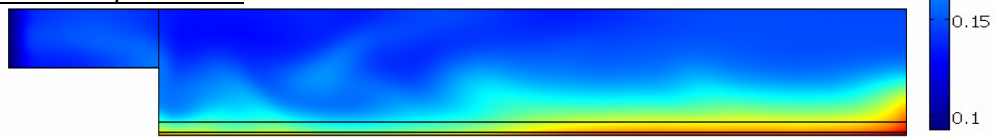Figure 6.7: Effects of pulsating amplitude variation on water mass fraction distribution along the cathode side of a PEM fuel cell; V = 0.32 Volts; T = 333 K; inlet velocity = 0.35 m/s; frequency = 10 Hz

139
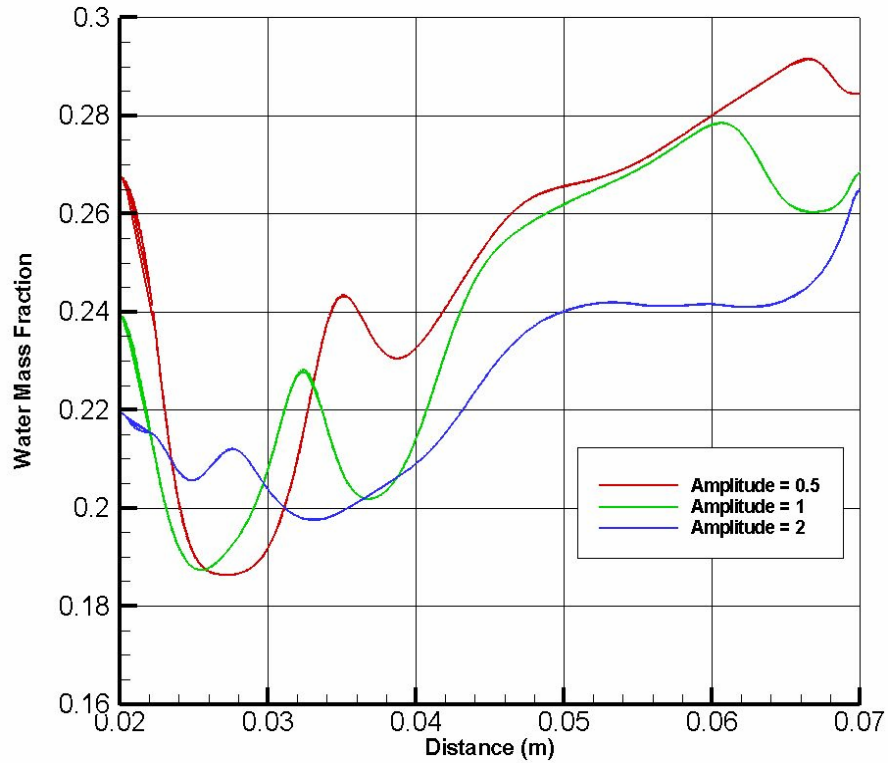
Figure 6.8: Variation of water mass fraction along the cathode catalyst layer at different pulsating amplitudes

Figure 6.8 shows a decrease in the water mass fraction along the cathode catalyst layer with the increase in the pulsating amplitude of the reactant air at the cathode side. Increasing the pulsating amplitude forces the reactant flow to pass through the GDL and reach the catalyst layer. Overall, an increase in the pulsating amplitude improves the diffusion rate of the reactant species along the GDL that consequently improves the electro-chemical reaction rate. Figure 6.9 shows the polarisation curves for the PEM fuel cell performance at different pulsating amplitudes.
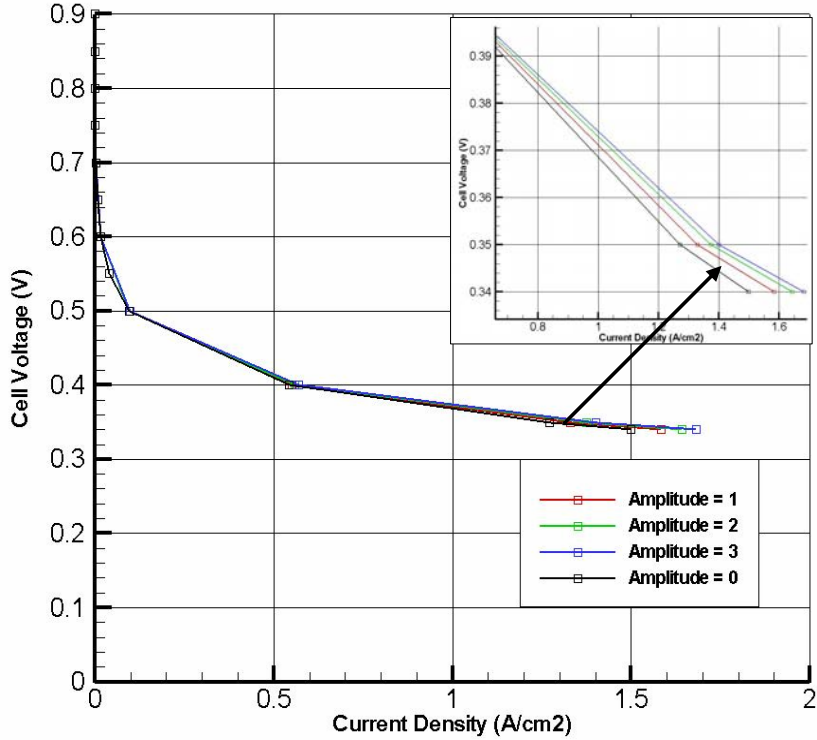
Figure 6.9: Performance polarisation curves at different pulsating amplitudes

Results obtained from studies of the effects of pulsation frequency and amplitude variation show that the effect of pulsating amplitude variation is more significant when compared to the pulsating frequency. The trends obtained from this numerical study are in good agreement with the experimental work done by Kim *et al.* [17]. Only general trends could be compared as Kim performed experimental analyses using a fuel cell stack of 10 PEM fuel cells, while the numerical work presented here only calculated the performance for a single PEM fuel cell.

6.3   Effect of Obstacle Placement in the Flow Domain: Passive Approach

The results presented in the section 6.2 showed that flow pulsations improve the performance of a PEM fuel cell, but to produce pulsations in the flow is not a straight forward process. It requires a complete set of systems which will require additional cost and effort. As mentioned earlier, one objective of this research is to reduce the operational cost of PEM fuel cells using simpler design concepts; therefore, to create the pulsations in the flow, a passive design is preferred.

One way of creating pulsations in the reactant flow is to place obstacles in the gas channel flow domain. These obstacles disturb the fluid flow pattern, creating pulsations. For this purpose, rectangular-shaped solid obstacles were used for this study. This section presents a 2D numerical study concerning the effect of rectangular-shaped obstacles in the flow domain on the flow behaviour. Figure 6.10 shows a schematic overview of the fuel cell domain under consideration.
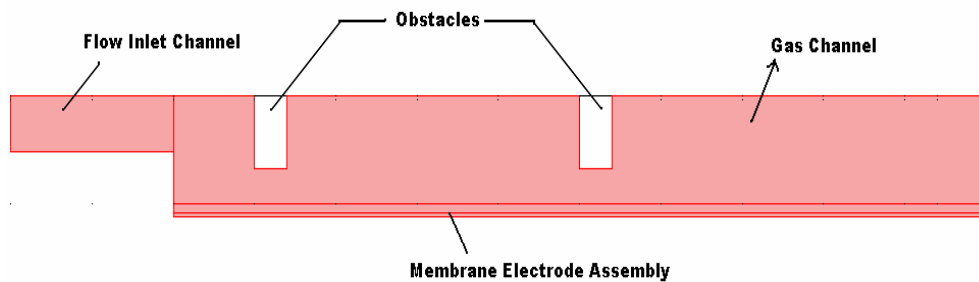
Figure 6.10: 2D schematic overview of the PEM fuel cell domain with two rectangular obstacles placed in the flow domain

This numerical study describes the effect of varying the number of obstacles, their position and angular placement in the flow domain on the overall flow behaviour along the fuel cell domain. The following sections present the results obtained from this numerical study.

6.3.1 Effect of the Number of Obstacles

This section presents a parametric study of the effect of obstacle placement on the flow behaviour in a PEM fuel cell gas channel. For the purpose of this numerical study, the effects of three different geometric configurations were analysed, where one, two and five obstacles were placed in the gas channel domain. Analyses showed a significant change in the flow pattern with increasing the number of obstacles in the gas flow channel. It was observed that the main influence was inflected on the pulsating frequency. Detailed analyses are carried out to explore this behaviour. The following figures show the velocity streamlines along the cathode side of the PEM fuel cell for three different design configurations.
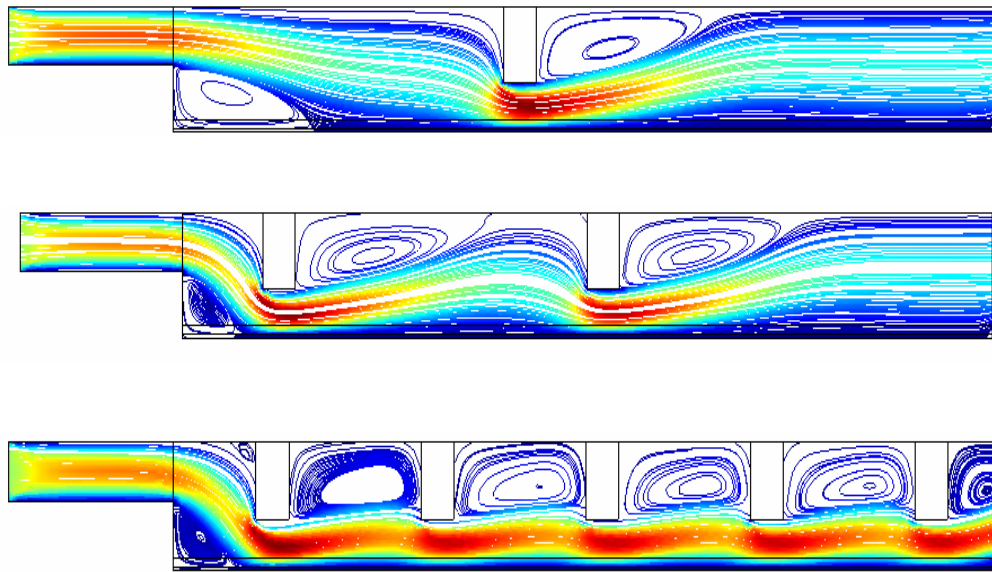
Figure 6.11: Velocity streamline patterns along the cathode side of the PEM fuel cell for three different numbers of obstacles

Figure 6.11 shows that when increasing the number of obstacles, a significant change in the flow pattern along the fuel cell domain arises. Increasing the number of obstacles improves the pulsating frequency of the reactant flow. These obstacles push the reactant flow downwards, and after passing below each obstacle, the flow again rises up, which leads to a pulsating effect in the flow.

143

The analysis also shows that the height of the obstacle plays an important role in this regard, and a study of obstacle height is presented in Section 6.3.3. Detailed analyses were carried out to study the effect of obstacle placement on the diffusion rate of reactant species. Results show that increasing the number of obstacles results in an improved oxygen mass fraction distribution. Figure 6.12 shows the variation of oxygen diffusion flux along the GDL/gas channel interface, and the distribution of oxygen mass fraction along the cathode catalyst layer for three different numbers of obstacles.

Figure 6.12: Oxygen diffusive flux along the GDL/Gas channel interface for three different numbers of obstacles in the flow domain

Figure 6.13: Distribution of oxygen and water mass fractions along the cathode catalyst layer for three different numbers of obstacles in the flow domain
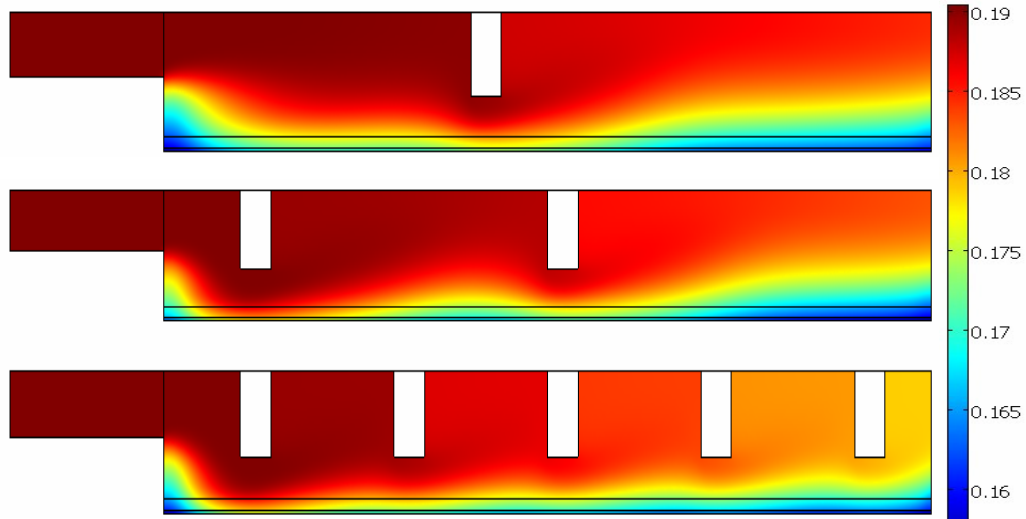
Figure 6.14: Variation of oxygen mass fraction along the cathode side of the PEM fuel cell for three different numbers of obstacles

145

With the increase in the number of obstacles, oxygen diffusive flux along the gas channel/GDL interface increases, effectively enhancing the mass fraction of oxygen along the cathode catalyst layer. One obvious effect of increasing the number of obstacles is the increase in vortex shedding. On one hand, such vortex shedding enhances the residence time and oxygen diffusion rate, but on the other hand it increases the amount of water flooding in some areas of the fuel cell. Although water flooding is reduced along the porous media of the fuel cell, analysis shows a high mass fraction of water in the areas behind the obstacles in the gas channel. In these areas, vortex shedding results in the passage of reduced amounts of air which are insufficient to remove the residual amounts of product water. Figure 6.15 shows the distribution of water mass fraction along the fuel cell domain for the three different numbers of obstacles.
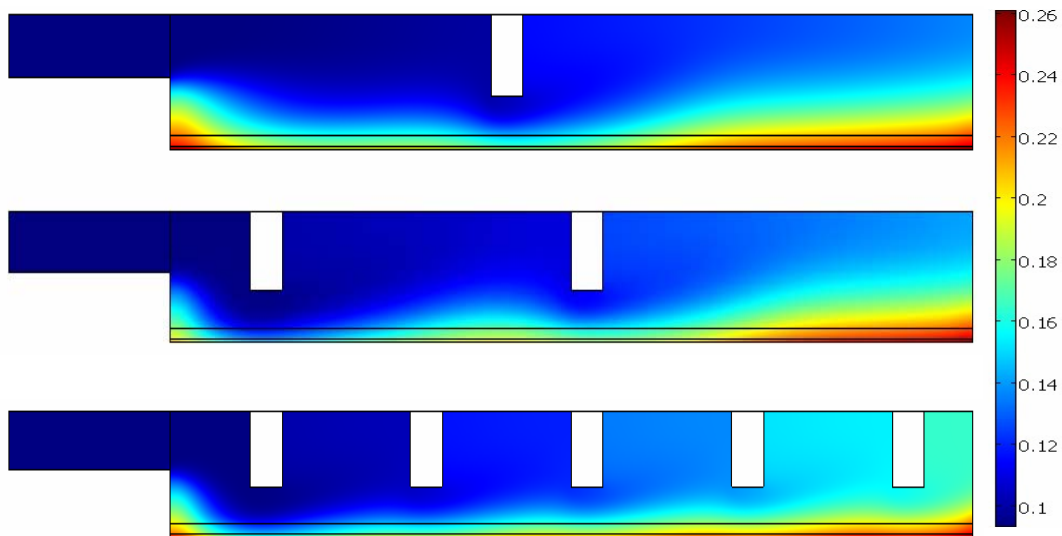
Figure 6.15: Variation of water mass fraction along the cathode side of the PEM fuel cell for three different numbers of obstacles

Such variations of water mass fraction do not considerably affect the fuel cell performance, as water flooding is considerably reduced along the porous media of the PEM fuel cell with increasing numbers of obstacles. One solution to the problem of high water accumulation behind the obstacles is to carry out a study to examine the effect of different obstacle placement angles, as they can disturb the

146

flow pattern to some extent. Keeping this issue aside, the overall analyses show that the performance of the PEM fuel cell increases with an increasing number of obstacles. Figure 6.16 shows the fuel cell performance polarisation curves for three different numbers of obstacles.
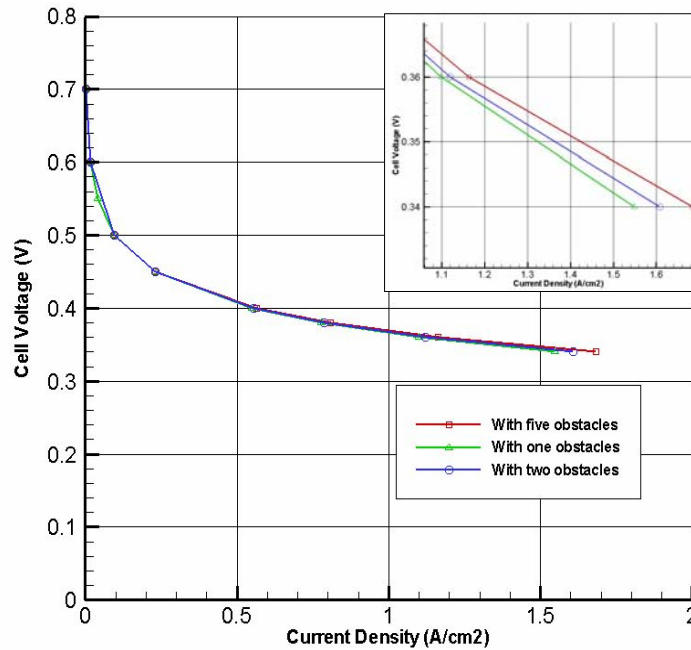
Figure 6.16: PEM fuel cell performance polarisation curves for three different numbers of obstacles.

Analysis of the effects of different numbers of obstacles in the fuel cell domain identified two new areas for further research;

1. Effect of obstacle height;
2. Effect of obstacle angle.

The following sections present studies of the effect of obstacle height and placement angle on the overall performance of the PEM fuel cell.

6.3.2 Effect of Obstacle Placement Angle

This section describes a study of the effect of obstacle placement angle on the flow behaviour in the fuel cell domain. The main purpose of this analysis is to study the effect of obstacle angular placement on the vortex shedding pattern behind each obstacle. All previous analyses have been carried out with an obstacle placement angle of 90 degrees as this configuration is easy to produce. During this study, two obstacles with a height of 3.5 mm each at three different angles; (60, 90 and 120 degrees) were placed in the two dimensional domain of the PEM fuel cell. Detailed numerical analyses were carried out to study the flow behaviour. Figure 6.17 shows the velocity streamlines in the fuel cell domain at three different angles of the obstacles.
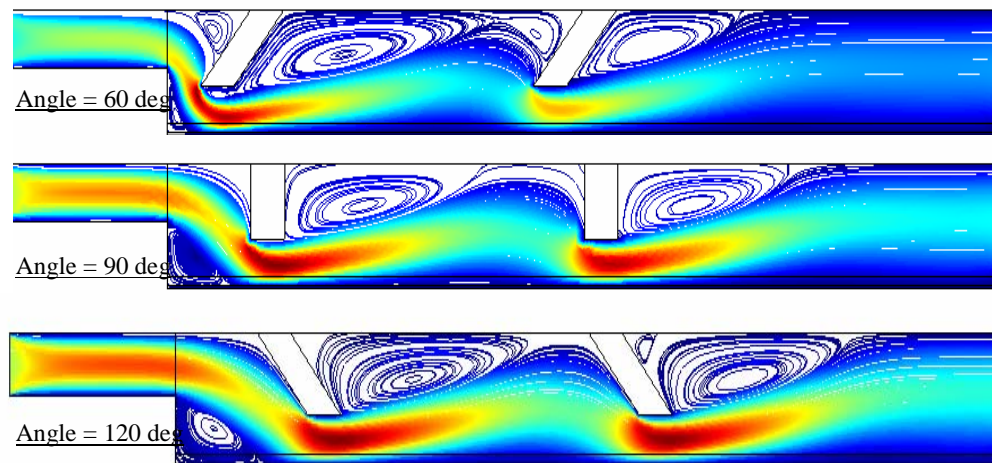
Figure 6.17: Velocity streamlines at three different obstacles angles in the PEM fuel cell domain

Results show that variation of the obstacle angle changes the flow behaviour in the fuel cell domain. At a 60 degree angle, (i.e. when the obstacle is tilted in a forward direction) the flow behaviour is quite different from the case of a 120 degree angle (where the obstacle is tilted backward). There is considerable change in the strength of the vortex shedding behind the obstacle with variation of the angle. Such variation in the vortex shedding leads to changes in the overall behaviour of the flow. Figures 6.18 and 6.19 shows the diffusion rate of oxygen

148

along GDL/gas channel interface and the resulting distribution of reactant species along the cathode catalyst layer for these three different design configurations.
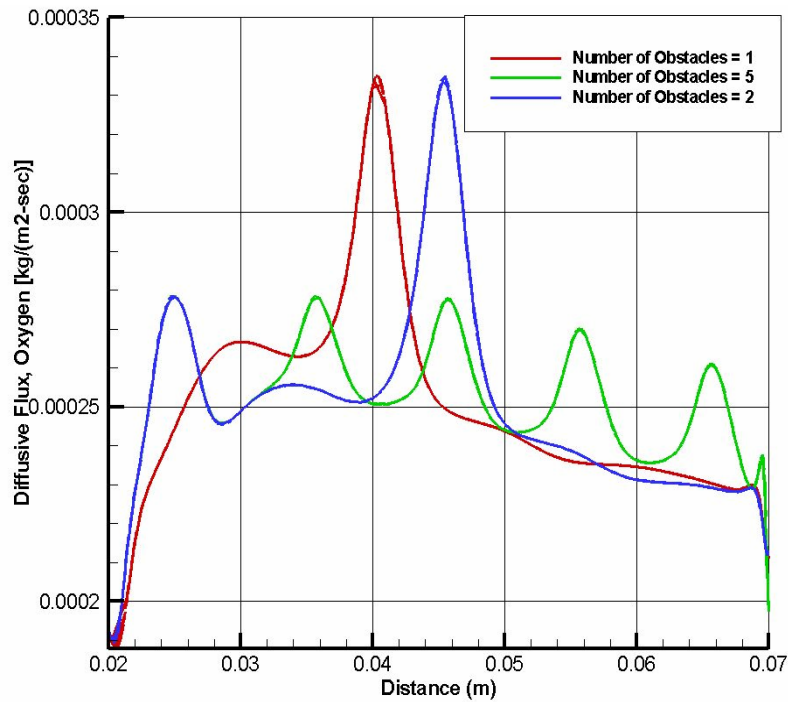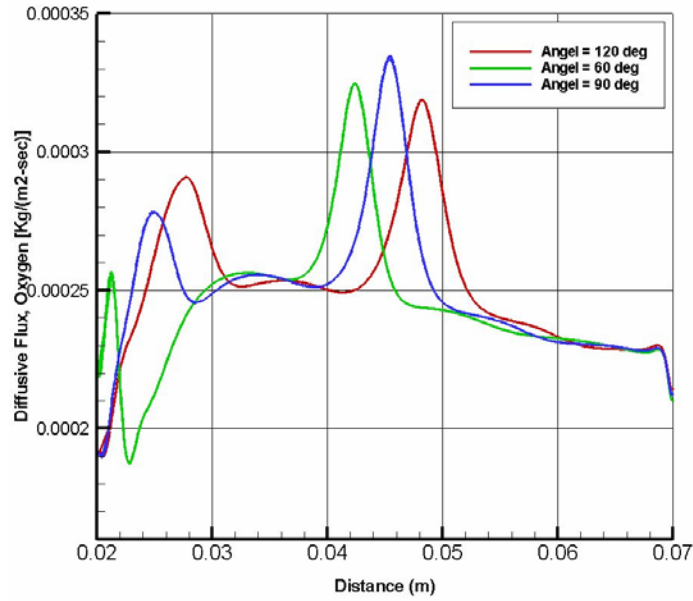

Figure 6.18: Oxygen diffusive flux along the GDL/Gas channel interfaces for three different angles of obstacles in the flow domain
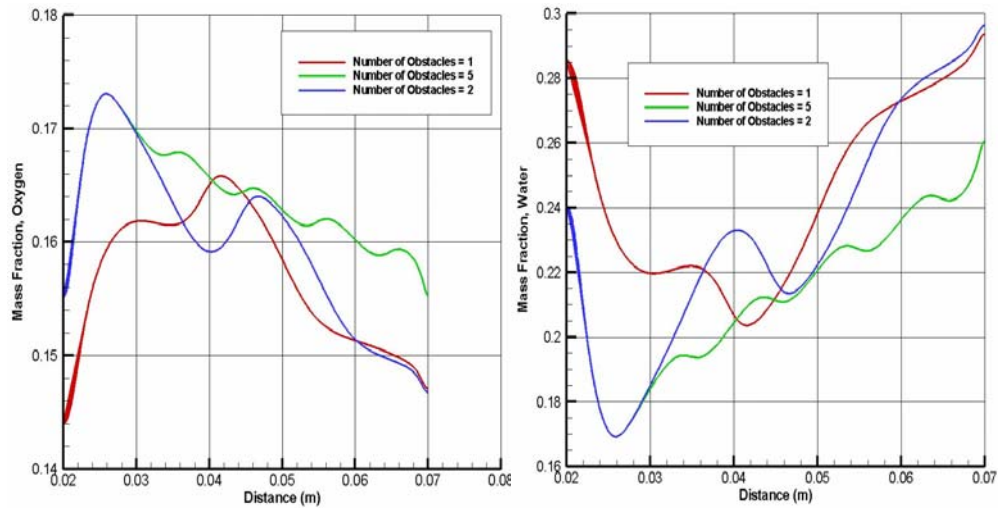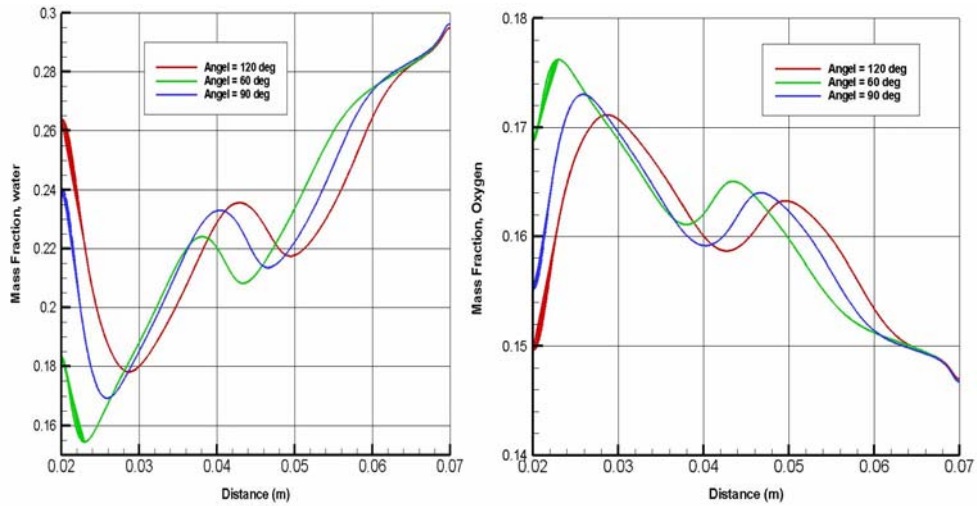

Figure 6.19: Distribution of oxygen and water mass fraction along the cathode catalyst layer for three different angles of obstacles in the flow domain

It is also deduced from the analyses that increasing the obstacle angle causes the diffusion rate of oxygen along the porous media of the fuel cell to increase. Analysis of the vortex shedding and especially the water accumulation behind the obstacle show that the increase in obstacle angle reduces, to a certain extent, the amount of water accumulation behind the obstacle. Figure 6.20 shows the distribution of water along the cathode side of the PEM fuel cell.
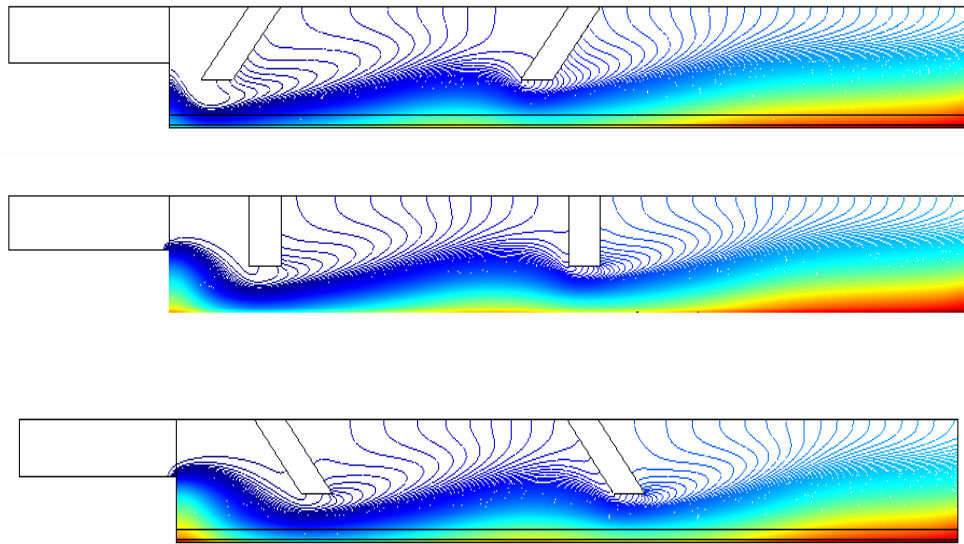
Figure 6.20: Distribution of water mass fraction along the PEM fuel cell domain for three different obstacle angles

6.3.3 Effects of Obstacle Height

This section presents a study of the effects of varying obstacle height on the flow behaviour and on the overall performance of the PEM fuel cell. Two dimensional numerical analyses were carried out using three different obstacle heights; 2.5, 3.5 and 4 mm respectively, at an angle of 90 degrees. Velocity streamline profiles along the fuel cell domain at three different heights show that varying the obstacle height results in a considerable change in flow behaviour. Figure 6.21 shows the streamline velocity profile at three different obstacle heights.

Height = 2.5 mm

Height = 3.5 mm

Height = 4 mm
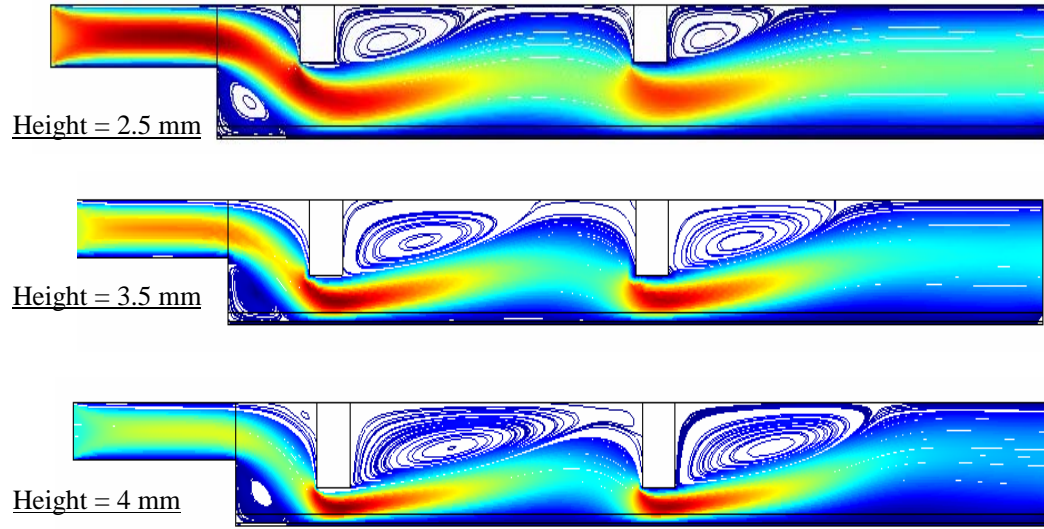
Figure 6.21: Velocity streamlines along the fuel cell domain for three different heights of obstacles

With increases in obstacle height, the length of the vortex shedding region behind the obstacle increases, leading to improvements in the residence time of the reactant species, as well as increasing their diffusion rate. Figure 6.22 and 6.23 show the analysis of the effects of obstacle height variation on the diffusive flux and reactant species mass fraction distribution along the cathode catalyst layer. Results show a significant improvement. An obvious disadvantage of increasing the obstacle height is the increase of water accumulation in the vortex shedding region. However, this problem can be solved to some extent by changing the placement angle of the obstacles.
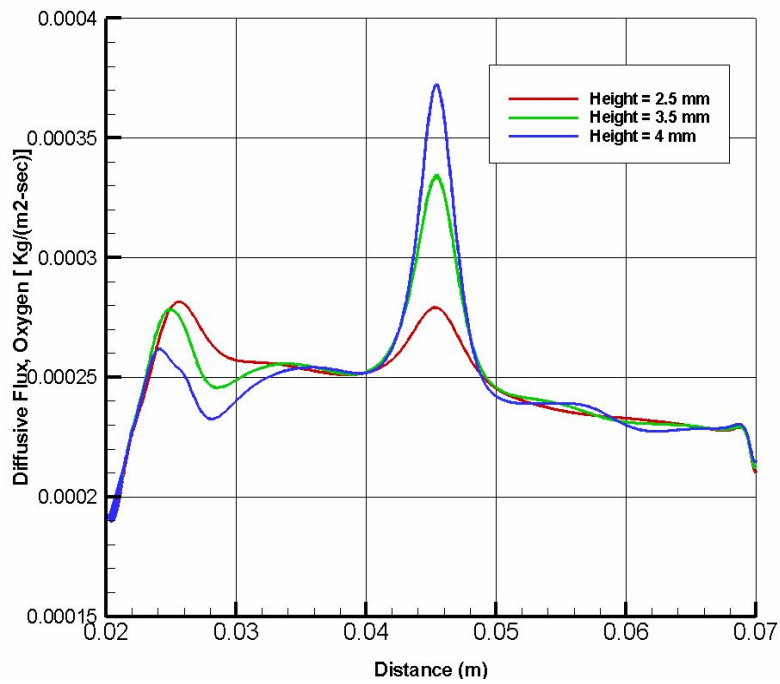
Figure 6.22: Oxygen diffusive flux along the GDL/gas channel interface for three different heights of obstacles in the flow domain
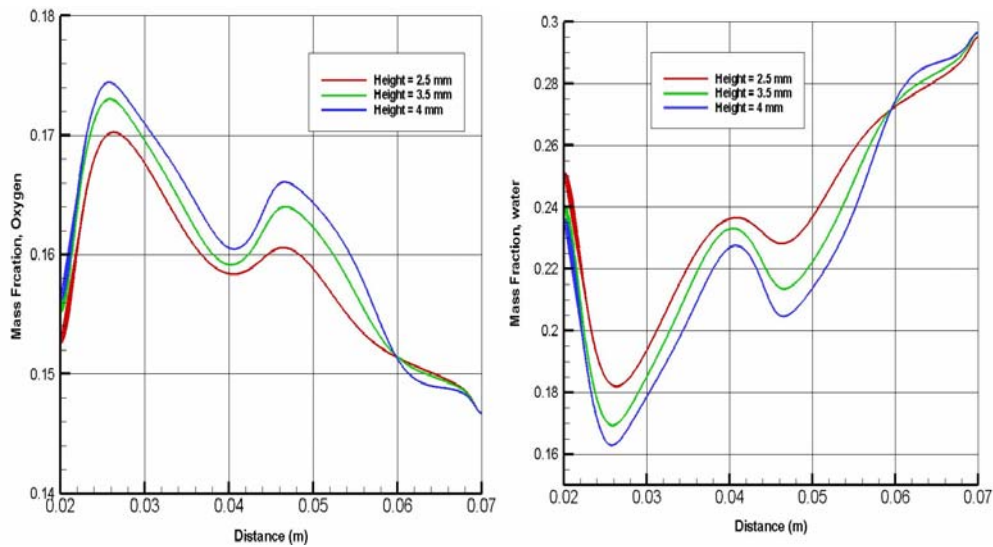
Figure 6.23: Distribution of oxygen and water mass fractions along the cathode catalyst layer for three different heights of obstacles in the flow domain

6.4 Findings

The following are some important findings based on the results of the numerical study of the effects of flow pulsation generated by the placement of different numbers of obstacles at alternative angles along the fuel cell domain on the performance of PEM fuel cells:

i. The diffusion rate of reactant species can be improved by introducing a pulsating effect in the flow, which consequently improves the overall performance of the PEM fuel cell;

ii. There is no significant influence of the variation of pulsation frequency on the performance of the PEM fuel cell;

iii. The performance of the PEM fuel cell significantly improves with an increase in pulsation amplitude;

iv. The placement of obstacles in the fuel cell domain affects the flow behaviour; Increasing the number of obstacles mainly improves the pulsating frequency;

v. Variation in the obstacle angle affects the vortex shedding pattern, but does not significantly influence the overall performance of the PEM fuel cell;

vi. Increasing the obstacle height increases the strength of vortex shedding; and improves the pulsation amplitude, leading to an increase in the overall performance of the PEM fuel cell.

6.5 Summary

This chapter described the numerical analyses of the effects of cathode flow pulsation on the diffusive properties of reactant species and the overall performance of the PEM fuel cell. Both passive and active pulsation generation methods were studied. Results obtained from the numerical study were compared with experimental trends and a good agreement was found.

To actively generate flow pulsations, a time-averaged pulsating flow velocity was assumed at the fuel cell inlet. This time-averaged pulsating flow velocity was a function of pulsating amplitude and frequency. Analyses were carried out to study the effect of pulsating frequency and amplitude variation, and results showed that the effects of pulsating amplitude variation were more significant than the effects of pulsating frequency variation.

To passively generate the flow pulsations, rectangular-shaped solid obstacles were placed at regular intervals in the PEM fuel cell gas flow channel. A detailed parametric study was carried out to numerically model this geometry, and the effect of the number of obstacles, their placement angle and height on the pulsating behaviour and overall performance of the PEM fuel cell were analysed. Increases in the number of obstacles improve the pulsating frequency, whereas the pulsating amplitude improved with the obstacle height. Overall, the results showed that the diffusive properties and overall performance of the PEM fuel cell was improved by the introduction of flow pulsations.

CHAPETR 7

7   Discussion

7.1   Introduction

This chapter discusses the important findings of this research work. Two different design approaches has been analysed and discussed in the following sections.

7.2   PEM Fuel Cell with a Perforated-Type Gas Flow Distributor

The performance analyses of a PEM fuel cell with a perforated-type gas distributor were categorised into three phases during this research work. In the first phase, numerical analyses were carried out to understand the coupling of different transport phenomena and the distribution of reactant and product species along the perforated type PEM fuel cell domain. The performance analyses of this new design configuration of the PEM fuel cell were initiated using a simple two dimensional numerical model that provided a basic understanding of the coupling and transport phenomena taking place inside the fuel cell. Later, the two dimensional model was extended to a full scale three dimensional numerical model. The results obtained from the three dimensional numerical analyses were compared with experimental data and a good agreement was found. A comparison study was also carried out with a PEM fuel cell constructed with a serpentine-shaped gas flow distributor to validate the performance of the proposed design.

After the initial numerical analysis and validation of the concept, a detailed parametric study was carried out to explore the effects of varying different operating and geometric parameters on the overall performance of the perforated-

type PEM fuel cell. The following sections summarise and discuss the important findings of this study.

7.2.1 Preliminary Numerical Analysis and Model Validation

Initially, a simple two dimensional model was used to numerically model the transport phenomena of the PEM fuel cell. This provided a basis for further, more detailed three dimensional numerical analyses. These numerical analyses provided an insight into the distribution of reactant and product species along a perforated-type PEM fuel cell domain, which was not possible through the experimental techniques.

The numerical results showed a parabolic velocity profile along the gas flow channel domain at both anode and cathode sides, where the velocity near the wall was very slow compared to the velocity in the centre of the gas flow channel. Such velocity profiles passively force the reactant flow near the wall to pass through the perforated holes of the gas distributor. The passive deflection of the reactant flow towards the holes was not easily achieved when the flow velocity was high near the walls of the domain; hence passive flow of the species through the perforation holes and the gas diffusion layers under high velocities of flow was limited. Furthermore, the flow behaviour in the fuel cell domain shows that the reactant flow follows the shortest possible route from the inlet to the outlet of the PEM fuel cell domain.

The main purpose of using perforated-type gas flow distributors instead of the more conventional types of gas flow distributors based on graphite was to simplify the design configuration and to improve the distribution of reactant/product species along the PEM fuel cell domain. In the case of conventional types of fuel cell gas flow distributors, pressurization of the flow is usually required to force the reactant flow through the small channels between the inlet and outlet, requiring additional compressor systems. Moreover, the manufacturing of such small gas flow channels requires extra manufacturing cost and time, whereas in the case of a perforated-type gas flow distributor, the need for pressurisation is eliminated and manufacturing is simpler and less costly. All of the numerical analyses during this research work were carried out at atmospheric pressure conditions.

156

Numerical analyses of the flow behaviour in the perforated-type gas flow channel showed that the flow passing through the holes of the perforated stainless steel electrodes undergoes frictional losses arising from the side wall shear stresses that results in a thick boundary layer in these holes. To address this issue in more detail, a parametric study was carried out examining different shapes of the perforated holes, and was reported in Section 5.4.

After passing through the perforated holes, the reactant species reach the gas diffusion layer (GDL). The porous media of the GDL offers resistance to the flow reactants that pass through it. This resistance is a function of the GDL porosity. The porous media of the GDL generally consists of a honey comb structure and plays an important role in the distribution of reactant and product species along the catalyst layer. Performance of the GDL decreases due to blockage of these porous holes by water generated as a product of the electro-chemical reaction. Such blockage of porous holes by water restricts the ability of species to pass through the GDL, which negatively affects the overall performance of the PEM fuel cell.

After passing through the gas diffusion layer, the reactant species reach the catalyst layer. At the anode side hydrogen atoms split into their constituents (protons and electrons). Positively charged protons travel through the electrolyte membrane, while the negatively charged electrons travel through an external circuit to reach the cathode side. At the cathode side, electrons and protons coming from the anode side react with the reduced oxygen atoms at the cathode catalyst layer to generate heat and water in addition to the intended electrical current. The splitting of hydrogen and Oxygen into their constituents along the cathode and anode catalyst layers depends upon the amount of catalyst surface available. The electrochemical reactions along the cathode catalyst layer also depend upon the rate of oxidation and distribution of the reactant species.

The analyses showed a high value of oxygen mass fraction along the cathode catalyst layer near the inlet section of the PEM fuel cell domain that reduced towards the outlet section of the PEM fuel cell. Close to the inlet section, the mass flow-rate of air and its effective diffusive flux was high, which lead to a high mass fraction of oxygen along the cathode catalyst layer below this section.

157

Such a high mass fraction of oxygen results in an increase in the electro-chemical reaction rate, hence, more water is produced. Some of this water moves back towards the electrolyte membrane to keep it wet, while the majority of the water moves towards the gas flow channels in the PEM fuel cell. The porous media of the GDL retains some of this water due to capillary action and surface tension, which can lead to the blockage of the pores of the GDL, hence resulting in gas concentration problems in the fuel cell.

Analyses of the activation and Ohmic over-potential distributions along the perforated-type PEM fuel cell domain showed a high value of Ohmic losses and low value of the activation losses below the open sections of the perforated plate. Activation over-potential depends upon the material properties and availability of the reactant species to activate the electro-chemical reaction. Numerical analysis showed a low value of activation over-potential below the open section of the perforated plate, whereas a high value of activation over-potential was observed below the solid section of the perforated plate.

Polarisation curves were used to analyse the performance of the PEM fuel cell. Results obtained from the numerical analyses were found to be in good agreement with experimental data (Figure 4.10). Results showed that the numerical analysis predicted higher values in comparison with the experimental data at high current densities. Such variation is mainly due to the single phase flow assumption used in the model. In actual fact, the water in a PEM fuel cell domain exists in both liquid and vapour forms, but for the initial numerical analyses, the water was assumed to be only in the vapour form.

The numerical analyses also showed higher values of activation over-potential when compared to experimental data. The increase in activation over-potential was found to be mainly due to the limitations of the numerical modelling with regards to material properties. Activation over-potential mainly depends upon the material properties of the electrodes. Due to the complex chemical structure of the fuel cell electrodes, accurate numerical modelling was not possible at this time. However, despite the above mentioned variations, a good agreement was found between both numerical and experimental results.

158

To compare the performance of the perforated-type PEM fuel cell with a conventional serpentine-type fuel cell, detailed numerical analyses were carried out. Analyses showed a better distribution of reactant species in the case of a perforated-type gas distributor when compared to a serpentine-type gas flow distributor. Serpentine-shaped gas flow channels require a high pressure flow supply, whereas in the case of the perforated type gas flow channels, such high pressures are not necessary. Overall, the PEM fuel cell with the perforated-type gas distributor showed a better performance when compared to the PEM fuel cell with the serpentine-shaped gas channel at atmospheric pressure conditions.

7.2.2 Effect of Operating Parameters Variation: A Parametric Study

Two dimensional, steady state numerical analyses were carried out to explore the effects of varying different operating parameters, such as gas diffusion layer porosity, operating temperature and exchange current density on the overall performance of the perforated-type PEM fuel cell. Two dimensional numerical analyses were carried out instead of three dimensional analyses for this parametric study in order to reduce computational requirements, as the parameters studied were not significantly influenced by the geometry of the fuel cell domain.

The parametric study of the effects of the gas diffusion layer (GDL) porosity variation showed that increasing the GDL porosity resulted in an increase in the performance of the PEM fuel cell. This increase in performance was mainly due to the improved distribution of the reactant species along the catalyst layer when the GDL porosity was increased. The resistance offered by the gas diffusion layer to the reactant species reduced to a certain extent when GDL porosity was increased, leading to the presence of high mass fractions of reactant species along the catalyst layer that effectively improved the rate of the electrochemical reaction and the overall performance of the PEM fuel cell.

The numerical analyses of the effect of operating temperature variation on the PEM fuel cell performance showed that increasing the operating temperature improved the rate of the electro-chemical reaction and reduced the activation over-

159

potential of the PEM fuel cell. However, increases in the operating temperature could also lead to possible dryness of the membrane that could reduce the performance of the PEM fuel cell. A small amount of heat was also produced as a by-product of the electro-chemical reaction that also increased the operating temperature of the PEM fuel cell.

The two dimensional non-isothermal study showed that for an inlet air temperature of 298 K (25°C), the operating temperature of the PEM fuel cell rose to 312 K (42°C). This increase in operating temperature was mainly due to the heat generated by the electro-chemical reaction along the cathode catalyst layer. Increases in temperature can be controlled to some extent by increasing the effective flow rate of the reactant air, and certain design changes can be used to improve the diffusive flux of the air through the porous media. An optimum balance is required between the operating temperature and the reactant flow rate.

The exchange current density is a function of material composition, surface roughness and electrode surface impurities. Increasing the exchange current density improves the rate of oxidation and reduction, which increases the rate of the electro-chemical reaction. Activation over-potential is significantly reduced with increasing exchange current density. No detailed analyses were carried out to explore this behaviour, as it entirely depends upon the chemical composition of the material, which is out of the scope of this research work. Overall, analyses showed that increasing the exchange current density magnitude significantly improved the performance of the PEM fuel cell.

7.2.3 Effect of Geometric Parameters Variation: A Parametric Study

Three dimensional numerical analyses were carried out to study the effects of geometric parameters on flow behaviour and the overall performance of the perforated-type PEM fuel cell. The effect of different geometric parameters, such as perforated holes diameter, gas channel height, inlet hole diameter and its location were analysed. The idea behind this parametric study was to identify and optimise the performance of this new design of PEM fuel cell without any major design changes.

The perforated hole diameter is an important design parameter for this novel design configuration. It determines the effective open area of the perforated plate. Two different perforated holes diameters (2.5 and 5 mm) were studied. Analysis showed that increasing the hole diameter resulted in an increase in the performance of the PEM fuel cell. This occurs for two reasons; firstly, increasing the perforated hole diameter results in a corresponding increase in the effective open area of the perforated plate, which improves the distribution of reactant species along the PEM fuel cell domain; secondly, such an increase in the perforated hole diameter reduces the frictional losses of the reactant flow by side wall shear stresses. As a consequence, the wetted surface area of the membrane electrode assembly increases, which consequently improves the performance of the PEM fuel cell.

The perforated hole shape is another design parameter that affects the effective flow rate of the reactant species along the fuel cell domain. Two different shapes of perforated holes (circular and trapezoidal) were analysed during this study. Analyses showed that the overall performance of the PEM fuel cell increased with the trapezoidal hole shape at high load conditions. Such increases in performance were mainly due to the increase in the effective open area of the perforated hole adjacent to the GDL, and a reduction in side wall shear stresses due to the trapezoidal shape of the hole. However, this performance increase was not significant.

The gas channel height affects the flow behaviour in the fuel cell gas flow channel. Increase in the gas channel height reduced the side wall shear stresses and increased the convective flux of the reactive flow. Increase in the gas channel height also reduced the diffusive flux of the reactant species. Numerical analyses showed that an increase in gas channel height caused a reduction in the mass fraction of the oxygen along the cathode catalyst layer. This indicated a reduction in diffusive flux of the reactant species with an increase in gas channel height. Overall, the analyses showed that increasing the gas channel height resulted in a reduction in the overall performance of the PEM fuel cell.

Three different inlet hole diameters were taken into consideration to study their effect on the species distribution and the overall performance of this new

design of PEM fuel cell. Circular-type inlet/outlet ports were assumed for this study. Analysis showed that an increase in the inlet hole diameter caused the performance of the PEM fuel cell to increase. This increase in performance was due to an increase in the effective mass flow-rate and Reynolds number of the reactant species.

Inlet/outlet port locations in the PEM fuel cell affect the distribution of reactant species, as any change in the location varies the wetted area of the fuel cell domain covered by the reactant species. During preliminary three dimensional analyses, it was observed that in the case of central locations of the inlet/outlet holes, the fluid flow did not cover the full area of the perforated type PEM fuel cell domain. The flow species did not reach the corners of the fuel cell domain. Due to this behaviour, a small parametric study was carried out to understand the effect of inlet/outlet hole locations on the performance of the fuel cell. Two different locations of the inlet/outlet holes (centre and corner) were analysed during this study. Results showed that in the case when the holes were located at opposite corners, the performance of the PEM fuel cell increased, as reactant species covered a larger area, but the overall influence on fuel cell performance was not very significant.

7.3   Effects of Flow Pulsation on the Performance of the PEM Fuel Cell

Flow pulsation is a time-dependant phenomena, where the time-averaged pulsating velocity is a function of pulsation frequency and amplitude. Flow pulsations affect the diffusive/convective properties of the fluid flow. Kim *et al.* [17] studied the effects of flow pulsation on the performance of the PEM fuel cell using experimental techniques, but no numerical analysis has been carried out to explore the effect of flow pulsation on the overall performance of the PEM fuel cell. Numerical analyses were carried out during this research work to explore the effects of flow pulsation and to identify the effects of different parameters such as pulsation frequency and amplitude variation on the pulsating behaviour, and particularly on the overall performance of the PEM fuel cell.

One way of generating pulsations in the reactant flow is to use an electro-kinematics device, while another way is by passive methods whereby pulsations are induced by placing obstacles in the flow domain. Transient, two dimensional numerical simulations were carried out to study the effects of flow pulsations by both active and passive approaches. Results showed that by introducing pulsations into the reactant flow, the diffusive flux of the reactant species increased along the GDL/gas channel interface of the PEM fuel cell. This increase consequently improved the performance of the fuel cell. To explore this behaviour further, a more detailed parametric study was carried out to identify the parameters that significantly influence the flow pulsation.

To study the effect of pulsating frequency variation, three different values of pulsating frequencies (0, 10 and 30 Hz) were taken into consideration. Results showed that increase in the pulsating frequency caused an increase in the diffusive flux of the reactant species. Such increase in the diffusive flux increased the performance of the fuel cell, but overall the effect was not significant.

To study the effects of pulsating amplitude variation, four different values of pulsating amplitude (0 to 3) were taken into consideration. Analysis showed that increasing the pulsating amplitude significantly affected the performance of the PEM fuel cell. The diffusive flux of the reactant species increased considerably with an increase in pulsating amplitude, which improves the electro-chemical reaction rate.

Studies into the effects of the number of obstacles in the fuel cell gas channel when using passive pulsation showed that the increase in the number of obstacles affected the flow behaviour along the fuel cell domain. Numerical analyses were carried out assuming three different numbers of obstacles (1, 2 and 5). Analyses showed that varying the number of obstacles mainly affected the pulsating frequency and the strength of vortex shedding behind each obstacle. Increase in the vortex shedding strength increased the diffusive flux of the reactant species along the porous media of the membrane electrode assembly.

A major disadvantage of the increased strength of vortex shedding was the increase in the water amount in the areas behind the obstacles. To overcome this problem, some design changes were essential in terms of the placement and dimensions of the obstacles placed in the PEM fuel cell gas channel. A further parametric study was carried out to explore this phenomenon. Overall, the numerical analyses showed that the increase in the number of obstacles enhanced the pulsating effect, consequently improving the performance of the PEM fuel cell.

Increasing the number of obstacles would increase the manufacturing cost and complexity. To solve this problem, some alternative methods are required. Simple design changes, such as a change in obstacle height and placement angle were proposed by the author. Parametric analyses were carried out to explore the effect of these design changes on the overall performance of the PEM fuel cell.

To study the effect of obstacle height, a fuel cell domain with two obstacles was modelled, in which three different obstacle heights (2.5, 3.5 and 4 mm) were analysed. Results showed that increasing the obstacle height improved the effect of pulsating amplitude. Increasing the obstacle height resulted in the reactant flow being deflected down sharply and during the recovery; it enhanced the strength of vortex shedding. Both these phenomena increased the pulsating amplitude in the domain, the matter which increased the diffusive rate of reactant species, and effectively improved the performance of the PEM fuel cell.

Analyses showed that vortex shedding behind the obstacle was influenced by the variation in the number of obstacles and their height. To an extent, such increases in the vortex shedding improved the residence time and effective diffusivity of the reactant species along the fuel cell domain. However, such increases in the vortex shedding increased water flooding in the areas behind the obstacle. To solve this problem, the angular placement of the obstacle needed to be adjusted.

To study the effect of angular placement of the obstacles on flow behaviour and water flooding in the fuel cell gas channel, three different obstacle placement

angles (60, 90 and 120 degrees) were taken into consideration. Results showed that by increasing the obstacle angle from 60 to 120 degrees, the flow behaviour behind the obstacle was considerably disturbed, which affected the water flooding behind the obstacle, but generally it did not significantly affect the performance of the PEM fuel cell.

All of these analyses showed that the overall performance of the PEM fuel cell could be increased by introducing pulsations into the reactant flow. Placing obstacles in the flow is a good alternative method for generating pulsations in the flow, instead of using complex and costly electro-kinematics systems. The parametric examination of obstacles also showed that although increasing the number of obstacles improved fuel cell performance, it also involved additional manufacturing complexities; therefore, other alternative methods, such as changing the obstacle height and placement angle were also analysed to study their effects.

CHAPETR 8

8   Conclusions & Recommendations

This chapter summarizes the important findings based upon the performance analyses of two new design configurations of the PEM fuel cell and recommendations for future work are proposed.

8.1   Conclusions

8.1.1   Performance Analyses of Perforated-Type PEM Fuel Cells

Following are the important findings of this study based upon the performance analyses of the perforated type PEM fuel cell:

i.   Perforated type gas flow distributors can be a good alternative to conventional PEM fuel cell gas flow channels. Extra manufacturing effort and cost is required for conventional gas flow channels, whereas perforated gas flow distributors are easy to manufacture and are readily available in the market. Moreover, perforated-type gas distributors can be easily customised according to the requirements of the fuel cell design;

ii. Compared to the serpentine-shaped conventional gas distributor, a better distribution of reactant species along the fuel cell domain was shown with a perforated type gas distributor. Results showed that for the serpentine-shaped gas channels, a high pressure flow was required at the fuel cell inlet, whereas for the perforated gas flow channel, no high pressure flow was required and operation can be performed at atmospheric conditions. Overall, the perforated type flow channels gave better performance compared to the serpentine-shaped gas distributor at atmospheric pressure conditions;

iii. Analyses of the reactant species distribution showed high values of oxygen mass fraction and low values of water mass fraction below the open areas of the perforated gas flow distributor. Closer to the outlet section, this concentration is reduced because of oxygen consumption. Similarly, at the anode side, a high value of hydrogen and water mass fraction is observed near the inlet section, which is continuously reduced closer to the outlet section due to consumption of hydrogen and water. Hydrogen is split up into its constituents while water is consumed to keep the electrolyte membrane wet;

iv. Analysis of water generation along the membrane/catalyst interface at the cathode side showed a high value of water content at low cell voltages. This was due to an increase in the rate of electro-chemical reaction rates at these low cell voltages;

v. The water content generated by the electro chemical reaction moves from the membrane/catalyst interface to the gas channel. Some of this water gets stuck in the pores of gas diffusion layer, causing an increase in concentration losses of reactant species along the cathode GDL;

vi. Increasing the operating temperature improves the rate of electro-chemical reactions along the cathode catalyst layer, which leads to an increase in the overall performance of the PEM fuel cell. This increase in operating temperature can also lead to the dryness and possible rupture of the electrolyte membrane, but on the other hand, the increase in electro-chemical reactions causes more water to be generated as a reaction by-product. Some part of this waste water moves back to the membrane due to back-diffusion and keeps the membrane wet. This behaviour is allowable up to a certain temperature level, but at very high temperatures this can lead to dryness and rupturing of the membrane;

vii. The non-isothermal analyses show that heat is generated as a by-product of the electrochemical reactions along the cathode catalyst layer. Such heat gets distributed along the PEM fuel cell domain and increases the operating

temperature of the PEM fuel cell. Results show that such heat generation is more significant at the cathode side, while at the anode side there is no significant variation in operating temperature, and the temperature remains almost constant;

viii. Increasing the GDL porosity improves the efficiency with which the reactant species permeate the GDL. Overall, the performance of the PEM fuel cell increases with an increase in GDL porosity;

ix. The exchange current density affects the rate of oxidation and reduction at the cathode and anode sides respectively. Activation over-potential is significantly reduced with increasing the exchange current density. Overall, the analyses show a significant improvement in the PEM fuel cell performance when the cathode exchange current density is increased;

x. The performance of the PEM fuel cell with a perforated-type gas distributor is strongly influenced by the effective open area of the perforated gas channel. There are two methods to increase the effective open area of the perforated plate: either by increasing the number of perforated holes or increasing the diameter of each hole. Increasing the number of holes means extra manufacturing costs and added design complexity. Therefore, the analysis carried out studied different diameters of perforated holes. Results showed that with an increase in perforated hole diameter, the performance of the PEM fuel cell increases. This increase in performance was mainly due to improved reactant species distribution along the fuel cell domain, and to some extent a reduction in the side wall shear stress offered by each perforated hole to the flow while passing through it;

xi. Increasing the gas channel (trough) height affects the wall shear stresses in the gas channel domain, which consequently affect the performance of the PEM fuel cell. An increase in gas channel height reduces the residence time of the reactant flow in the gas channel, which leads to an increase in the convective flux. Analyses of the variation of the oxygen diffusive flux at

different gas channel heights showed a considerable increase in the oxygen diffusive flux when the gas channel height was decreased;

xii. Increases in inlet hole diameter of the PEM fuel cell increases the effective mass flow-rate, which leads to an increase in fuel cell performance. Analyses show that increasing the inlet hole diameter results in an increased effective area of the fuel cell domain covered by the reactant species;

xiii. Changing the inlet/outlet port location from the centre to the corners improved the reactant species distribution along the fuel cell, but generally this change was not significant.

8.1.2 Effect of Cathode Flow Pulsation on PEM Fuel Cell Performance

The following are some important findings based upon the results obtained from the numerical analyses of cathode flow pulsations on the species distribution and overall performance of the PEM fuel cell:

i. Time-averaged pulsating velocity is a function of pulsating frequency and amplitude. Analyses show that variations of pulsating frequency have no significant influence on fuel cell performance, but the effect of pulsating amplitude is significant;

ii. A pulsating flow improves the diffusion rate of the reactant species which consequently improves the performance of the PEM fuel cell;

iii. The placement of obstacles in the fuel cell domain affects the flow behaviour in the fuel cell domain; these obstacles passively induce a pulsating effect into the reactant flow;

iv. Increasing the number of obstacles improves the pulsating frequency, but generally does not improve the performance of the PEM fuel cell significantly;

169

v.   Variation in the obstacle placement angle affects the flow behaviour behind the obstacle, but overall it does not significantly affect the performance of the PEM fuel cell;

vi.   The flow amplitude increases with an increase in obstacle height. Overall, the performance of the fuel cell increases with an increase in obstacle height.

8.2   Recommendations for Future Work

The research work presented in this thesis mostly dealt with a parametric study into the effects of varying different operating and geometric parameters on the overall performance of two new design configurations for PEM fuel cells. This research work was based upon some initial assumptions to ease the resources required to conduct the numerical analyses. The following are proposed recommendations suggested by the author for further research work in the future:

▪ The numerical analysis in this research work has been carried out assuming a single phase flow (vapour form) in the fuel cell domain. This assumption has been taken into consideration to minimise computational requirements for the numerical simulation. In actual fact, the water in the PEM fuel cell domain exists in both liquid and vapour form. Although this assumption does not significantly influence the numerical results, more realistic numerical analyses in the future should be carried out assuming two phase flow in the fuel cell domain;

▪ Most numerical analyses in this research work were isothermal. Although some two dimensional, non-isothermal analyses were carried out, no full scale three dimensional and non-isothermal numerical analyses were carried out due to limitations in computational power. Therefore, full scale, three dimensional non-isothermal numerical simulations should be carried out in the future to explore the heat generation due to electro-chemical reactions and temperature distributions along the fuel cell domain in a more realistic way;

- Transient numerical analyses are generally more realistic and provide a better picture of the overall scenario. Numerical analyses of the PEM fuel cell with a perforated-type gas distributor were carried out under steady state conditions because the main purpose of this study was to validate the model and analyse the performance at different operating and geometric conditions. For further research, some full scale, three dimensional and time dependant numerical simulations are vital for a better understanding of the reactant species and temperature distributions along the domain of this new design of PEM fuel cell;

- Improved knowledge of material properties plays an important role in improving numerical analyses. Material properties of the membrane electrode assembly (GDL), catalyst layer and electrolyte membrane are complex. Continuous research is ongoing by researchers in order to gain improved understanding of the membrane electrode assembly. It is recommended by the author to use this knowledge in developing more comprehensive numerical models of the fuel cell.

- During this research work, a parametric study was carried out for different operating and geometric conditions. This parametric study provided a basis for the effect of different parameter variations. For further research, it will be worthwhile to use these results as a basis and couple the numerical solver with optimisation routines to predict an optimum value of these operational and geometric parameters for specific conditions.

References:

1. Coppoa, M., N.P. Siegel, and M.R.v. Spakovsky, *On the influence of temperature on PEM fuel cell operation.* Journal of Power Sources, 2006. **159**: p. 560-69.

2. Park, J. and X. Li, *An experimental and numerical investigation on the cross flow through gas diffusion layer in a PEM fuel cell with a serpentine flow channel.* journal of Power source, 2007. **163**: p. 853-863.

3. Djilalib, N. and B.R. Sivertsena, *Computational modelling of polymer electrolyte membrane (PEM) fuel cells: Challenges and opportunities.* Energy, 2007. **32**: p. 269-280.

4. Fernga, Y.M., A. Su, and S.M. Lu, *Experiment and Simulation investigations for effect of flow channel patterns on PEMFC Performance.* International Journal of Energy Research, 2008. **32**: p. 12-23.

5. YING and M. Ouyang, *Three Dimensional Heat and Mass Transfer analysis in an air-breathing Proton Exchange Membrane Fuel Cell.* journal of Power source, 2007. **164**: p. 721-729.

6. Nguyen, P.T., *A Three-Dimensional Computational Model of PEM Fuel Cell with Serpentine Gas Channels*, in *Department of Mechanical Engineering*. 2003, Institute of integrated energy system. University of Victoria, Canada.

7. Japanese Economy Davison, J.J.e.r., *Japan's Fuel Cell Industry*. May 2006.

8. Larmine, J. and A. Dicks, *Fuel Cell Systems Explained.* 2000: John Willey & Sons. 303.

9. Mennola, T., *Design and Experimental characterization of Polymer Electrolyte Membrane Fuel Cells*, in *Department of Engineering Physics and Mathematics*. 2000, Helsinki University of Technology: Espoo. p. 92.

10. Hu, G., et al., *Three Dimensional Numerical Analyses of Proton Exchange Membrane Fuel Cells (PEMFC) with conventional and interdigitised flow fields.* journal of Power source, 2004. **136**: p. 1-9.

11. Grujicic, M. and K.M. Chittajallu, *Design and Optimization of Polymer Electrolyte Membrane (PEM) Fuel Cell.* Applied Surface Science, 2004. **227**: p. 56-72.

12. Hontanon, M.J. Escudero, and C. Bautista, *Optimisation of flow-field in polymer electrolyte membrane fuel cells using computational fluid dynamics techniques.* Journal of Power Sources, 2000. **86**: p. 363-68.

13. Meng, H., *A Three Dimensional Mixed Domain PEM Fuel Cell model with fully Coupled Transport Phenomena.* journal of Power source, 2007. **164**: p. 688-696.

14. Ren, G.p., L.J. Yu, and M.j. Qin, *Transport mechanisms and performance simulation of a PEM fuel cell.* International Journal of Energy Research, 2008. **32**(6): p. 514-530.

15. Chen, F., M.H. Chang, and C.F. Fang, *Analysis of Water Transport in a Five Layer Model of PEMFC.* journal of Power source, 2007. **164**: p. 649-658.

16. Um, S. and C.Y. Wang, *Three Dimensional Analysis if Transport And Electrochemical reactions in polymer electrolyte fuel cells.* journal of Power source, 2004. **125**: p. 40-51.

17. Kim, Y.H., H.S. Han, and S.Y. Kim, *influence of cathode flow pulsation on performance of proton-exchange membrane fuel cell.* journal of power sources, 2008. **185**: p. 112-117.

18. Chu, H.S., F. Tsau, and Y.Y. Yan, *The development of a small PEMFC combined heat and power system.* journal of power sources, 2008. **176**(2): p. 499-514.

19. Appleby, A.J. and F.R. Foulkes, *Fuel Cell Handbook.* 1989, New York: Van Nstrand Reinhold.

20. Curry, B.E. *National Fuel Cell Seminar Abstracts.* 1981.

21. http://physics.nist.gov/MajResFac/NIF/Images/FuelCellBasic.gif.

22. Henke, M., *Fuel Cell System for Automotive Application*, in *Faculty of Engineering and Computing.* 2008, Coventry University: Coventry. p. 97.

23. http://www.fctec.com/fctec_types_pafc.asp.

24. http://www.fctec.com/fctec_types_mcfc.asp.

25. http://www.iit.edu/~smart/garrear/Fuel_C3.jpg.

26. larmine, J. and A. Dicks, *Fuel Cell systems Explained.* 2000: Willey International.

27.	Balkin, A.R., *MODELLING A 500W POLYMER ELECTROLYTE MEMBRANE FUEL CELL*, in *Faculty of Engineering*. 2002, University of Technology, Sydney: Sydney.

28.	Haufe, S. and U. Stimming, *Proton conducting membrane based on electrolyte filled micro porous matrices.* Journal of Membrane Science, 2001. **185**: p. 95-103.

29.	Mikkola, *Experimental studies on polymer electrolyte membrane fuel cell stacks.* 2001, Helsinki University of Technology.

30.	Mustafa, M.Y.F.A., *Design, construction and testing of a 5KW PEM fuel cell stack based on sulphonated Naphthalenic Copolyimides Membrane*, in *AADE*. 2005, University of Hertfordshire, UK: Hertfordshire. p. 83.

31.	Kreuer, K.D., *On the development of Proton conducting polymer membranes for hydrogen and methanol fuel cells.* Journal of Membrane Science, 2001. **185**: p. 29-39.

32.	Smitha, B., S. Sridhar, and A.A. Khan, *Soild Polymer Electrolyte Membranes for Fuel Cell Applications - A review.* Journal of Membrane Science, 2005. **259**: p. 10-26.

33.	Rikukawa, M. and K. Sanui, *Proton conducting polymer electrolyte membrane based on hydrocarbon polymers.* Progress in Polymer Science, 2000. **25**: p. 1463-1502.

34.	Mehta, M. and J.S. Cooper, *Review and analysis of PEM fuel cell design and manufacturing.* journal of Power source, 2003. **114**: p. 32-53.

35.	Castro, D. and S. Emory. *New ELAT Materials for Ambient Fuel Cell Operation. Commercialization of small fuel cells & the Latest Battery Technology for Portable Applications*. 1999. Bethseda, MD, USA: The Knowledge Foundation Inc.

36.	Bevers, D. and R. Rogers, *Examination of the influence of PTFE coating on the properties of carbon paper in PEFCs.* Journal of Power Sources, 1996. **63**: p. 193-201.

37.	Wilson, M.S. and S. Gottesfeld, *Thin film catalyst layers for polymer electrolyte fuel cell electrodes.* Journal of applied Electro-chemistry, 1992. **22**(1): p. 1-7.

38. Fern`andez, R. and P.F. Aparicio, *PEMFC Electrode Preparation: Influence of the solvent composition and evaporation rate on the catalytic layer microstructure.* Journal of Power Sources, 2005. **151**: p. 18-24.

39. Sabir, I. and X. Li, *Review of bipolar plates in PEM fuel cells: Flow Field Design.* Int Journal of Hydrogen Energy, 2005. **30**(4): p. 359-371.

40. Kumara, A. and G. Ramana, *Materials and design developments for bipolar/endplates in fuel cells.* Journal of Power Sources, 2004. **129**: p. 62-67.

41. Wang, H. and M.A. Sweikart, *Stainless Steel as bipolar plate arterial for polymer electrolyte membrane fuel cells.* Journal of Power Sources, 2003. **115**: p. 243-251.

42. Makkus, R.C. and A. Janssen, *Use of Stainless steel for cost competitive bipolar plates in the SPFC.* journal of Power source, 2000. **86**: p. 274-282.

43. Hantall, P.L. and G.O. Mepsted, *New materials for polymer electrolyte membranes fuel cell current collecters.* journal of Power source, 1999. **80**: p. 235.

44. Watkins, D.S. and K.W. Dircks, *D.G.Epp.* 1992: US.

45. Watkins, D.S., *Novel fuel cell Fluid flow field plate.* US Patent 4988583, 1991.

46. Pollegri, A. and P. Spaziante, *US Patent 4197178.* 1980.

47. Wilson and Mahlon, *Fuel cell with interdigitated porous flow field.* US patent 5641586, 1997.

48. Berning, T. and N. Djilali, *Three dimensional computational analyses of transport phenomena in a PEM fuel cell.* journal of Power source, 2002. **106**: p. 284-294.

49. Wang, C.Y., *Fundamental Models of Fuel cell Engineering.* Chem Rev, 2004. **104**: p. 4727-4766.

50. Robalinho, E., E.F. Cunah, and A.B. Andrade. *COMSOL modelling and simulation of PEM fuel cell's flow channels.* in *COMSOL User Conference 2007.* 2007. Boston, USA.

51. Springer, T.E., T.A. Zawodzinski, and S. Gottesfeld, *Polymer electrolyte fuel cell model.* J. Electrochemical. Soc., 1991. **138**(8): p. 2334-2342.

52.   Bernardi, D.M. and M.W. Vebrunge, *A mathematical model of the solid polymer electrolyte fuel cell,* Journal of Electrochemical Society, 1992. **139**(9): p. 2477-2491.

53.   Broka and Ekdunge, *Modelling the PEM fuel cell cathode.* J Appl Electrochemical, 1997. **27**(1997): p. 281-289.

54.   Nguyen, T.V. and R.E. White, *A Water and Heat Management Model for Proton Exchange-Membrane Fuel Cells.* journal of electrochemical society, 1993. **140**(8): p. 2178-2186.

55.   Lampinen and Fomino, *Analysis of free energy and entropy changes for half-cell reactions.* Journal of Electrochemical Society, 1993. **140**(12): p. 3537-46.

56.   T.F. Fuller, J.N., *Water and thermal management in solid polymer electrolyte fuel cell.* J. Electrochemical. Soc., 1993. **140**(5): p. 1218-1225.

57.   Nguyen, T. and R. White, *A water, heat management model for Proton exchange membrane fuel cells.* Journal of electrochemical Society, 1993. **140**(1993): p. 2178-2186.

58.   Gurau, V., H. Liu, and S. Kakac, *Two dimensional model for proton exchange membrane fuel cells.* AIChE J, 1998. **44**(11): p. 2410-2422.

59.   Wang, Z.H., C.Y. Wang, and K.S. Chen, *Two phase flow and transport in the air cathode of PEM fuel cell.* Journal of Power Sources, 2001. **94**(1): p. 40-50.

60.   Yi, J. and T. Nguyen, *An Along the channel model for Proton Exchange Membrane Fuel Cell.* journal of electrochemical society, 1999. **146**: p. 38.

61.   Dutta, S. and S. Shimpalee, *Three Dimensional numerical simulation of straight channel PEM fuel Cells.* Journal of Applied Electrochemical, 2000. **30**: p. 135-146.

62.   MARS, A.B. and A.J. HAKS, *Parametric and optimization study of a PEM fuel cell performance using three-dimensional computational fluid dynamics model.* Renewable Energy, 2007. **32**: p. 1077-1101.

63.   Shimpalee, S. and S. Dutta, *Effect of Humidity on PEM Fuel Cell Performance. Part II. Numerical Simulation,* Heat Transfer Davison, ASME, 1999. **364-1**: p. 367-374.

64. Bradean, R., K. Promislow, and B. Wetton, *Transport phenomena in the porous cathode of a proton exchange membrane fuel cell.* Numerical Heat Transfer, 2002. **42**(2002): p. 121-138.

65. Guvelioglu, G.H. and H.G. Stenger, *Computational fluid dynamics modelling of polymer electrolyte membrane fuel cells.* Journal of Power Sources, 2005. **147**: p. 95-106.

66. Baschuk, J.J. and X. Li, *Modelling of polymer electrolyte membrane fuel cells with variable degrees of water flooding,* J. Power Sources, 2000. **86**: p. 181-196.

67. Wang and K.S. Chen, *Computational fluid dynamics modelling of proton exchange membrane fuel cells,* Journal of Electrochemical Society, 2000. **147**(12): p. 4485-4493.

68. You, L. and H. Liu, *A Two Phase flow and transport model for the cathode of PEM fuel cells.* Int. J. Heat Mass Transfer, 2002. **45**(2002): p. 2277-2287.

69. Natarajan and Nguyen, *Three Dimensional effect of liquid water flooding in cathode of PEM fuel cells.* journal of Power source, 2003. **115**: p. 66-80.

70. Berning, T. and N. Djilali, *A 3D multiphase, multi-component model of the cathode and anode of a PEM fuel cell.* journal of electrochemical society, 2003. **150**: p. A1589-A1598.

71. Hu, M., A. Gu, and M. Wang, *Three dimensional two phase flow mathematical model of PEM fuel cell: Part 2. Analyses and Discussion of the internal transport mechanisms.* Energy Conservation and Management, 2004. **45**(2004): p. 1883-1916.

72. Hu, M., A. Gu, and M. Wang, *Three dimensional two phase flow mathematical model of PEM fuel cell: Part 1. Model Development.* Energy Conservation and Management, 2004. **45**(2004): p. 1861-1882.

73. Nguyen, T.V. and R.E. White, *A Water and Heat Management Model for Proton-Exchange-Membrane Fuel Cells,"* Journal of the Electrochemical Society, 1993. **140**(1993): p. 2178-2186.

74. Fuller, T.F. and J. Newman, *Water and thermal management in solid-polymer electrolyte fuel cells.* Journal of electrochemical society, 1993. **150**(5): p. 1218-1225.

75. Djilali, N. and D.M. Lu, *Influence of heat transfer on gas and water transport in fuel cells.* International Journal of Thermal Science, 2002. **31**(2): p. 141-149.

76. Fernga, Y.M. and A. Sub, *A three-dimensional full-cell CFD model used to investigate the effects of different flow channel designs on PEMFC performance.* International Journal of Hydrogen Energy, 2007. **32**: p. 4466-4476.

77. Akbari, M.H. and B. Rismanchi, *Numerical investigation of flow field configuration and contact resistance for PEM fuel cell performance.* Renewable Energy, 2007. **33**(8): p. 1775-1783.

78. Djilalib, N. and B.R. Sivertsena, *CFD-based modelling of proton exchange membrane fuel cells.* Journal of Power Sources, 2005. **141**: p. 65-78.

79. Taylor, R. and R. Krishna, *Multicomponent Mass Transfer.* 1993, New York: Willey.

80. Cussler, E.L., *Diffusion Mass Transfer in Fluid systems.* 2nd ed. 1997: Cambridge University Press.

81. Bird, R.B., W. Steward, and E.N. Lightfoot, *Transport Phenomena.* 1960: Wiley, New York.

82. Baca, C.M., R. Travis, and M. Bang, *Three Dimensional Single Phases Non Isothermal CFD Model of a PEM Fuel Cell.* Journal of Power Sources, 2008. **178**(1): p. 269-281.

83. Williams, M.V. and E. Begg, *Characterisation of Gas Diffusion layer for PEMFC.* journal of electrochemical society, 2004. **151**(8): p. A1173-A1180.

84. Dohle, H., R. Jung, and N. Kimiaie, *Interaction between the diffusion layer and the flow filed of Polymer electrolyte fuel cells experiment and simulation studies.* journal of Power source, 2003. **124**: p. 147-154.

85. Paganin, V.A., E.A. Ticcianelli, and E.R. Gonzalez, *development and electrochemical studies of gas diffusion electrodes for polymer electrolyte fuel cells.* Journal of applied Electro-chemistry, 1996. **26**(3): p. 297.

86. Inoue, G., Y. Matsukuma, and M. Minemoto, *Evaluation of the thickness of membrane and gas diffusion layer with simplified two dimensional reaction and flow analyses of polymer electrolyte fuel cell.* journal of Power source, 2006. **154**: p. 8-17.

178

87. Lee, H.K., J.H. Park, and D.Y. Kim, *A study on the characteristics of the diffusion layer thicknesses and porosity of the PEMFC.* journal of Power source, 2004. **131**: p. 147-154.

88. Jordan, L.R. and A.K. Shukla, *Diffusion layer parameters influencing optimal fuel cell performance.* Journal of Power Sources, 2000. **86**: p. 250-54.

89. Rismanchi, Akbari, and Golneshan. *Three-dimensional numerical modelling of a proton exchange membrane fuel cell.* in *Proceedings of the 10th fluid dynamics conference.* 2006. Yazd University,Yazd, Iran.

90. Nguyen, B. T, and D. N, *Computational model of a PEM fuel cell with serpentine gas flow channels.* J Power Sources, 2004. **130**: p. 149-57.

91. Kast, W. and R. Hohenthanner, *Mass transfer within the gas-phase of porous media.* International journal of heat and mass transfer, 2000. **43**: p. 807-823.

92. Hwang, J.J. and S.J. Liu, *Comparison of temperature distributions inside a PEM fuel cell with parallel and interdigitated gas distributors.* Journal of Power Sources, 2006. **162**: p. 1203-1212.

93. Bazylak, A., D. Sinton, and N. Djilali, *Dynamic water transport and droplet emergence in PEMFC gas diffusion layers.* journal of Power source, 2008. **176**: p. 240-246.

94. Lin, G., W. He, and T.V. Nguyen, *Modelling liquid water effects in gas diffusion and catalyst layers of cathode of PEM fuel cell.* journal of electrochemical society, 2004. **151**: p. A1999-A2006.

95. Natarajan, D. and T.V. Nguyen, *A Two dimensional, Two phase Multicomponenet, Transient model for cathode of PEM fuel cell using conventional gas distributors.* journal of electrochemical society, 2001. **148**: p. A1324-A1335.

96. Yang, X.J. and F.Y. Zhang, *Visualization of liquid water transport in a PEFC.* Electrochemical and solid state letters, 2004(7): p. A408-A411.

97. Quan, P., B. Zhou, and A. Sobiesiak, *Effects of hydropholic/hydrophobic properties on the water behaviour in the micro-channels of a PEM fuel cell.* Journal of Power Sources, 2006. **161**(2): p. 843-848.

98.   Jiao, K. and B. Zhou, *Innovative gas diffusion layers and their water removal characteristics in PEM fuel cell cathode.* Journal of Power Sources, 2007. **169**: p. 296-314.

99.   C.Y. Wang, *Fundamental model for fuel cell engineering.* Chem. Rev., 2004. **104**(2004): p. 4727.

100.   U. Pasaogullari, C.Y.W., J. Electrochemical. Soc., 2005. **152**(2005): p. A380.

101.   H Meng and C Y Wang, J Electrochemical. Soc., 2005. **152**(2005): p. A1733.

102.   Y. Wang and C.Y. Wang, J. Electrochemical. Soc., 2006. **153**(2006): p. A1193.

103.   Hamann, C.H., A. Hamnett, and W. Vielstich, *Electrochemistry*, ed. Wiley-VCH. 1998.

104.   Bard, A.J. and L.R. Faulkner, *Electrochemical models*. 1980, New York: Willey.

105.   Nitta, I., *Inhomogeneous Compression of PEMFC Gas Diffusion Layer*, in *Faculty of Information and Natural Sciences*. 2008, Helsinki University of Technology: Helsinki. p. 89.

106.   Lampinen, M.J. and M. Fomino, *Analysis of free energy and entropy changes for half-cell reactions,*. J. Electrochemical. Soc., 1993. **140**(12): p. 3537-3546.

107.   Sivertsen, B.R., *CFD-based modelling of proton exchange membrane fuel cells*, in *MSc Thesis*. 2003, Norwegian University of Science and Technology.

108.   T.E. Springer, T.A.Z., S. Gottesfeld,, *Polymer Electrolyte fuel cell model.* J. Electrochemical. Soc., 1991. **138**(8): p. 2334-2342.

109.   Ise, M., K.D. Kreuer, and J. Maier, *Electro osmotic drag in polymer membranes: an electrophoresis NMR study.* Solid state ionic, 1999. **125**: p. 213.

110.   Djillali, N. and T. Bearing, *Three dimensional computational analyses of transport phenomena in PEM fuel cell-a parametric study.* journal of Power source, 2003. **124**: p. 440-452.

111.   Motupally, S., A.J. Becker, and J.W. Weidner, *Diffusion of water in Nafion 115 membranes,*. J. Electrochemical. Soc., 2000. **147**(9): p. 3171.

112.   Dutta, S. and S. Shimpalee, *Numerical Prediction of Mass exchange between cathode and anode channels in a PEM fuel cell.* Int. J. Heat Mass Transfer, 2001. **44**: p. 2029-2042.

113.   Zawodzinski, C. Derious, and T. Springer, *Water Uptake by and transport through Nafion 117 membranes.* journal of electrochemical society, 1993. **140**(1993): p. 1041-45.

114.   Ren, K., T.E. Springer, and S. Gottesfeld, *Water and Methanol uptakes in Nafion membranes and membrane effect on direct methanol cell performance.* journal of electrochemical society, 2000. **147**(2000): p. 92.

115.   Walsby, Nadia, and Sami, *Water in different poly (styrene Sulphonic acid) grafted fluropolymers.* Journal of applied polymer science, 2002. **86**(2002): p. 33-42.

116.   Kumar, A. and R.G. Reddy, *Recent Developments in materials, design and concepts for bipolar/end plates in PEM fuel cell*, in *Advance e materials for energy conversion*, D. Chandra, Editor. 2004, University of Albama: Tuscaloosa.

117.   Reid, C.E. and G. Mclean. *Results and analysis of a PEMFC stack using metallic bipolar plates*. in *Processing of the 1998 Fuel Cell Seminar*. 1998. Palm Springs, California USA: United State Department of Defence.

118.   Wang, Y. and D.O. Northwood, *An investigation into the effects of a nano-thick gold interlayer on polypyrrole coatings on 316L stainless steel for the bipolar plates of PEM fuel cells.* Journal of Power Sources, 2008. **175**(1): p. 40-48.

119.   Davies, D.P. and P.L. Adcock, *Stainless steel as bipolar plate material for solid polymer fuel cells.* Journal of Power Sources, 2000. **86**(1): p. 237-242.

120.   Mustafa, M.Y., *Design and manufacturing of a proton exchange membrane fuel cell*, in *Mechanical Engineering*. 2009, Coventry University: Coventry. p. 240.

121.   Versteeg, H.K. and W. Malalasekera, *An introduction to computational fluid dynamics*. 1995, New York: John Willey & Sons. 257.

122. Ferziger, J.H. and M. Peric, *Computational Methods for Fluid Dynamics*. 1996, New York: Springer. 356.

123. Williams, A., T.N. Croft, and M. Cross, *A Group Based solution strategy for multiphysics simulations in parallel*, in *Applied Mathematical Modelling*. 2006.

124. Zimmerman, W.B.J., *Multiphysics Modelling with Finite Element Methods*. Series on Stability, Vibration and control of systems, ed. A. Guran. Vol. 18: World Scientific. 422.

125. *COMSOL User's Guide, Version 3.4*.

126. Narvekar, V.V. and Q. Fan. *Transport Phenomena in a Nafion Polypropylene Composite Membrane*. in *Comsol User Conference*. 2006. Boston.

127. Miley, G.H. *Development of a coupled 2D-3D fuel cell model for flow field analysis*. in *COMSOL User Conference*. 2006. Boston.

128. Hottinen, T., M. Mikkola, and P. Lund, *Evaluation of planer free breathing polymer electrolyte membrane fuel cell design*. journal of power sources, 2004. **129**(1): p. 68-72.

129. Ishino, Y., M. Suzuki, and T. Abe, *Flow and Heat Transfer Characteristics in pulsating pipe flows*. Heat Transfer, Japanese Research, 1998. **25**(5): p. 323-341.

130. Faghri, A., M. Faghri, and K. Javdani, *Effect of Flow pulsation on laminar heat transfer between two parallel plates*. Heat and mass transfer, 2005. **13**: p. 97-103.

131. Kurzweg, U.H. and L.D. Zhao, *Heat transfer by high frequency oscillation: A new hydrodynamic technique for achieving large effective thermal conductivities*. Physics Fluids, 1984. **27**(11): p. 2624-2627.

132. Kurzweg, U.H., *Enhanced heat conduction in oscillating viscous flows with in parallel plate channels*. Journal of Fluid Mechanics, 1985. **156**: p. 291-300.